

Peder Gjestvang

# Buckling of Non-spherical MOSS-LNG Tanks

Master's thesis in Marine Technology

Supervisor: Jørgen Amdahl

June 2020

**NTNU**  
Norwegian University of Science and Technology  
Faculty of Engineering  
Department of Marine Technology



Norwegian University of  
Science and Technology



Peder Gjestvang

# **Buckling of Non-spherical MOSS-LNG Tanks**

Master's thesis in Marine Technology  
Supervisor: Jørgen Amdahl  
June 2020

Norwegian University of Science and Technology  
Faculty of Engineering  
Department of Marine Technology





NTNU Norges teknisk-naturvitenskapelige universitet  
*Institutt for marin teknikk*

## MASTER THESIS 2020

for

Stud. techn. **Peder Sødal Gjestvang**

### **Buckling of Non-spherical MOSS-LNG Carriers**

*Knekking av ikke-sfæriske tanker i MOSS-LNG skip*

In recent years the demand for large LNG ships has increased. Ship owners are now requesting larger LNG ships with a cargo capacity up to 180 000 m<sup>3</sup>, with ship dimensions being compliant with the limitations of the new locks of the Panama Canal. A challenge with the Moss LNG tanks is that increase in cargo capacity is most efficiently dealt with by increasing the tank diameter. Spherical tank ships of cargo capacity 165 000 m<sup>3</sup> are in compliance with the Panama canal restrictions, but for larger capacities modification of tank shape is necessary, as discussed below.

The Moss-type LNG tank is an independent aluminium tank, supported by a cylindrical skirt, which provides the structural connection to the ship double bottom structure. The cylindrical skirt connects to the LNG tank through a central horizontal ring (the equator profile). The Moss LNG tank is very robust and is preferred by many ship owners, with more than 20 vessels in construction in early 2017.

As discussed above, increasing the cargo capacity without increasing number of tanks is challenging because the maximum ship width must remain within the Neo-panamax limitations. An option for increasing the cargo capacity is to modify the shape of the tank. An example of an altered tank shape is the apple-shaped tanks designed by Mitsubishi shown in Figure 1. The apple shape gives the tank a larger capacity than a spherical tank, while maintaining the ship width within the limitations of the Panama Canal. The center of gravity of the tank is also lower than for a vertically stretched tank, which makes it easier to meet the stability requirements. Although the tank shape is altered, the tank support system is not. Many of the important characteristics of the spherical Moss LNG tank are therefore maintained.

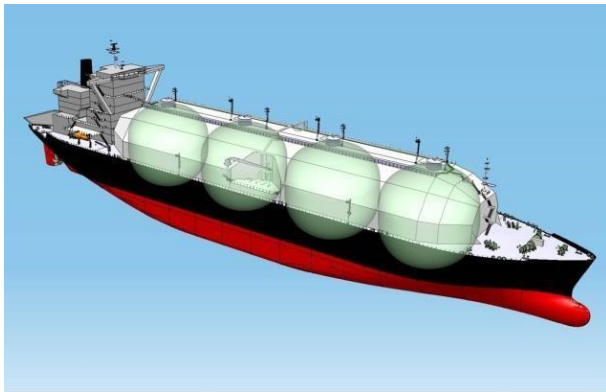


**Figure 1 Illustration of apple shaped tanks on a LNG Ship.**

Changing the tank shape to a non-spherical shape introduces some challenges with regard to calculating the tanks structural capacity for the Ultimate Limit State (ULS) especially.

Simplified equations for structural capacity available in Classification codes are only valid for purely spherical tanks. When the tank shape deviates from a pure sphere more complex analyses must be performed to verify the tanks ULS capacity. For the Mitsubishi design, nonlinear finite element analyses (NLFEA) were performed to verify the tank's structure integrity. One should however note that non-linear finite element analyses are very time consuming both with regard to modelling and computation time, and may not be an efficient tool in the design phase.

An accurate estimate of the buckling capacity of the tank shell when the shell has a different curvature in the different directions is needed. This should also include the secondary effects of thermal contraction, as the tank shape deviate from the initial shape once it is filled. Estimates for second order geometrical loads are easily included when performing NLFEA, so the focus should first be on establishing a method for determining the buckling capacity of a non-spherical tank.

NLFEA is not a very efficient method for designing structures even with the recent increases in computation capacities. Simple estimates are preferred in the design stage. The availability and validity of these simple methods is however not known.

Analysis of spherical tanks was conducted by Andreas Sanne in a master thesis in the spring of 2019. The idea of this master thesis work is to follow up the work conducted by Sanne.

The project work shall address the following topics:

1. A summary of relevant formulas for stresses in spherical/non-spherical and cylindrical shells as given in literature and relevant design rules and guidelines issued by ship classification societies



2. Discuss and investigate the effect of different imperfection amplitudes and shapes. The starting point is tolerances limits and measurements available in the literature. Describe methods that may be used to introduce imperfections.
3. Discuss relevant load cases for the tanks. Determine which load cases that will be subjected to further investigation, how this will be applied in nonlinear analysis and how they can be compared with rule formulations.
4. Conduct eigenvalue analysis and check the mesh size sensitivity. Determine how nonlinear material shall be modelled for the tanks.
5. Apply relevant imperfections and conduct nonlinear analysis with LS-DYNA. Perform systematic parametric studies where e.g. shell thicknesses, length of cylindrical sections are varied. To simplify parametric studies it is recommended to automatize this by developing scripts.
6. Compare the results from the finite element analyses with theoretical and rule formulations. Propose rule formulations that better represents the ultimate strength of non-spherical tanks. On the basis of the results perform an simple evaluation of the possible advantages of non-spherical tanks.
7. Conclusions and recommendations for further work

During the master thesis work, the project should focus on a shape deviating from a spherical shell, and compared with available buckling theory (if possible). Then, the learning from the nonlinear calculations should be condensed for future use by extension of analytical formula or proposal of new empirical calculation methods.

Moss Maritime will support the work with relevant background data and discussions throughout the work execution, such as examples of tank size/scantlings, measured as-built imperfections, proposed altered tank shape geometry etc.

Literature studies of specific topics relevant to the thesis work may be included.

The work scope may prove to be larger than initially anticipated. Subject to approval from the supervisor, topics may be deleted from the list above or reduced in extent.

In the thesis the candidate shall present his personal contribution to the resolution of problems within the scope of the thesis work.

Theories and conclusions should be based on mathematical derivations and/or logic reasoning identifying the various steps in the deduction.

The candidate should utilize the existing possibilities for obtaining relevant literature.



The thesis should be organized in a rational manner to give a clear exposition of results, assessments, and conclusions. The text should be brief and to the point, with a clear language. Telegraphic language should be avoided.

The thesis shall contain the following elements: A text defining the scope, preface, list of contents, summary, main body of thesis, conclusions with recommendations for further work, list of symbols and acronyms, references and (optional) appendices. All figures, tables and equations shall be numerated.

The supervisor may require that the candidate, in an early stage of the work, presents a written plan for the completion of the work. The plan should include a budget for the use of computer and laboratory resources which will be charged to the department. Overruns shall be reported to the supervisor.

The original contribution of the candidate and material taken from other sources shall be clearly defined. Work from other sources shall be properly referenced using an acknowledged referencing system.

The report shall be submitted in two copies: -

Signed by the candidate

- The text defining the scope included
- In bound volume(s)
- Drawings and/or computer prints which cannot be bound should be organised in a separate folder.

**Supervisor:**

Prof. Jørgen Amdahl

**Co-supervisor**

PhD-student - Martin Slagstad

**Deadline: June 10, 2020**

Trondheim, January 15, 2020

Jørgen Amdahl



---

## Abstract

The demand for large LNG-Carriers has increased. The easiest way to increase the capacity of the LNG-Carriers of the Moss-design with spherical tanks, is to increase the tank diameter, and consequently the ship beam. Due to the limitations of the Panama Canal concerning ship dimensions, the remaining way to increase the capacity of the vessels is to modify the shape of the tanks to improve the utilization of the ship displacement. This thesis has focused on the possibilities of a longitudinally elongated tank, which includes a cylindrical part between the two spherical end-caps.

The FEM-analysis has been limited to buckling analyses of such tanks, and comparison with the current rules and regulations of non-spherical LNG-tanks have been done. Several analyses with only external pressure as load have been done to study the buckling strength of longitudinally stretched tanks, focusing on critical stresses and comparison with current rules and regulations. Additionally, the load assumed to be the most critical to buckling of the tanks, which is the sloshing load has been analysed. Both a spherical and a longitudinally stretched tank with a cylindrical part was analysed, and the results were compared.

Based on the results obtained in this project, DNV GLs use of the equation for elastic buckling stress for short cylinders seems unsuitable. A modification to the current Class Guidelines has been suggested in this thesis.

The sloshing analyses indicate that the buckling strength of a longitudinally stretched tank is significantly lower than the strength of the original spherical tank. However, the buckling strength can be increased by increasing the thickness in critical parts of the LNG-tank, although this will have some negative consequences in terms of weight and cost. Based on the results obtained in this thesis there is no indication that the reduction in buckling strength will make the longitudinally stretched tanks unfeasible, and it is deemed likely that other structural aspects will be more severe.

Comparison of maximum allowable stresses by DNV GL and the critical buckling stresses obtained in the FEA indicates that the maximum allowable stresses proposed by DNV GL are quite conservative, where the FEA-results indicate that the maximum allowable stresses by DNV GL have a safety factor of around 2. Hence, it is possible that allowing larger design stresses in the tanks may lead to more cost-efficient LNG-Carriers without introducing safety issues. This observation is based exclusively on the results obtained in this thesis and would need to be verified before introducing any changes to the current rules and regulations.

---

## Sammendrag

Etterspørselen etter store LNG-skip har økt. Den enkleste måten å øke kapasiteten til Moss LNG-skip er å øke diameteren til de sfæriske tankene, og dermed også skipets bredde. På grunn av begrensningene på skipets dimensjoner i Panamakanalen, er ikke dette en ideell løsning. Dermed er det ønskelig å endre tankens form fra den sfæriske for å forbedre utnyttelsen av skipets deplasement. Denne oppgaven fokuserer på mulighetene for å "strekke" tankene i langskips retning, ved å introdusere en sylindrerformet del, mellom to halvkuler. FEM-analysene har vært begrenset til knekkingsanalyser av slike tanker, og sammenligning med gjeldende regelverk for slike tanker er gjort.

Flere av analysene er gjort med kun ytre trykk som last. Dette er en enkel måte å vurdere hvordan styrken til tankene varierer ved ulike konfigurasjoner, som for eksempel sylindrerdelens lengde. Å bruke kun ytre trykk som last er en enkel måte å finne kritisk spenning for tankene. I tillegg har sloshing-laster blitt analysert. Denne lasten er sett på som mer kritisk for tankene. Både en sfærisk tank og en langskips strekt tank med en sylindrisk del har blitt studert, og resultatene har blitt sammenlignet.

Resultatene antyder at DNV GLs bruk av likningen for elastisk knekkspenning for sylindre passer dårlig for sylindre med et så lavt lengde/radius forhold som slike sylindre vil ha. En modifikasjon til denne metoden, basert på resultatene fra analysene er foreslått i denne oppgaven.

Analysene med sloshing-laster indikerer at de strekte tankene er betydelig svakere enn de originale sfæriske tankene i forhold til knekking. Å øke tykkelsen på de strekte tankene i spesielt kritiske områder virker som en mulig og enkel løsning for å øke styrken. Dette vil dessverre også medføre økt vekt og byggekostnad. Basert på resultatene i denne oppgaven er det ingenting som tilsier at den reduserte knekkstyrken vil gjøre langskips strekte LNG-tanker til en umulig løsning. Det er vurdert som sannsynlig at andre strukturelle aspekter enn knekking av tanken vil være mer kritisk for en slik konfigurasjon.

Sammenligning av maksimalt tillatte spenningsverdier fra DNV GL og de kritiske knekkspenningene fra analysene indikerer at de foreslåtte maksverdiene fra DNV GL er konservative. Resultatene tilsier at maksimalt tillatte spenningsverdier fra DNV GL gir en sikkerhetsfaktor på omtrent to. Det er mulig at det å tillate høyere spenninger i tankene vil føre til mer lønnsomme LNG-skip uten at det går utover sikkerheten. Denne observasjonen er utelukkende basert på resultatene fra denne oppgaven, og videre analyse og verifikasjon vil være nødvendig før noen endringer kan gjøres i forhold til nåværende regelverk.

---

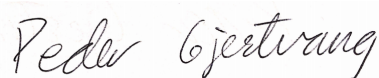
## Preface

This master thesis has been written at the Department of Marine Technology at the Norwegian University of Science and Technology. The thesis is the final work to conclude the five years of an Integrated Master in Marine Technology, with a specialisation in Marine Structures. The report reflects the work done in two courses at NTNU. A project thesis concerning the same topic was written during the fall semester of 2019. This work was the basis for the master thesis, and a major part of the literature study is based on the project thesis. The work with the project thesis gave more time for structural analysis during the master thesis, which has been very beneficial.

I would like to thank my supervisor Jørgen Amdahl for his contribution to the thesis. I am also grateful for the help and support provided by co-supervisor Martin Slagstad throughout the project. Due to the outbreak of the Covid-19 virus, the weekly meetings with the supervisors were carried out by video conference. This worked brilliantly, and has not lead to any significant challenges to this project.

I would also like to thank Andreas Sanne, who wrote his master thesis on the same topic in 2019. He has been most helpful in sharing his knowledge and experience, which has helped me a great deal.

Trondheim, June 8, 2020



---

Peder Gjestvang

---

# Contents

<b>1</b>	<b>Introduction</b>	<b>1</b>
1.1	Natural Gas . . . . .	1
1.2	Transport of Natural Gas . . . . .	2
1.3	Spherical LNG-tanks . . . . .	3
1.3.1	Dimensioning of Spherical LNG-tanks . . . . .	6
1.4	Non-Spherical LNG-tanks . . . . .	6
1.5	Objective & Scope of Work . . . . .	7
1.6	Outline . . . . .	8
<b>2</b>	<b>Theoretical background</b>	<b>9</b>
2.1	Buckling of Cylindrical Shells . . . . .	9
2.2	Buckling of Spherical Structures . . . . .	10
2.3	Spheres and Cylinders Exposed to External Pressure . . . . .	11
2.4	Buckling of Non-Spherical Shells . . . . .	12
2.4.1	Application of Imperfections in Shell Structures . . . . .	13
<b>3</b>	<b>DNV GL Design Rules</b>	<b>17</b>
3.1	Hull Structural Analysis . . . . .	17
3.2	Global Analysis . . . . .	17
3.3	Strength Analysis of the Spherical Cargo Tanks . . . . .	18
3.4	Buckling Check: Sphere . . . . .	20
3.5	Strength Assessment of Other Types of Spherical Geometry . . . . .	21
<b>4</b>	<b>Finite Element Method</b>	<b>24</b>
4.1	Linear Buckling Analysis . . . . .	24
4.2	Non-Linear Buckling Analysis . . . . .	24
4.3	Material . . . . .	25
4.3.1	Material Model . . . . .	26
4.4	Choice of Shell Element . . . . .	27
<b>5</b>	<b>Method</b>	<b>28</b>
5.1	Software . . . . .	28
<b>6</b>	<b>Mesh Convergence Study</b>	<b>30</b>
<b>7</b>	<b>Buckling Analyses of Stretched Tank Exposed to External Pressure</b>	<b>33</b>
7.1	Calculating Elastic Buckling Pressure according to DNV GL . . . . .	33
7.2	Linear Analyses . . . . .	34
7.3	Non-Linear Analyses . . . . .	36
7.4	Comparison of Results . . . . .	38
7.5	Comparison of Simple Cylinder and Half-sphere . . . . .	39
7.5.1	Only Cylinder . . . . .	39
7.5.2	Only Hemisphere . . . . .	40
7.6	Results of Comparison . . . . .	41
<b>8</b>	<b>Study of the Impact of Cylinder Length in Stretched Tank</b>	<b>42</b>
8.1	Comparison with Vertically Stretched Tank . . . . .	44
<b>9</b>	<b>Imperfection Sensitivity Study</b>	<b>46</b>
9.1	DNV GL Class Guidelines . . . . .	46
9.2	Eigenmodes as Imperfections . . . . .	46

9.3	Chosen Imperfection Shapes . . . . .	50
<b>10</b>	<b>Non-Spherical LNG-tank With Different Thicknesses</b>	<b>51</b>
10.1	Comparison of Linear Analysis with External Pressure . . . . .	51
10.2	Comparison of Non-Linear Analysis with External Pressure, Without Imperfections . . . .	53
10.3	Comparison of Non-Linear Analysis with External Pressure, With 1. Mode as Imperfection	53
10.4	Comparison of Non-Linear Analysis with External Pressure, Computed Imperfection . . .	54
<b>11</b>	<b>Sloshing Analyses with Conservative Thicknesses</b>	<b>56</b>
11.1	Acceleration on Material . . . . .	56
11.2	Sloshing Load . . . . .	56
11.2.1	Difference Between Spherical and Non-Spherical Tank . . . . .	57
11.2.2	Application of Loads . . . . .	57
11.3	Spherical Tank, 23 % Filling, 20° . . . . .	59
11.3.1	External Pressure of 0.005 MPa . . . . .	60
11.4	Stretched Tank, Longitudinal Sloshing, 23 % Filling, 20° . . . . .	63
11.5	Stretched Tank, Transverse Sloshing, 23 % Filling, 20° . . . . .	67
11.6	Summary of Section 11 . . . . .	70
<b>12</b>	<b>Analysis of Spherical Tank Exposed to Only Vertical Acceleration</b>	<b>71</b>
<b>13</b>	<b>Sloshing Analyses With Realistic Thicknesses</b>	<b>72</b>
13.1	Spherical Tank, 20° Heel and 50 % Filling . . . . .	72
13.2	DNV GL Buckling Check of Spherical Tank . . . . .	75
13.3	Transverse Sloshing in Stretched Tank, 20° heel and 50 % Filling . . . . .	77
13.4	DNV GL Buckling Check of Stretched Tank . . . . .	79
13.4.1	Spherical Caps . . . . .	79
13.4.2	Cylindrical Part . . . . .	80
13.5	Comparison of Spherical and Stretched Tank . . . . .	81
13.6	Attempt with Linear Elastic Material Model . . . . .	83
<b>14</b>	<b>Discussion</b>	<b>84</b>
14.1	Limitations of the Project & Sources of Error . . . . .	84
14.1.1	Simplifications of the Tank . . . . .	84
14.1.2	Choice of Material . . . . .	84
14.1.3	Application of Imperfections . . . . .	85
14.1.4	Determination of Buckling Load . . . . .	85
14.2	Elastic Buckling Stress of Cylinders . . . . .	86
14.3	Advantages and Disadvantages of Stretched LNG-tanks . . . . .	87
<b>15</b>	<b>Conclusion</b>	<b>89</b>
15.1	Further Works . . . . .	89
	<b>Appendices</b>	<b>i</b>
<b>A</b>	<b>Additional Results Section 8</b>	<b>i</b>
<b>B</b>	<b>Python Scripts</b>	<b>v</b>
B.1	Mesh Convergence Script . . . . .	v
B.2	Script for Making Imperfection Files . . . . .	vii
B.3	Script 1 for Computed Imperfection . . . . .	viii
B.4	Script 2 for Computed Imperfection . . . . .	viii
B.5	Force/Displacement Plot . . . . .	x

---

B.6	Script for Stress Development Plots . . . . .	xii
B.7	Buckling Check Sphere . . . . .	xv
B.8	Buckling Check Cylinder . . . . .	xvi

## List of Figures

1	Emissions per Produced Energy for Different Energy Sources [30] . . . . .	1
2	World Total Energy Consumption by Source 2015 [30] . . . . .	2
3	Moss Rosenberg LNG-tanker, provided by Moss Maritime . . . . .	3
4	Moss Rosenberg LNG-Tank, provided by Moss Maritime . . . . .	4
5	Nomenclature of LNG-tank [7] . . . . .	5
6	Zones in LNG-tank by Moss Maritime, provided by Moss Maritime . . . . .	5
7	Structural drawing of spherical LNG-tank [25] . . . . .	6
8	KHI's new non-spherical Moss tank [29] . . . . .	7
9	Longitudinally Stretched LNG-tank . . . . .	7
10	Equilibrium Paths for Perfect and Imperfect Shells [1] . . . . .	9
11	Influence of Axisymmetric Imperfections on the Buckling Load of a Cylinder. [1] . . . . .	10
12	Cylinder with Internal Pressure . . . . .	11
13	Sphere with Internal Pressure . . . . .	11
14	Illustration of Cylindrical Tank with Spherical Caps . . . . .	12
15	Illustration of the Cassini ovoidal geometry [4] . . . . .	12
16	The Buckling Strength for Ovoidal Shells with Different $k_c$ -values [4] . . . . .	13
17	Imperfection-sensitivity of Cylindrical and Spherical Sells Exposed to Uniaxial Compression and External Pressure [15] . . . . .	14
18	Illustration of Egg-parameters [32] . . . . .	15
19	Contour Plot of Buckled Egg [32] . . . . .	15
20	Knock-Down Factors for Different Egg-shapes (SI) with Different Imperfection Sizes [32] . . . . .	16
21	Proper Mesh for the Hull Structural Analysis [7] . . . . .	17
22	Global FE Model With Pressure From the Wave Load Analysis [7] . . . . .	18
23	DNV GL Load Conditions [7] . . . . .	19
24	Illustration of a Stretched Cargo Tank with a Cylindrical Belt Above Equator [7] . . . . .	21
25	Illustration of the Arc-Length Method [24] . . . . .	25
26	Hardening Rules [24] . . . . .	26
27	Stress-Strain Curve Aluminium Al 5083-0 . . . . .	27
28	Tank Model Before Meshing in Patran . . . . .	30
29	Mesh Convergence Study, 1. Eigenmodes with Different Mesh Sizes . . . . .	31
30	Mesh Convergence Study, 1. Eigenmodes with Different Mesh Sizes (2) . . . . .	32
31	Mesh Convergence: Critical Load . . . . .	32
32	Mesh Convergence: Computational Time . . . . .	32
33	Linear Analysis: Sphere: 50 mm, Cylinder: 100 mm . . . . .	34
34	Linear Analysis: Sphere: 35 mm, Cylinder: 100 mm . . . . .	35
35	Linear Analysis: Sphere: 30 mm, Cylinder: 100 mm . . . . .	36
36	Linear Analysis: Sphere: 30 mm, Cylinder: 100 mm . . . . .	36
37	Non-Linear Analysis: Cylinder: 100 mm . . . . .	37
38	Non-Linear Analysis: Cylinder: 100 mm (2) . . . . .	38
39	Comparison of Results from FEA and Relevant Formulas . . . . .	39
40	Linear Analysis of Cylinder with Thickness 100 mm . . . . .	40
41	Linear Analysis of Half Sphere with Thickness 50 mm . . . . .	41
42	Comparison of FEA-results and DNV GL Equations . . . . .	43
43	% Offset of FEA-Results from DNV GL equations . . . . .	44
44	Illustration of Stretched Tank from Class Guidelines [7] . . . . .	44

45	Boundary Conditions for Horizontal Tank . . . . .	45
46	Vertical Tank Model . . . . .	45
47	Vertical Tank, Mode 1 . . . . .	45
48	Linear Buckling Analysis, 1. Mode, Buckling Pressure = 0.185 MPa . . . . .	47
49	Non-Linear Buckling Analysis, No Imperfection, Buckling Pressure = 0.179 MPa . . . . .	48
50	Knock-Down factor With Increasing Imperfection Amplitude . . . . .	49
51	Experimental Test of Imperfections on Buckling of Cylinder [1] . . . . .	49
52	Imperfection Sensitivity Study with Computed Imperfections . . . . .	50
53	Meshed Model With Different Thicknesses . . . . .	51
54	Linear Analysis . . . . .	52
55	Non-Linear Analysis Without Imperfection . . . . .	53
56	Non-Linear Analysis With 1. Eigenmode as Imperfection . . . . .	54
57	Non-Linear Analysis With Computed Imperfection . . . . .	55
58	Illustration of Sloshing Load as Hydrostatic Pressure . . . . .	57
59	Plot Illustrating the Application of Loads . . . . .	58
60	Sloshing Load on Spherical Tank with 23 % Filling, and 20° angle . . . . .	59
61	Displacement Scaled With a Factor of 100 . . . . .	60
62	Sphere: 20 deg pitch, 23 % Filling; Buckling Deformation . . . . .	61
63	Sphere: 20 deg pitch, 23 % Filling; Meridional Stress . . . . .	61
64	Sphere: 20 deg pitch, 23 % Filling; Circumferential Stress . . . . .	62
65	Sphere: 20 deg pitch, 23 % Filling; von Mises Stress . . . . .	62
66	Force/Displacement Relation Sphere (23 % Filling) . . . . .	63
67	Longitudinal Sloshing Load on Stretched Tank with 23 % Filling, and 20° angle . . . . .	64
68	Longitudinal Sloshing, 20 deg pitch, 23 % Filling: Scaled Displacement of Tank (Factor=50) . . . . .	65
69	Longitudinal Sloshing, 20 deg pitch, 23 % Filling: Longitudinal Stress . . . . .	65
70	Longitudinal Sloshing, 20 deg pitch, 23 % Filling: Vertical Stress . . . . .	66
71	Longitudinal Sloshing, 20 deg pitch, 23 % Filling: Von Mises Stress . . . . .	66
72	Force/Displacement Relation, Longitudinal Sloshing (23 % Filling) . . . . .	67
73	Transverse Sloshing, 20 deg heel, 23 % Filling: Scaled Displacement of Tank (Factor=20) . . . . .	68
74	Transverse Sloshing, 20 deg heel, 23 % Filling: Longitudinal Stress . . . . .	68
75	Transverse Sloshing, 20 deg heel, 23 % Filling: Vertical Stress . . . . .	69
76	Transverse Sloshing, 20 deg heel, 23 % Filling: Von Mises Stress . . . . .	69
77	Force/Displacement Relation, Transverse Sloshing (23 % Filling) . . . . .	70
78	1. Eigenmode, Linear Analysis . . . . .	71
79	Displacement, Non Linear Analysis . . . . .	71
80	Illustration of Sloshing Load with 50 % Filling, and 20° angle . . . . .	72
81	Spherical Tank with Realistic Scantlings: Displacement/Force Relation . . . . .	73
82	Sphere with Realistic Scantlings: Buckling Deformation . . . . .	74
83	Sphere with Realistic Scantlings: Circumferential Stress . . . . .	74
84	Sphere with Realistic Scantlings: Meridional Stress . . . . .	75
85	Sphere with Realistic Scantlings: Von Mises Stress . . . . .	75
86	Spherical Tank: Principal Stress Components . . . . .	76
87	Stretched Tank with Realistic Scantlings: Displacement/Force Relation . . . . .	77
88	Stretched Tank with Realistic Scantlings: Buckling Deformation . . . . .	78
89	Stretched Tank with Realistic Scantlings: von Mises Stress . . . . .	78
90	Stretched Tank with Realistic Scantlings: Longitudinal Stress . . . . .	79
91	Stretched Tank with Realistic Scantlings: Vertical Stress . . . . .	79
92	Stretched Tank: Principal Stress Components in Spherical Part . . . . .	80
93	Stretched Tank: Principal Stress Components in Cylindrical Part . . . . .	81
94	Development of Compressive Stresses in Spherical and Stretched Tank Based on Extrapolation . . . . .	82
95	Force/Displacement Relation with Linear Elastic Material . . . . .	83

96	Example of Force/Displacement Relation . . . . .	85
97	Percentage Offset of FEA-Results from DNV GL equations . . . . .	86
98	Experimental Results and Fitted Regression Line . . . . .	87
99	4 meter Cylindrical Part, Mode 1 . . . . .	i
100	8 meter Cylindrical Part, Mode 1 . . . . .	i
101	12 meter Cylindrical Part, Mode 1 . . . . .	ii
102	16 meter Cylindrical Part, Mode 1 . . . . .	ii
103	20 meter Cylindrical Part, Mode 1 . . . . .	iii
104	32 meter Cylindrical Part, Mode 1 . . . . .	iii
105	48 meter Cylindrical Part, Mode 1 . . . . .	iv
106	64 meter Cylindrical Part, Mode 1 . . . . .	iv

## List of Tables

1	Properties of Al 5083-0 . . . . .	25
2	Parameters for Ramberg Osgood Equation (Al-5083-0) . . . . .	27
3	Mesh Convergence Analysis Parameters . . . . .	31
4	Parameters for Thickness Relationship Study . . . . .	33
5	Buckling Coefficients for Hydrostatic Pressure - DNV GL . . . . .	33
6	Critical Buckling Pressures for Important Combinations of Coefficients . . . . .	34
7	Buckling Pressure for 50 mm Sphere, Linear Analysis . . . . .	34
8	Buckling Pressure for 35 mm Sphere, Linear Analysis . . . . .	35
9	Buckling Pressure for 30 mm Sphere, Linear Analysis . . . . .	36
10	Linear Elastic Buckling Pressures for Stretched Tank . . . . .	37
11	Result from Cylinder Analysis . . . . .	40
12	Result from Half Sphere Analysis . . . . .	40
13	Parameters for Study Effect of Cylinder Length . . . . .	42
14	Results of Cylinder Length Parameter Test . . . . .	42
15	Comparison of Strength of Horizontal and Vertical Tank . . . . .	45
16	Parameters for Study Effect of Cylinder Length . . . . .	47
17	Results of Imperfection Test using 1 Eigenmode as Imperfection . . . . .	48
18	Thicknesses for Sectioned Non-Spherical Tank . . . . .	51
19	General Parameters for Homogeneous and Sectioned Model . . . . .	52
20	Thicknesses for Homogeneous Model . . . . .	52
21	Linear Buckling Pressures . . . . .	53
22	Non-Linear Buckling Pressures Without Imperfections . . . . .	53
23	Non Linear Buckling Pressures With 1. Mode as Imperfection . . . . .	54
24	Non-Linear Buckling Pressures With Computed Imperfections . . . . .	54
25	Sloshing Analysis on Sphere with Different External Pressures and Imperfections . . . . .	60
26	Thicknesses for Sectioned Non-Spherical Tank . . . . .	64
27	Comparison of Critical Buckling Loads . . . . .	70
28	Imperfection Effect on Longitudinal Sloshing (20 deg heel and 29 % Filling) . . . . .	71
29	Realistic Thicknesses For Spherical Tank . . . . .	73
30	Load Table for Analysis of Tanks with Realistic Thicknesses . . . . .	73
31	Imperfection Effect on Spherical Tank (20 deg heel and 50 % Filling) . . . . .	74
32	Buckling Check (DNV GL) with Extracted Stresses . . . . .	76
33	Realistic Thicknesses for Sectioned Non-Spherical Tank . . . . .	77
34	Imperfection Effect on Transverse Sloshing (20 deg heel and 50 % Filling) . . . . .	78
35	Buckling Check (DNV GL) For Spherical Caps . . . . .	80
36	Buckling Check (DNV GL) for Cylindrical Part . . . . .	81
37	Comparison of Spherical and Stretched Tank . . . . .	81



38 Comparison of Spherical and Stretched Tank (Linear Elastic Material Model) . . . . . 83

## Nomenclature

$\bar{\xi}$	Normalised Imperfection Amplitude
$\eta$	Usage Factor
$\eta_{all}$	Maximum Allowable Usage Factor
$\gamma_m$	Material Factor
$\kappa$	Slenderness Factor
$\lambda_E$	Slenderness Parameter
$\Lambda_{CR}$	Critical Buckling Condition Including Effects from Geometrical Imperfections and Material Plasticity
$\Lambda_E$	Elastic Buckling, Elastic Knock Down due to Geometrical Imperfections Included
$\nu$	Poisson's Ratio
$\psi$	Plate Buckling Coefficient
$\rho$	Knock-down Factor
$\sigma$	Normal Stress
$\sigma_{10}$	Circumferential Design Stress
$\sigma_{20}$	Meridional Design Stress
$\sigma_\theta$	Circumferential Stress
$\sigma_{e0}$	Equivalent Design Stress
$\sigma_E$	Elastic Buckling Stress
$\sigma_z$	Axial Stress
$\tau$	Shear Stress
$\xi$	Curvature Parameter
$a_R$	Relative Sloshing Acceleration
$p$	Pressure
$p_c$	Critical Buckling Pressure
$R, r$	Radius
$R_{eH}$	Yield Stress
$\delta$	Imperfection Amplitude
$\gamma_{sum}$	Safety Factor
$\sigma_{vm}$	Von Mises Stress
$g$	Buckling Check Criterion
$h$	Buckling Check Criterion
$l$	Length
$t$	Thickness

# 1 Introduction

This chapter will describe the background of the issue addressed in this thesis. The background includes an introduction to the market and transportation of natural gas. Furthermore, the scope of work and the main objective will be presented, along with an outline of the structure of the thesis.

## 1.1 Natural Gas

Natural gas is a fossil energy source that is formed deep beneath the earth's surface. The largest component of natural gas is methane but it also contains smaller amounts of natural gas liquids and non-hydrocarbon gases, such as carbon dioxide and steam. As for oil, gas has been made during millions of years starting as biological material such as plants and animals. This biological material has been buried, and with pressure and heat it can develop into coal, oil or natural gas [30].

Natural gas can be used for most fossil fuel purposes such as transportation fuel, heating, supporting the industry with energy, and most of all electricity production are the main applications for natural gas. The main disadvantages are the explosion hazard and storage difficulties.

Natural gas is often characterised as the most beneficial fossil fuel, as it has lower emissions than oil and coal [30]. With renewable energy making up only 9 % of the global energy mixture and nuclear power generation being phased out in large parts of the world, it may be necessary to use the fossil energy sources with less emissions, and reduce the use of coal and oil.

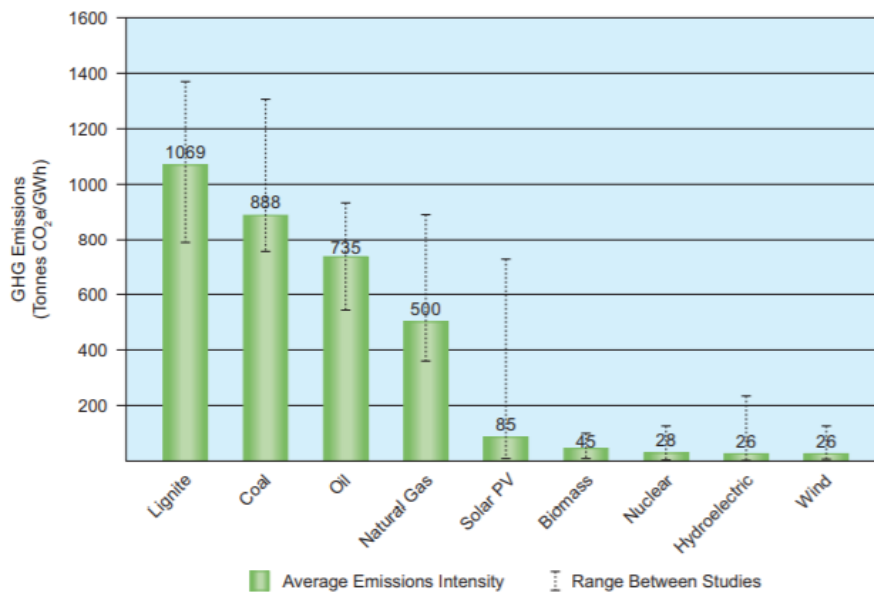


Figure 1: Emissions per Produced Energy for Different Energy Sources [30]

Figure 2 reflects the world's energy consumption and its reliance on fossil fuels. Coal, oil and gas make up 87 percent of the world energy consumption, where gas has the smallest percentage of the three. There are several estimates on the different emissions per energy ratios, but the reduction in emissions using natural gas would be approximately 25-30 % compared to oil, and 30-40 % compared to coal [30]. The reduction of emissions by using gas instead is significant, and gives reason to believe that the gas demand will be stable for the foreseeable future.

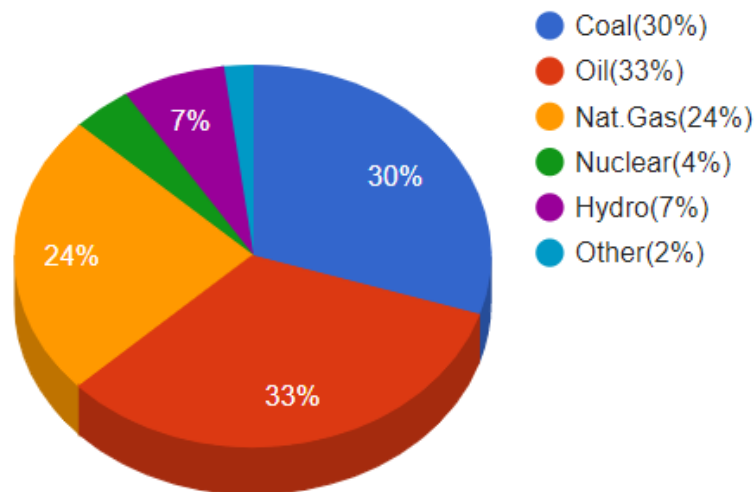


Figure 2: World Total Energy Consumption by Source 2015 [30]

## 1.2 Transport of Natural Gas

After the gas has been processed, the gas has to be transported from the processing facility to the customer. This is mainly done by pipelines or by ships. Pipelines are only used where large amounts of gas have to be transported and when the seabed makes it beneficial. One example reflecting the use of pipelines is the transportation of gas by pipelines between several countries in northern Europe.

Gas carriers can be divided into three categories, made for different purposes. The categories are as follows:

- Fully pressurised gas carriers
- Semi-pressurised gas carriers
- Fully refrigerated gas carriers

The fully pressurised gas carriers do not use a lot of power to cool the gas to liquid form. This makes the capacity smaller, but liquefying gas is an energy demanding process, which one avoids for a fully pressurised gas carrier. These ships are suitable for shorter transportation between terminals. Fully refrigerated gas carriers carry liquefied natural gas (LNG) at temperatures around  $-163^{\circ}$  and at atmospheric pressure. This is the normal type for longer transportation and the one studied in this thesis. Semi-pressurized gas carriers also carry liquefied gas, but at higher temperatures allowing higher pressures than the atmospheric pressure in the fully refrigerated tanks.

Within the fully refrigerated gas carriers there are also different tank types. These are listed below as described by DNV GL [7].

- Integral tanks form a part of the hull and are influenced by the same loads as the adjacent hull structure. As a consequence, they also contribute to the global ship strength. However, the fact that the tanks are exposed to the global loads is a major disadvantage and leads to stricter demands concerning tank strength.
- Membrane tanks are non-self-supporting structures consisting of a thin membrane layer supported through insulation by the adjacent hull structure. Thermal strains or other forms of expansions and contractions are compensated for without inducing stresses in the membrane.

- Semi-membrane tanks means that parts of the tanks are supported through insulation by the adjacent hull structure. The rounded parts of this layer connecting the above-mentioned supported parts are designed to also accommodate the expansions and contractions of the membrane.
- Independent tanks are defined as tanks that does not form a part of the hull and the influence on the tanks due to deformation of the hull is minimised. The tanks will not contribute much to the hull girder strength, especially not against the vertical bending moment which often yield the most critical stresses in a ship. Normally, an independent tank only has longitudinally rigid fixture to the hull in one transverse plane. Independent tanks are quite common, and there are several configurations within this category. The tanks in question in this project are independent tanks.

Independent tanks type A are prismatic and consist of plane surfaces. The tanks sharp edges or corners makes it more exposed to leakage which leads to a demand of a secondary containment system for such tanks. This buffer between the inner and outer tank must be filled with inert gas.

Independent tank type B is most often a spherical shape but can also consist of flat surfaces like type A tanks. However, they are not in need of the secondary containment system in the same way as type A tanks. For such tanks the secondary containment barrier is only necessary for the part of the sphere below deck.

Independent Type C tanks are designed for high pressures and can be both spherical or cylindrical. The secondary barrier is not necessary for pressurised tanks.

### 1.3 Spherical LNG-tanks

The spherical tanks in the Moss Rosenberg design are of type B, and is the basis of this project. An example of such a tanker can be seen in Figure 3.



Figure 3: Moss Rosenberg LNG-tanker, provided by Moss Maritime

Furthermore, an example of a spherical tank can be seen in Figure 4. The spherical tank is supported along the equator. A cylindrical skirt is mounted on the ship bottom, supporting the tank at the equator. A sufficiently strong steel foundation is needed close to the bilge of the vessel to support the forces from the cylindrical skirt carrying the tank. The tower in the middle has the function of loading and unloading of LNG. A drip tray is placed below the tank to collect any leakage of LNG from the tank. Insulation is used between the tank and the dome, in order to keep the LNG at a low temperature. In addition to acting as a

second barrier, the dome contributes to the global strength of the vessel.

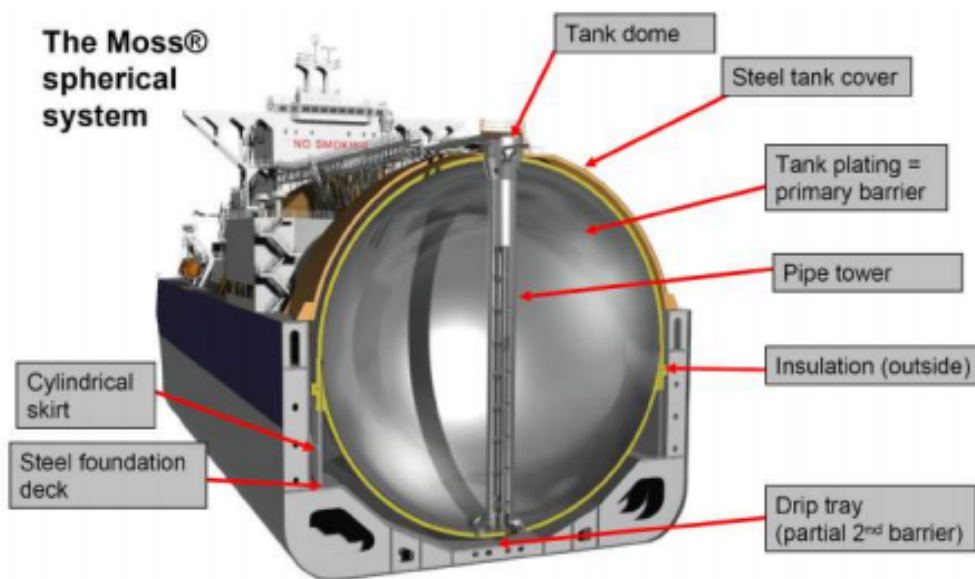


Figure 4: Moss Rosenberg LNG-Tank, provided by Moss Maritime

An important part of the tank design is the different thicknesses of the sections. A tank will have several sections with different thickness depending on the required strength for each individual section. Especially the equator is significantly thicker than the other zones. The division into zones is particularly interesting as this makes the basis for the strength of the tank and are the main parameters for optimising the spherical LNG-tanks.

In addition to the LNG-tank representations above, a Figure from DNV GL with relevant nomenclature for LNG-tanks is included in Figure 5 and an illustration of how the tanks are divided in sections can be seen in Figure 6.

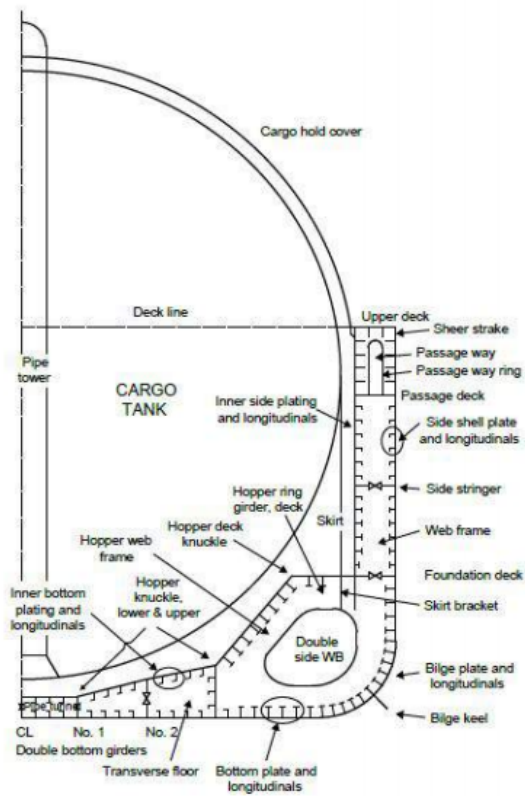


Figure 5: Nomenclature of LNG-tank [7]

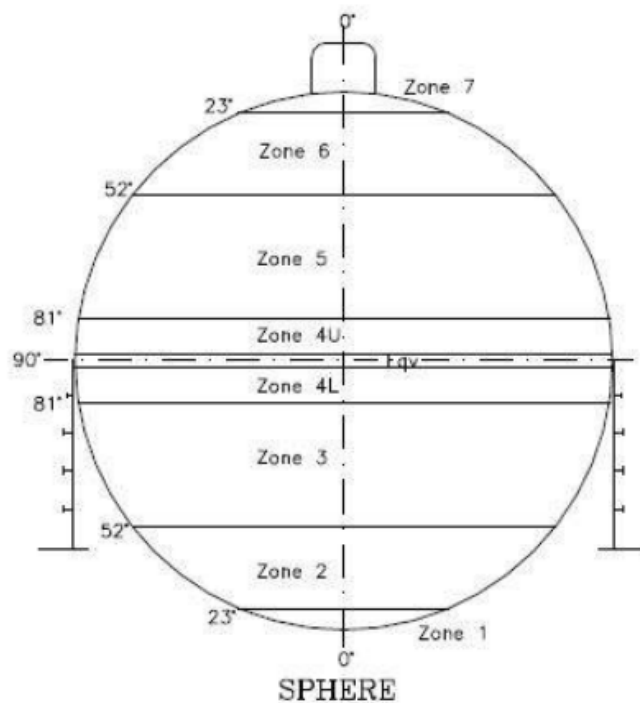


Figure 6: Zones in LNG-tank by Moss Maritime, provided by Moss Maritime

### 1.3.1 Dimensioning of Spherical LNG-tanks

Depending on the type of tank, there are different practices for what tensions that can be allowed [25]. For integrated tanks the tensions are specified based on practice for general ship structures, whilst for membrane tanks these allowed tensions must be decided for each individual tank. According to J Odland, the stresses in the tanks can be categorised as following: [25]

- Primary stresses: A stress induced by applied loads to balance the external loads and moments. Hence, primary stresses are not self-limiting.
- Primary membrane-stress: A primary membrane stress has the property that no stress rearrangement happens after yielding.
- Primary local membrane stress: A disturbance in the dominant stress distribution due to discontinuities.
- Secondary stress: A stress due to a constraint in the structure. Contrary to primary stresses, the secondary stresses are self-limiting.

A spherical-LNG tank, continuously supported along the equator can be seen in Figure 7. Usually, these tanks are analysed numerically using FEM-sofwares. However, it is possible to obtain decent estimates of the stress distribution based on membrane theory for spherical shells [25].

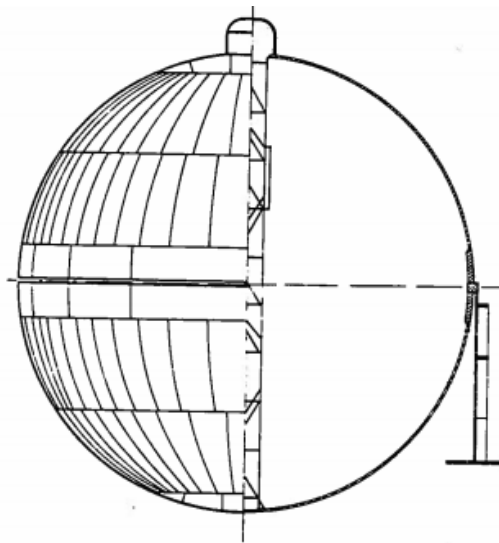


Figure 7: Structural drawing of spherical LNG-tank [25]

### 1.4 Non-Spherical LNG-tanks

In order to increase the cargo volume it is of interest to alter the shape of the spherical Moss Tank. For this purpose, Kawasaki Heavy Industry has developed an apple shaped tank. KHI state that the new tank has the same reliability as the spherical tank, and the capacity is increased by 15 % [29]. DNV GL has carried out comprehensive analyses, which yielded satisfactory results. The tank can be seen in Figure 8.



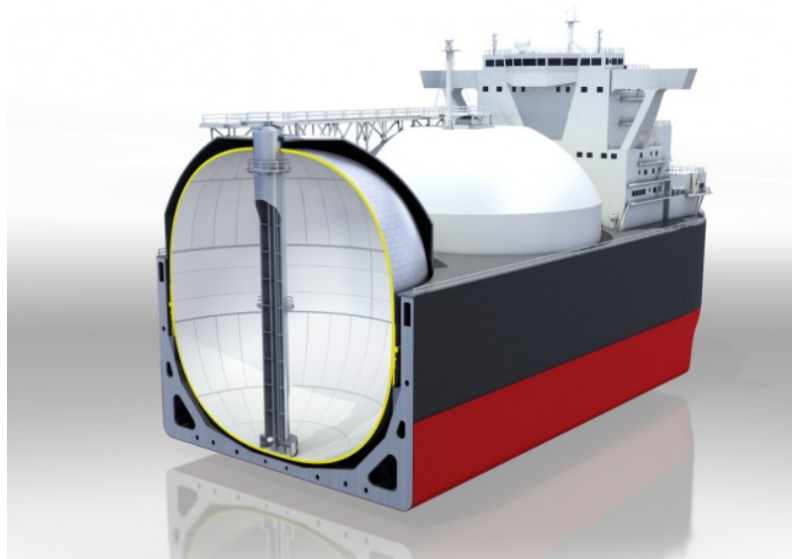


Figure 8: KHI's new non-spherical Moss tank [29]

This is one possible solution to increase the capacity of LNG-carriers. Another interesting possibility is to extrude the tank in the longitudinal direction, by making a tank with a cylindrical part with half-spheres at each end. The possibility to stretch the tank longitudinally will be the focus in this thesis. An illustration of such a tank can be seen in Figure 9. Similar to elongation of the tanks longitudinally, the tanks can be extended vertically with a similar cylindrical part. This modification will increase the center of gravity of the vessel, and lead to instability. Thus, the length of the cylinder will be limited to a few meters.

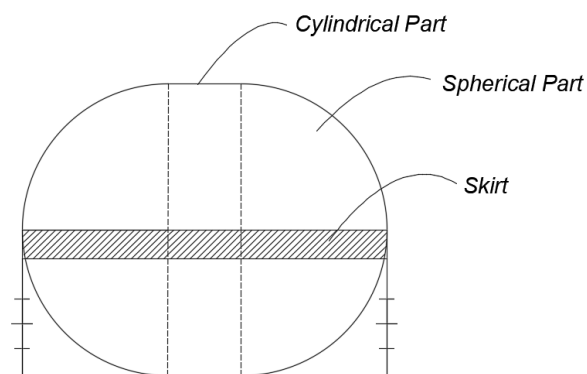


Figure 9: Longitudinally Stretched LNG-tank

## 1.5 Objective & Scope of Work

The objective for this work has been to analyse the buckling strength of longitudinally stretched LNG-tanks and compare with the strength of the traditional spherical tanks. Additionally, the current rules and guidelines provided by DNV GL on the topic are compared to the results of the FEM-analyses. The main target is to increase the knowledge on the topic of non-spherical tanks, which can lead to further development of the design of LNG-Carriers. Increased capacity of LNG-carriers can lead to reduction of both costs and emissions, without aggravating safety, for both personnel and environmental hazards.

The scope of the project includes:

1. A summary of relevant formulas for stresses in spherical/non-spherical and cylindrical shells as given in literature and relevant design rules and guidelines issued by ship classification societies has been written
2. The effect of different imperfection amplitudes and shapes. The starting point is tolerances limits and measurements available in the literature. Methods to introduce imperfections have been addressed.
3. Relevant load cases for the tanks have been studied. How the loads should be applied to the model, and how to compare the results has also been determined.
4. Mesh size sensitivity has been studied by conducting linear eigenvalue analysis. A suitable elasto-plastic material model has been identified.
5. Non-linear analysis has been conducted in LS-DYNA. Varying parametric studies has been performed. In some cases, scripts have been developed to automatise the studies.
6. The results from the finite element analyses is compared with theoretical and rule formulations. Certain changes to the rules have been proposed. An evaluation of the possible advantages and disadvantages of a stretched tank will be done based on the obtained results.

No important deviations to the original scope of work provided by the task assignment has occurred. The scope of work presented in this thesis corresponds well with the original scope of work presented in the task assignment.

## 1.6 Outline

The outline of the thesis is presented below:

- **Chapter 2:** Presents relevant theoretical background, mostly concerning the buckling of shell structures.
- **Chapter 3:** Brief review of the most important part of the Class Guidelines from DNV GL, as well as detailed explanations of the strength assessment of spherical and cylindrical shells.
- **Chapter 4:** Brief introduction to Finite Element Method and the most important choices made in LS-DYNA.
- **Chapter 5:** Explains in detail how the analyses were executed, and how the different software were used.
- **Chapter 6-13:** These eight chapters deals with the different analyses done in the project. More specific description of how the analyses were done (method) is also included. The results are briefly discussed throughout these chapter as they in most cases make the basis of the next analyses.
- **Chapter 14:** A more general discussion, discussing both possible sources of errors and the most important results obtained in this project.
- **Chapter 15:** Conclusion and further works

The references are presented in the Bibliography at the end of the document, as well as the Appendices.

## 2 Theoretical background

This chapter presents relevant theoretical background concerning buckling of shell structures, especially focusing on spherical and cylindrical thin-walled structures. The application and effects of imperfections on the buckling strength of shell structures are also addressed.

### 2.1 Buckling of Cylindrical Shells

Cylindrical shells are important elements in offshore structures and are often exposed to external pressure. Due to the vast use of cylindrical shells, a major part of the literature on buckling of shells is focused on cylindrical shells specifically. This project concerns the difference between spherical tanks and non-spherical tanks that will include a cylindrical part.

A major aspect concerning the buckling of shells in general, is the importance of imperfections. These thin shell structures are more vulnerable to small imperfections as a small imperfection makes up a larger part of the shell cross-section. Additionally, buckling is a highly non-linear phenomenon, which means that a small imperfection can yield large reductions of capacity. Figure 10 illustrates the large difference between perfect shells and imperfect shells. This underlines the need of including imperfections and analysing the impact, when studying the strength of shell structures.

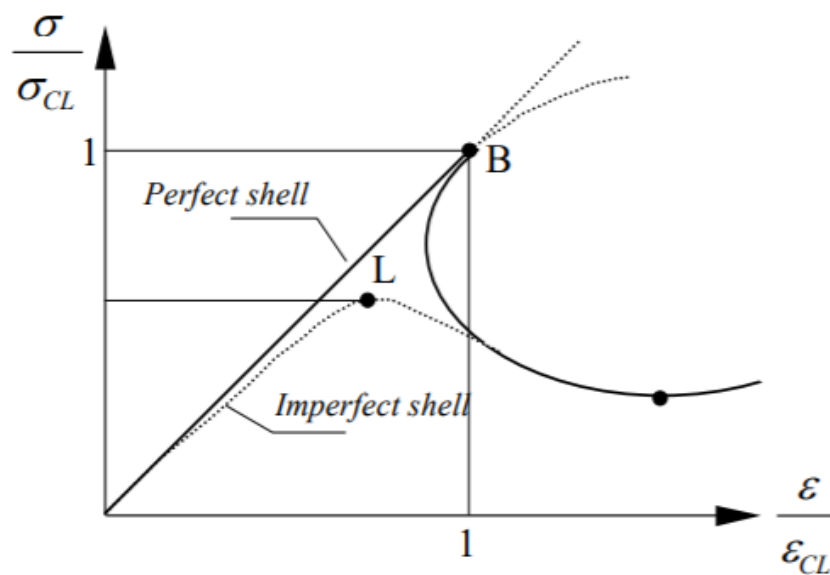


Figure 10: Equilibrium Paths for Perfect and Imperfect Shells [1]

Figure 11 shows a lower boundary for the effect of imperfections on a cylinder exposed to axial loading. An imperfection of only 10 % reduced the capacity to 60 % of a perfect shell, and an imperfection of around 2 % could even reduce the capacity with around 20 %. Due to this effect, for the design of cylindrical shells, a so-called "knock-down" factor is used. This is an empirical reduction factor that modifies the theoretical load.

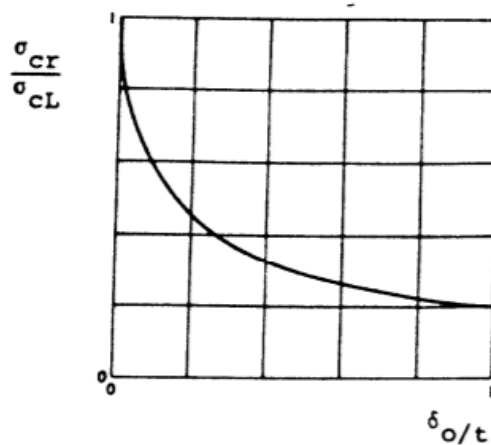


Figure 11: Influence of Axisymmetric Imperfections on the Buckling Load of a Cylinder. [1]

The elastic buckling strength of an unstiffened circular cylinder is defined as seen below, according to DNV GL [6].  $\psi$  represents a plate buckling coefficient,  $\xi$  represents a curvature parameter, and  $\rho$  is a knock-down factor [1].

$$\sigma_E = C \frac{\pi^2 E}{12(1-\nu^2)} \left(\frac{t}{l}\right)^2 \quad (1)$$

$$C = \psi \sqrt{1 + \left(\frac{\rho \xi}{\psi}\right)^2} \quad (2)$$

## 2.2 Buckling of Spherical Structures

The majority of research on elastic buckling pressure for thin spherical shells is based on the equation obtained by Robert Zoelly in 1915 [33]. The elastic buckling pressure is based on the classical theory of small deflections and the solution of linear differential equations. The theoretical critical buckling pressure for a thin spherical shell was found to be:

$$p_c = \frac{2E}{\sqrt{3(1-\nu^2)}} \left(\frac{t}{R}\right)^2 \quad (3)$$

For a typical value of  $\nu=0.3$ , the equations simplify to:

$$p_c = 1.21E \left(\frac{t}{R}\right)^2 \quad (4)$$

This is a strictly theoretical value, and experimental data have shown that the buckling pressure could be as low as 25 % of the pressure given by the Zoelly equation. This result was obtained by von Karman and Tsien [18]. Although deviations were expected, a factor of four was unexpected, and the reasons for the major deviations were researched. Von Karman and Tsien simplified the theory and developed a formula for the lower elastic limit of collapse pressure for a spherical shell with  $\nu=0.3$ : The Zoelly-equation (equation 4) represents the upper limit.

$$p_c = 0.37E \left(\frac{t}{R}\right)^2 \quad (5)$$

The reasons for such a difference between upper and lower limit is mainly due to the difference between flat and curved plates, and especially imperfections. As mentioned, these limits are based on elastic theory

and does not take plasticity into account.

### 2.3 Spheres and Cylinders Exposed to External Pressure

As described in Chapter 1, the purpose of this work is to investigate the opportunities of altering the shape of the current Moss tanks to a more cylindrical shape to increase the capacity of the LNG-tankers. Hence, the difference between a spherical and a cylindrical tank exposed to pressure is important for such a configuration.

For a circular cylinder, the circumferential stresses can be found by fulfilling horizontal equilibrium in Figure 12. Independent of where one cuts this circular shape, the stress will be the same. By solving the equilibrium equation, and making a minor simplification using the mean radius, it can be shown that the circumferential stress in the cylinder is:

$$\sigma_{\theta} = \frac{pr}{t} \quad (6)$$

For the spherical tank, the same argument can be used concerning where the cut is made. Hence, the membrane stresses in the shell have to be equal in each point. Figure 13 shows a half-sphere in horizontal equilibrium. Horizontal equilibrium yields the following solution.

$$p\pi r_i^2 = (\pi r_y^2 - \pi r_i^2)\sigma_z \quad (7)$$

$$\sigma_z = \frac{pr}{2t} \quad (8)$$

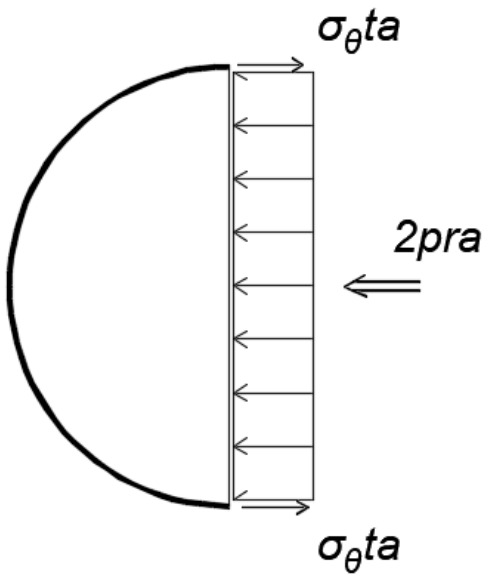


Figure 12: Cylinder with Internal Pressure

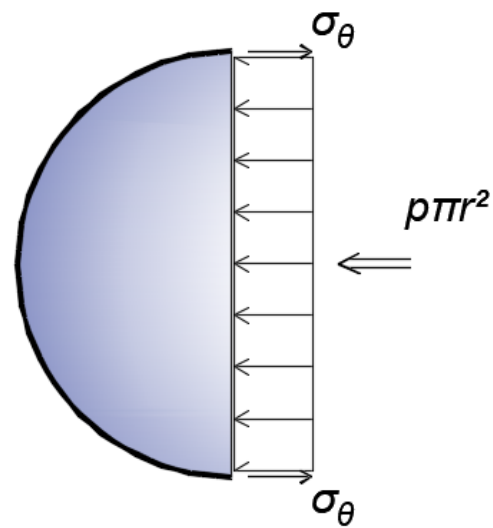


Figure 13: Sphere with Internal Pressure

The calculations above show that there is a major difference between the stresses in a cylinder and a sphere, exposed to internal or external pressure. In the illustrations, the pressure is internal. However, this does not make any difference concerning the calculations. This observation is fundamental for the tanks to be designed as spheres, and also highlights some of the difficulties when it comes to increasing the tank capacity. Figure 14 illustrates the difficulties of combining a circular cylinder with hemispheres at both ends. Due to the stresses being higher in the cylindrical part than in the hemispheres, the strain and the deformations increase. The joint between the cylinder part and the hemispheres leads to strong local curvature. This leads

to high bending- and shear stresses in the transition. Especially the bending stresses in this area can be critical to the structure due to the thin walls with low bending stiffness. Normally, these stresses will act in a limited area. However, they can be quite large and often lead to the need of local stiffening. The challenge concerning the joint will increase for more sharp transitions. A flat circular end-plate will therefore be the least suitable solution, and one would benefit stress-wise from making the transition between the cylinder and the spherical end-caps, as smooth as possible.

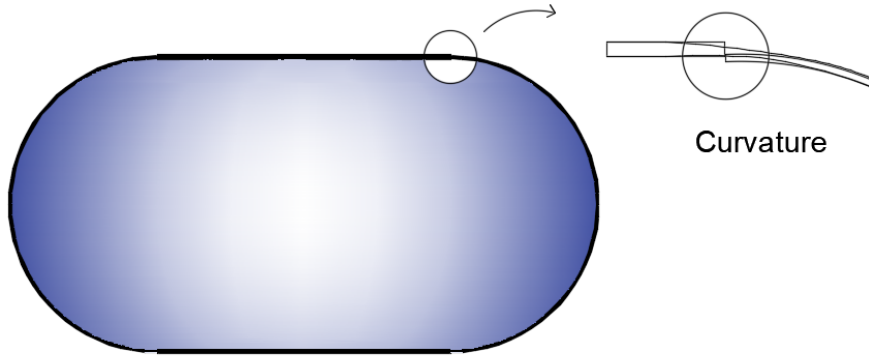


Figure 14: Illustration of Cylindrical Tank with Spherical Caps

## 2.4 Buckling of Non-Spherical Shells

The main goal of this project is to investigate the consequences of stretching a tank in the longitudinal direction. Relevant literature on the topic has been studied, in order to be able to perform the analyses correctly, and to verify the reliability of the results.

Jasion and Magnucki researched the buckling of ovoidal shells with a Cassini ovoidal geometry, and how the curvature and area of the middle cross-section affect the strength of the shell structure exposed to external pressure [4]. The geometry of such a shell is illustrated in Figure 15. In Figure 15 the curvature of the middle of the shell is zero. The main purpose of this article is to study the effect of the size of this curvature. This includes increasing the value of  $r_0$  which leads to a more spherical shape, and to decrease the radius leading to a shell structure with the geometry similar to that of a peanut. The assumption here is that the buckling strength will be larger for a spherical shape and smaller as the radius decreases. The objective is to study how the buckling strength develops depending on the radius  $r_0$ .

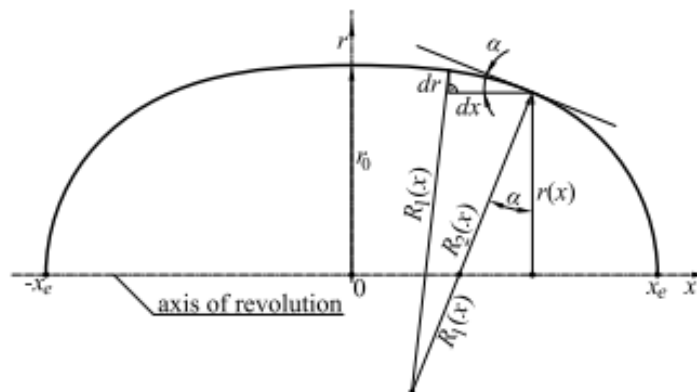


Figure 15: Illustration of the Cassini ovoidal geometry [4]

The plot in Figure 16 illustrates the buckling strength normalised by the strength of the plano-convex (no

curvature) shell.  $k_c$  is a dimensional parameter describing the shell geometry.

$$k_c = \frac{c}{s} \quad (9)$$

$c$  and  $a$  are parameters of Equation 10 describing the plane curve of the Cassini ovoidal shell.

$$y(x) = \left[ \sqrt{4c^2x^2 + a^2} - (c^2 + x^2) \right]^{1/2} \quad (10)$$

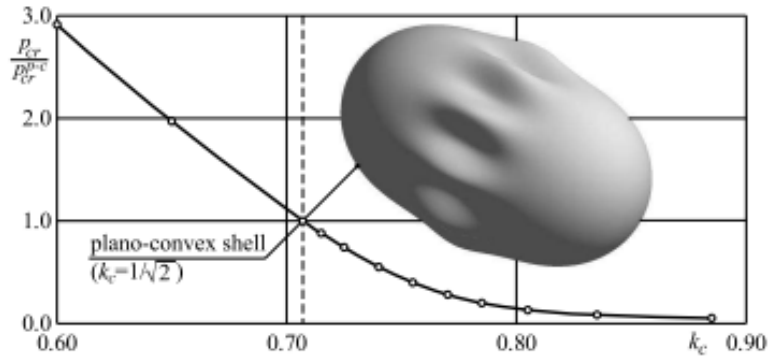


Figure 16: The Buckling Strength for Ovoidal Shells with Different  $k_c$ -values [4]

Figure 16 shows that the strength decreases drastically when the shape of the shell deviates from a spherical shape. The major reduction in buckling strength, due to a minor increase in  $k_c$ , confirms the challenges concerning altering the spherical shape of the Moss tanks.

#### 2.4.1 Application of Imperfections in Shell Structures

The application of imperfections is of great importance in this study, and subsequently, relevant literature has been studied to examine how imperfections should be applied and what consequences the imperfections may lead to.

JW Hutchinson studied the knockdown factors for both cylindrical and spherical shells [15]. This study is particularly interesting as it compares analytical, experimental, and numerical results. The article also describes how the imperfection is applied. The imperfection is applied as a buckling mode, where the deviation from a full spherical geometry is a small fraction of the modal shape.

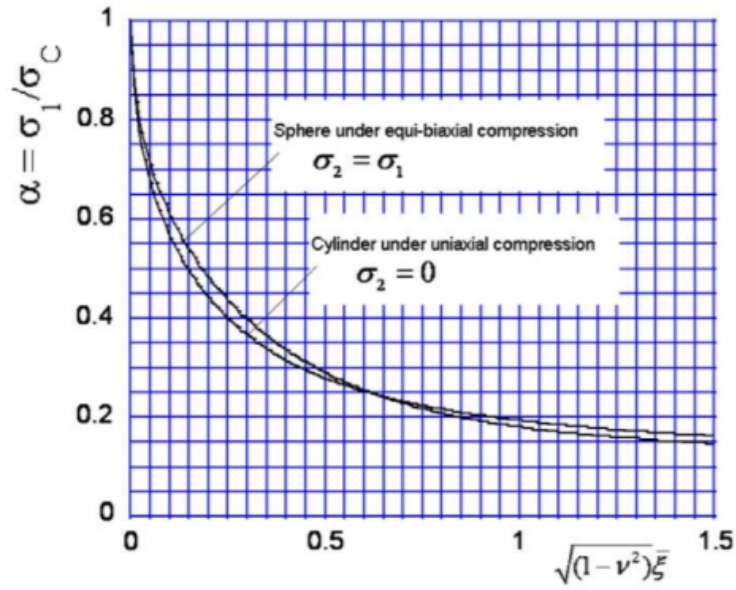


Figure 17: Imperfection-sensitivity of Cylindrical and Spherical Shells Exposed to Uniaxial Compression and External Pressure [15]

Figure 17 illustrates how the knock-down factor develops as the imperfection amplitude increases. The parameter  $\bar{\xi}$  is the normalised imperfection amplitude. The buckling mode applied in this paper is of the form:

$$\bar{W} = \bar{\xi} t \cos\left(q \frac{x_1}{R}\right) \quad (11)$$

The normalised imperfection amplitude is scaled according to the thickness. Hence, a  $\bar{\xi}$  of 1 implies an imperfection amplitude equal to the thickness of the shell.

Zhang et al. performed a numerical study concerning the buckling of egg-shaped structures exposed to external pressure [32]. Egg-shapes of increasing length to width ratio was analysed, and the strength and imperfection sensitivity was studied. The parameter describing the relation between the length and the width of an egg is the shape index (SI).

$$SI = \frac{B}{L} \quad (12)$$

It can be seen that for  $SI=1$ , the shell will be spherical, while a low SI-value will mean a longer and more slender egg.



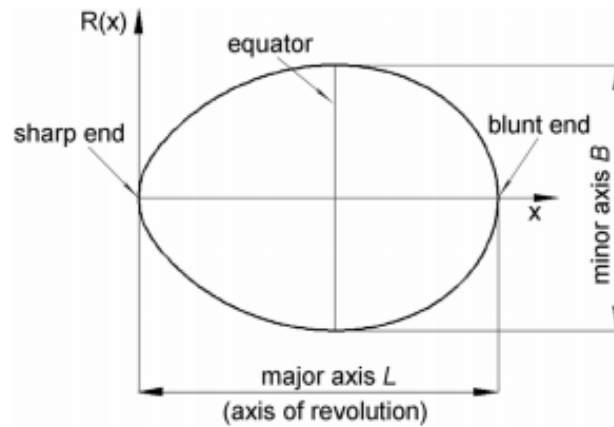


Figure 18: Illustration of Egg-parameters [32]

Both a linear and a non-linear analysis with imperfections were performed. The non-linear buckling analysis will be the focus for this purpose. According to Zhang et al. geometrical imperfections and non-linear material properties, both having a significant effect on the buckling loads was implemented in such a manner that an additional knock-down factor was unnecessary [32]. Eggs with imperfections of 20, 40, and 60 % of the egg thickness were analysed. The differences between the SI values in the mentioned range was deemed to be of minor significance. The results for a mean value of  $SI=0.69$  was therefore the focus of the results. Figure 19 shows the contour plot of the buckling shape of such an egg.

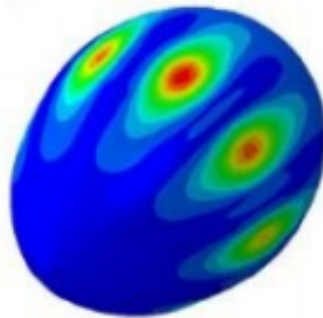


Figure 19: Contour Plot of Buckled Egg [32]

Figure 20 shows how the knock-down factor depends on imperfection amplitude and the shape index. Higher amplitude leads to a lower knock-down factor, meaning a larger reduction in capacity. However, the most interesting observation may be that  $SI=1$ , which implies a spherical shell is significantly more sensitive to imperfections than the elongated shapes, more similar to a cylinder.

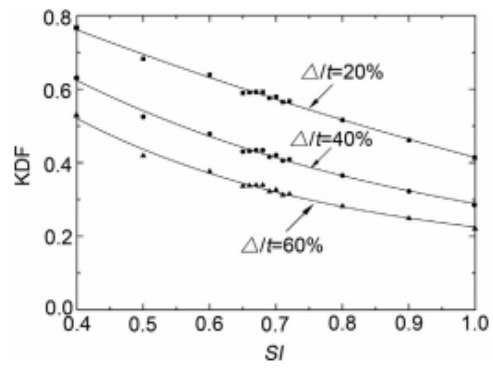


Figure 20: Knock-Down Factors for Different Egg-shapes (SI) with Different Imperfection Sizes [32]

### 3 DNV GL Design Rules

The relevant rules for the design of spherical LNG-tanks of type B are given in Class Guideline DNVGL-CG-0134: Liquefied gas carriers with spherical cargo tank of type B [7]. The documentation from DNV GL has been used throughout the project for defining parameters, loads, boundary conditions etc. Evaluation of the results has also been based on the Class Guidelines.

The Class guideline describes both a hull structural analysis, a general global analysis, a strength analysis of cargo hold covers and supporting structures, and a strength analysis of the spherical cargo tank, in addition to strength analyses of other elements. The analysis of the spherical cargo tank is key for this work. However, the other topics will also be briefly discussed, focusing on how the different analyses are connected.

#### 3.1 Hull Structural Analysis

The hull structural analysis is relevant for the analysis of the tanks. In addition to confirming the scantlings of the cargo area, the hull structural analysis provides interaction forces/deflections in the tank and the skirt structure. The input for the strength evaluation of the tank system is computed in this section. For this purpose, a larger model is made for the hulls middle part. As mentioned, the focus is the strength of the hull structure and the interaction with the tanks. Hence, a fine mesh is needed for the hull, while the mesh of the tanks only needs to be of such a quality that the interaction forces are calculated accurately. This can be seen in Figure 21.

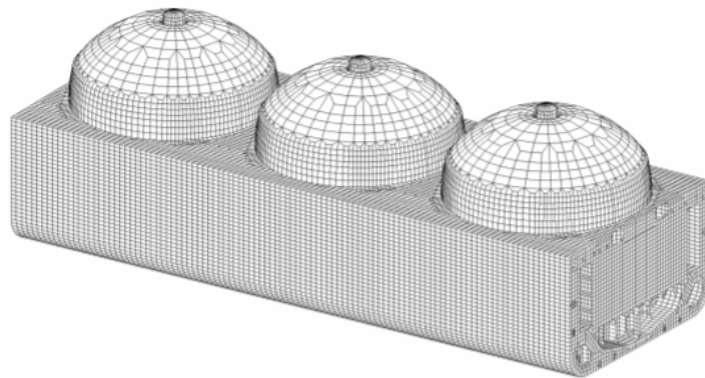


Figure 21: Proper Mesh for the Hull Structural Analysis [7]

#### 3.2 Global Analysis

The global analysis has a broader perspective, and also here the tanks are analysed, together with the rest of the structure. The global model should be exposed to a set of forces, including all dynamic loads, hull girder loads, local loads, and dimensioning accelerations for the tank design, based on hydrodynamic analysis. An example of such a model can be seen in Figure 22. In this case the mesh is coarse for the fore and aft part of the ship, but refined for the midship section. This may vary based on load case.

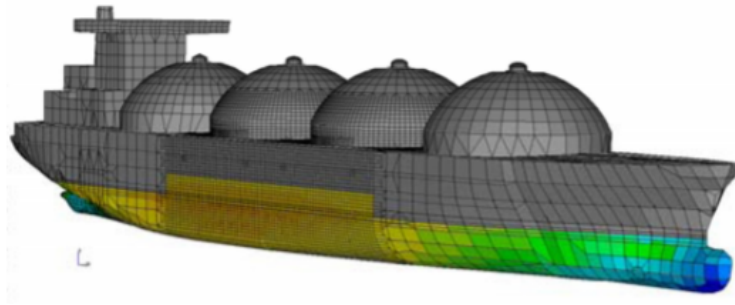


Figure 22: Global FE Model With Pressure From the Wave Load Analysis [7]

### 3.3 Strength Analysis of the Spherical Cargo Tanks

This section defines the acceptable procedures for strength analysis of the cargo tanks. DNV GL defines ten types of analyses necessary for Class approval [7].

- Wave load analysis of the ship
- Assessment of interaction forces
- Analysis of sloshing loads in cargo tanks
- Analysis of skirt and tank structure including stationary thermal loads
- Buckling analysis
- Fatigue analysis
- Crack propagation analysis
- Leak rate analysis
- Steady-state temperature and stress analysis to determine the temperature distribution in the tank system. The temperature gradient in the upper part of the skirt is of particular significance.
- Transient thermal stresses (cool down analysis). This is not a design analysis as such but has to be carried out on the final tank design in order to ensure that the tank (i.e. the equator area) is not overstressed due to too rapid cool down and filling up of the tank.

Before narrowing the scope to the buckling analysis, the general guidelines concerning FEM-analysis of the spherical tank will be addressed. The Guidelines recommend the sphere to be modelled using 8-node shell elements with a typical mesh size of  $d/30$ ,  $d$  being the tank diameter. Alternatively, one can use flat 4-node quadrilateral elements. However, this would lead to a demand of mesh size in the order of  $d/150$ , which would yield a system of equations about 4-5 times larger than for the 8-node shell elements. The skirt is recommended to be modelled using 4-node quadrilateral shell elements of size  $d/30$  or equal to the stiffener spacing. Areas where especially high stress concentrations may be expected, are recommended to be modelled by very fine meshed solid element models. These areas may include the tower connection area, the dome connection area, and the equator profile.

Concerning material properties of the tank, DNV GL recommends using standard material properties for rolled Al 5083-0, which is the typical aluminium alloy used for the cargo tank. The material properties are found in DNVGL-RU-SHIP Sec.10 Table 4 [12]. Special considerations can be made in some cases due to enhanced yield and tensile strength at temperatures below  $-105^{\circ}$  Celcius.

For a separate model of the spherical tank, as in this analysis, the following boundary conditions may apply [7].

- The lower edge of the skirt should be restricted from rigid body displacement and rotation.
- The interaction load cases (still water interaction forces and dynamic interaction forces) should be applied along the bottom of the skirt as vertical and circumferential interaction displacements calculated in the integrated cargo hold model.

The number of load cases to be applied, combining all the ten mentioned types of analyses are numerous. Only the load-cases significant in terms of buckling will be addressed. The load cases necessary for the buckling analysis are described in DNVGL-CG-0134 Chapter 5.6 Table 6 and presented below [7].

- Tank test condition
- Sea going with empty tank
- Sea going with part filling

For the load case; Tank test condition the loads are:

- Tank system self-weight(tank material, insulation and piping etc.)
- Partial filling of fresh water
- Static interaction force due to still water bending moment and external static pressure

For the load case; Sea going with empty tank:

- Tank system self-weight(tank material, insulation and piping etc.)
- Static interaction force due to still water bending moment and external static pressure
- External pressure 0.005 MPa
- Dynamic interaction force due to wave bending moment and external wave pressure

For the load case of; Sea going with partial filling:

- The same four loads as in the second load case
- Partial filling of cargo; static and dynamic part combined based on resulting skewed acceleration  $a_R$  from the acceleration ellipse

The three different load conditions relevant for the buckling analysis are illustrated in Figure 23. The third load case is mainly analysed in this thesis. However, both the static and dynamic interaction forces between the tank and the hull are not included in this project.

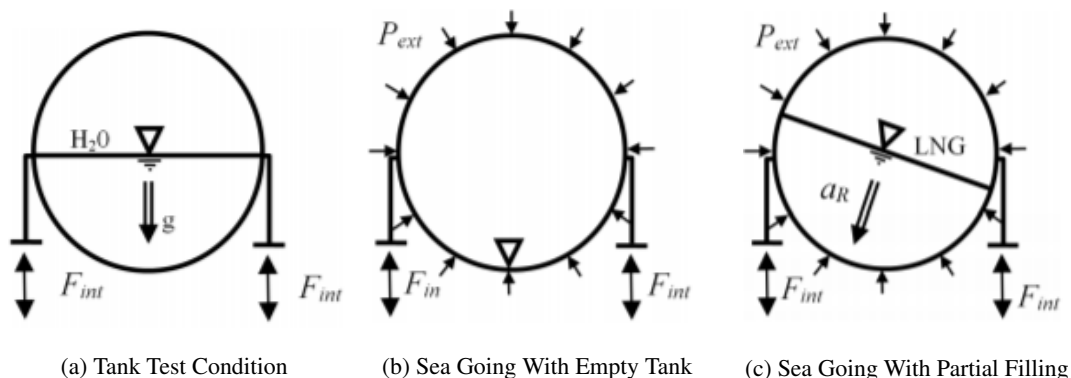


Figure 23: DNV GL Load Conditions [7]

### 3.4 Buckling Check: Sphere

DNV GL recommends to do non-linear analyses concerning buckling of spherical shapes. Two limit states in a partial safety format have to be checked.

- Elastic buckling: A spherical shell segment may collapse before the yield stress has been reached in any part of the shell.
- Elasto-plastic buckling: A spherical shell segment may collapse due to the initiation of material yielding in the most severely loaded part of the shell.

The combined elastic and elasto-plastic buckling strength criterion to be satisfied is:

$$g > 0 \text{ or } h > 1.0 \quad (13)$$

where  $g$  and  $h$  are defined as:

$$g = \Lambda_{CR} - \gamma_{sum} \quad \text{and} \quad h = \frac{\Lambda_{CR}}{\gamma_{sum}} \quad (14)$$

The critical buckling parameter  $\Lambda_{CR}$  is defined by use of the yield stress, the von Mises stress, and the reduced slenderness parameter.

$$\Lambda_{CR} = \frac{1}{\sqrt{1 + \lambda_E^4}} \frac{R_{eH}}{\sigma_{e0}} \quad (15)$$

The reduced slenderness is defined as:

$$\lambda_E = \sqrt{F_E \frac{R_{eH}}{\sigma_{e0}}} \quad (16)$$

The Von Mises stress in two dimensions is found based on the two design stresses:

$$\sigma_{e0} = \sqrt{\sigma_{10}^2 + \sigma_{20}^2 - \sigma_{10}\sigma_{20}} \quad (17)$$

$\gamma_{sum}$  is the safety factor and is found using the partial safety factors  $\gamma_m$  and  $\kappa$ .

$$\gamma_{sum} = \gamma_m^\kappa \quad (18)$$

where  $\gamma_m$  and  $\kappa$  represent the material factor and the slenderness factor, respectively. They should be determined as described by the equations below:

$$\gamma_m = 1.15 \quad (19)$$

$$\begin{aligned} \kappa &= 1.0 && \text{if } \lambda < 0.2 \\ \kappa &= 0.925 + 0.375\lambda && \text{if } 0.2 < \lambda < 1.0 \\ \kappa &= 1.3 && \text{if } \lambda > 1.0 \end{aligned} \quad (20)$$

$F_E$  consist of  $\rho$  and the classical elastic buckling parameter  $\Lambda_{CL}$

$$F_E = \frac{1}{\rho \Lambda_{CL}} \quad (21)$$

where  $\rho$  is found by iteration to fulfill the following equation:

$$0 = (1 - \rho)^{3/2} \left( \frac{3\sqrt{3}}{2} \right) \gamma_P \sqrt{-b} \left( \frac{\delta}{t} \right) \rho \quad (22)$$

It is seen that  $\Lambda_{CL}$  is the ratio between the design compressive stress, and the classical elastic buckling stress. The classical elastic buckling strength is seen as the Zoelly buckling pressure mentioned in Section 2.2, multiplied by  $R/2t$ .

$$\Lambda_{CL} = \frac{\sigma_{CL}}{\sigma_{10}} \quad (23)$$

$$\sigma_{CL} = \frac{E}{\sqrt{3(1-\nu^2)}} \frac{t}{R} \quad (24)$$

The challenge of the buckling analysis is to find the load combinations that are most severe for buckling. In this project, the design stresses  $\sigma_{10}$  and  $\sigma_{20}$  have been found using FEM-software.

The equations for the load factors and partial safety factors are given on page 147 and 148 in DNVGL-CG-0134. The principal stresses can also be found through FEM-analysis, and used directly in the procedure to find  $g$  and  $h$ .

The application and effect of imperfections are of great importance to the strength of spherical shell structures. Two different imperfection amplitudes are defined,  $\delta_1$  and  $\delta_2$ . For an aluminium sphere, the imperfections should not be less than:

$$\delta_1 = \frac{0.01g}{1+g/R} \quad \text{or} \quad \delta_2 = \frac{r}{750} \quad (25)$$

In addition to a regular non-linear calculation, DNV GL states that it might be necessary to carry out a linear eigenvalue calculation.

### 3.5 Strength Assessment of Other Types of Spherical Geometry

The DNV GL guidelines also describe the methods for strength assessment of tank systems deviating from an ideal spherical shape. These altered shapes generally result in increased thickness to compensate for increased stresses.

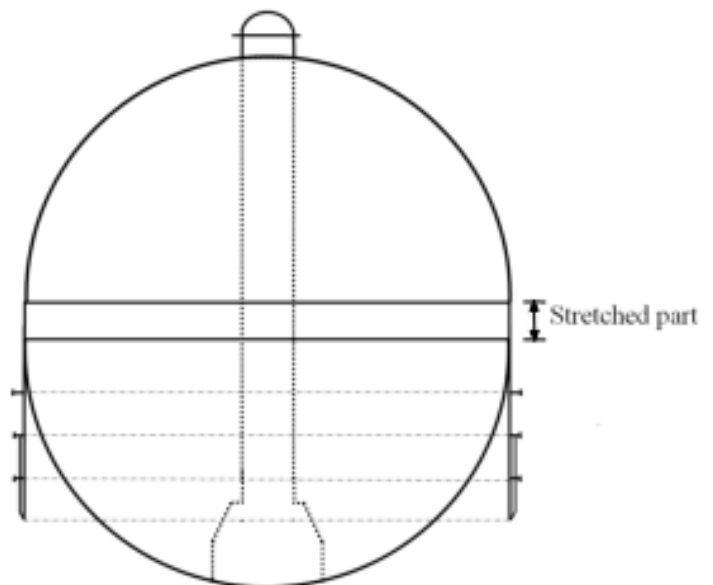


Figure 24: Illustration of a Stretched Cargo Tank with a Cylindrical Belt Above Equator [7]

For the buckling stress analysis of a stretched tank, the rules for ideal spherical tanks can be used for the northern and southern hemispheres with some minor modifications concerning the application of loads. For the cylindrical part, a finite element analysis checking several filling conditions and skew angels has to be done. In addition, DNV GL has developed a simplified method. This method is similar to that of the spherical part of the tank. It is a very important calculation procedure in this thesis, and will be used for comparison with FEM-results.

The characteristic buckling resistance is defined as:

$$\sigma_{ecr} = \frac{R_{eH}}{\sqrt{1 + \lambda^4}} \quad (26)$$

where the reduced slenderness parameter is defined as:

$$\lambda^2 = \frac{R_{eH}}{\sigma_{vm}} \left( \frac{\sigma_{z0}}{\sigma_{Ez}} + \frac{\sigma_{\theta 0}}{\sigma_{E\theta}} + \frac{\tau}{\tau_E} \right) \quad (27)$$

The von Mises stress is calculated with the design stresses.

$$\sigma_{vm} = \sqrt{\sigma_z^2 + \sigma_\theta^2 - \sigma_z \sigma_\theta + 3\tau^2} \quad (28)$$

For an unstiffened circular cylindrical shell the elastic buckling resistance may be taken as:

$$\sigma_E = C \frac{\pi^2 E}{12(1 - \nu^2)} \left( \frac{t}{\ell} \right)^2 \quad (29)$$

where C is the "reduced buckling coefficient" defined as:

$$C = \psi \sqrt{1 + \left( \frac{\rho_\xi}{\psi} \right)^2} \quad (30)$$

where the parameters are found in Table 8 in DNVGL-CG-0134 [7]. It is emphasised that  $\sigma_{E\varphi}$ ,  $\sigma_{E\theta}$ , and  $\tau_E$  are all found by use of Equation 29, and that C depends on type of stress and the load.

Note that the buckling check from DNV GL concerning the cylindrical part is based on the classical elastic buckling pressure mentioned in Section 2.1, similarly to the buckling check of the sphere.

Furthermore, the usage factor based on the design stresses is defined as:

$$\eta = \frac{\sigma_{vm}}{\sigma_{ecr}} \quad (31)$$

and the maximum allowed usage depends on the safety factors and is defined as:

$$\eta_{all} = \frac{1}{\gamma_m \kappa} \quad (32)$$

The material factor  $\gamma_m$  and the slenderness factor  $\kappa$  are defined as:

$$\gamma_m = 1.15 \quad (33)$$

$$\begin{aligned} \kappa &= 1.0 && \text{if } \lambda < 0.2 \\ \kappa &= 0.925 + 0.375\lambda && \text{if } 0.2 < \lambda < 1.0 \\ \kappa &= 1.3 && \text{if } \lambda > 1.0 \end{aligned} \quad (34)$$



If the design stresses are in order, the usage factor will be smaller than the maximum usage factor and the buckling check is passed.

It can be seen that the two buckling checks presented by DNV GL concerning the buckling of a sphere and a cylinder, are very similar. Both methods are based on the classical elastic buckling pressure, and the design limit is modified to take into account both geometrical imperfections and material plasticity.

## 4 Finite Element Method

This chapter describes linear and non-linear buckling analysis. Additionally, it describes the material used in this thesis, focusing on the material model used in LS-DYNA. Choice of shell element is also briefly explained.

### 4.1 Linear Buckling Analysis

The linear buckling analysis computes the theoretical buckling loads and modes for a structure, by solving the eigenvalue problem. The software assumes a small perturbation in each element and the reduction in stiffness due to compression, is analysed by solving to find the point where the axial force is of such a magnitude that the stiffness is zero. Especially for thin structures such as LNG-tanks, the sensitivity to imperfections yield that the results of the linear analysis are of small value unless a proper knock-down factor is known. However, the linear analysis is a useful tool to obtain mode shapes used as imperfections in the non-linear analysis.

### 4.2 Non-Linear Buckling Analysis

The non-linear analysis takes non-linear geometric behavior into account and most often non-linear material behavior as well. This analysis will take several effects into account, including yielding of the material as a way to fail as well as buckling. As buckling is an instability phenomenon, one often needs something to trigger this instability. This might be a trigger load, or applied imperfections to the geometry. With regards to buckling analysis it is common to use the mode shapes obtained in a linear analysis as imperfections for the non-linear analysis.

For non-linear analyses, one of the more important choices is the solution technique. For this project LS-DYNA uses the arc-length method. This method is known to be very accurate and especially useful for problems where the response after the limit point (maximum strength) is of interest. In this case, this is of importance to identify the nature of the collapse. More explicitly, it is important to see if it is a ductile or brittle collapse. Another major reason for using the arc-length method instead of a simpler method is that for many structures, the first limit point on the force-displacement curve does not represent the ultimate strength of the whole structure.

Figure 25 illustrates the arc-length method. The increment is made from the first point along the tangent. Furthermore, it is corrected by iteration to find the second point, which is the basis for the next time step. There are several methods to find the arc length. In Figure 25 a normal plane is used as the basis for the iteration. This can vary from solver to solver, and the arc-length method is a collective name for a group of methods with minor differences.

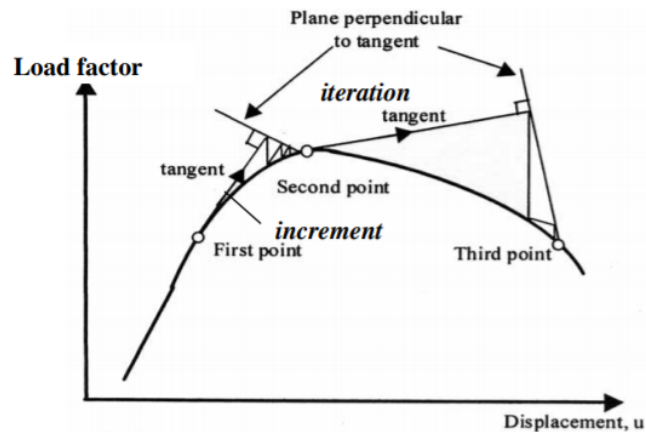


Figure 25: Illustration of the Arc-Length Method [24]

LS-DYNA uses the BFGS-algorithm for iterations at each timestep. The BFGS-solver is a quasi-Newton method. Briefly explained, the BFGS-method uses the stiffness matrix which is inverted and used for ten iterations, but with a small improvement for every iteration using a rank two update. This exercise is very inexpensive. This is done for a maximum of 10 iterations. If equilibrium has not been reached during the 10 iterations, a new stiffness matrix is computed and inverted. It can be seen that if the maximum number of iterations is reduced from 10 to 1, the method is the full Newton method. Inverting the stiffness matrix is demanding in terms of computational capacity, which is the reason for choosing not to compute and invert a new stiffness matrix at every iteration.

### 4.3 Material

According to the mentioned DNV GL Class Guidelines the aluminium alloy most commonly used in LNG-tanks is Al 5083-0. This alloy is used in a wide range of industries, and is especially used in shipbuilding due to its resistance against corrosion. The fact that the alloy can handle the cold temperature of the LNG, and the rapid cooldown makes it especially suitable for LNG-tanks. The properties of Al 5083-0 can be seen in the Table 1.

Table 1: Properties of Al 5083-0

Property	Value
Density	$265 \text{ g/cm}^3$
Melting Point	$570 \text{ }^\circ\text{C}$
Thermal Expansion	$25 \times 10^{-6} / \text{K}$
Modulus of Elasticity	71 GPa
Thermal Conductivity	121 W/m.K
Electrical Resistivity	$0.05810^{-6} \Omega.m$

Not only the choice of material has to be decided. The material model to be used in the analyses is something that can impact the analyses greatly. To find the most suitable way to model the material is an important matter. For non-linear analyses one needs to find a non-linear material model. The aluminium will be modelled as elasto-plastic, which means that it has one strain range where the stress-strain relationship is constant, before the stress-strain relationship becomes strain-dependant. Especially three important behaviours need to be defined when it comes to elasto-plastic material behavior.

The yield criterion defines at what stress level yield occurs, and is often defined as the tensile yield strength.

The hardening rules describe how the yield strength is affected by the historic loading leading to yield. Figure 26 illustrates two ways to model the hardening of an elasto-plastic material. For the case of isotropic hardening one can see that the elastic range increases when yield occurs, and the range becomes  $2\sigma_B$ . For the kinematic hardening the elastic stress range remains constant, but is displaced along the stress axis. That means that a given increase in tensile yield strength due to plastic deformation will lead to a decrease of the same magnitude for the yield strength in compression. This is not important in this case, but more important in i.e. a fatigue analysis.

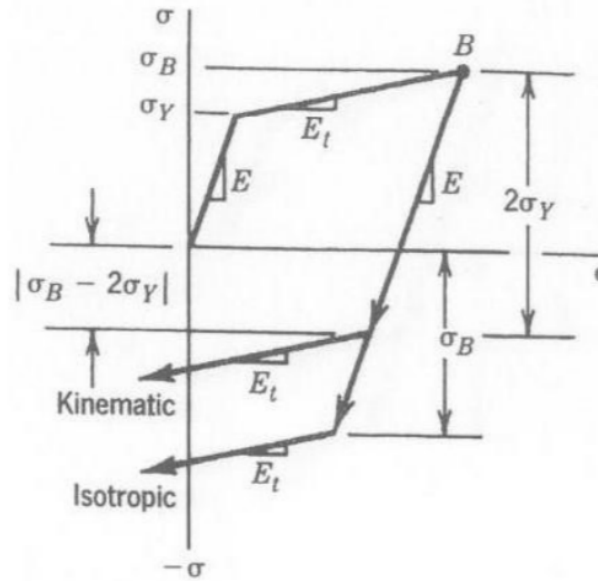


Figure 26: Hardening Rules [24]

A flow rule also has to be defined, which describes the stress-strain relation after yield. This is a very important part of the material model for the analyses in this thesis.

#### 4.3.1 Material Model

The material model used in this project is to a great extent based on the experimental work presented by Misovic et al. [23]. The article presents results of experiments on stress-strain behaviour of two aluminium alloys, including Al-5083. Based on experimental data, the Ramberg-Osgood relationship is suggested as a suitable material model for both alloys. The Ramberg-Osgood relation is seen below.

$$\varepsilon = \frac{\sigma_e}{E} + \left(\frac{\sigma_R}{K}\right)^{\frac{1}{n}} \quad (35)$$

Suggestions for suitable parameters in the Ramberg-Osgood equation is also suggested, based on experimental data. Material Model 18 in LS-DYNA is based on the Ramberg-Osgood relationship, and has the same material input variables as proposed by Misovic et al. [23]. These input variables can be seen in Table 2, and the stress-strain relationship defined by the Ramberg-Osgood relation and the parameters in Table 2 can be seen in Figure 27.

Table 2: Parameters for Ramberg Osgood Equation (Al-5083-0)

Property	Explanation	Value
$\sigma_e$	Stress at elastic limit	134 MPa
$\sigma_R$	Real stress	<i>Variable</i>
E	Modulus of Elasticity	71 GPa
K	Strength coefficient	426 MPa
n	Strain hardening component	0.2004

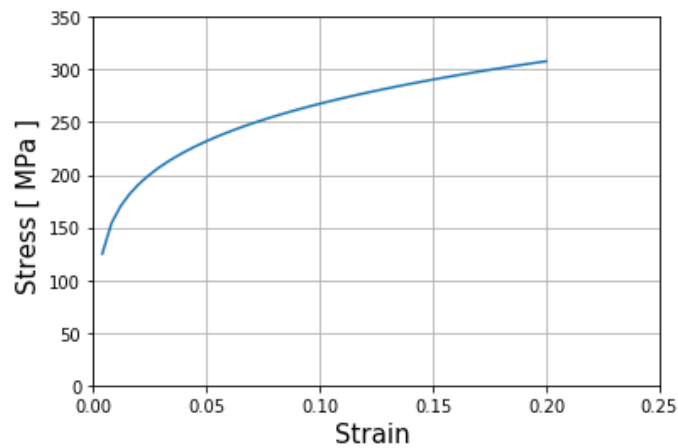


Figure 27: Stress-Strain Curve Aluminium Al 5083-0

#### 4.4 Choice of Shell Element

One of the major choices in any project concerning FEM is the selection of which elements to use. In this project, only one shell element has been used in the model, and the same shell element has been used for all analyses.

The Hughes-Liu Shell element in LS-DYNA has been used in this analysis. It is a four-node shell element with uniformly reduced integration. One additional version of the Hughes-Liu shell is Hughes-Liu with full integration. Full integration increases the need for computational capacity severely, which is the main reason it has not been seen as favorable. Some of the most important qualities of the Hughes-Liu shell element are listed below [21].

- It is less complicated than several other options, leading to high computational efficiency.
- It includes transverse shear strains.
- Rigid body rotation does not induce strain

Initial analysis has been done with the chosen shell element to verify the validity of the element. This was done in the project thesis written in the course TMR4500 at NTNU.

## 5 Method

This chapter will give a brief description of the work process of this project. Additionally, the use of different software is described.

The research done in this thesis is quantitative, as the main method is the Finite Element Method, where LS-DYNA is the solver. First, a literature review was done to build a relevant foundation of knowledge. Furthermore, analyses were carried out and the results were evaluated and compared with relevant theory. The results have been discussed continuously with supervisors through weekly meetings. The results obtained throughout the work have been decisive for the further analyses, which in most cases build on the prior analysis. This includes additional analyses computed for verification purposes, or making the analysis more advanced, either by applying additional loads or making the model more advanced.

### 5.1 Software

The modelling of the structures analysed throughout the project has been done in Patran. Patran is a Pre/Post-processing software, compatible with several solvers, including LS-DYNA. The work done in Patran includes modelling of the structure, including choice of shell element, computation of mesh, as well as applying thicknesses and material to all parts of the structure. The thicknesses and the material was easily changed also in LS-PREPOST, after exporting to a KEYWORD-file, compatible with LS-DYNA.

LS-PREPOST is a Pre/Post-processing software made for LS-DYNA. Application of boundary conditions and loads was done using LS-PREPOST. Furthermore, the material was changed for the non-linear analyses to the elasto-plastic model described in Section 4.3.1. The Keyword `*MAT POWER LAW PLASTICITY` was used to define the non-linear material, and the linear elastic material used for the linear analysis was defined using the Keyword `*MAT ELASTIC`.

The application of loads consisted of two parts. The part of the structure exposed to the load, as well as the direction was defined using either `*LOAD SHELL` or `*LOAD SEGMENT`. The size and how the load developed over time was defined using the keyword `*DEFINE CURVE`.

LS-PREPOST was also used to define the nature of the analyses. Both linear eigenvalue analyses and non-linear analyses, with and without imperfections have been done. To define the computation of the linear analyses, the essential keywords are:

- `*CONTROL IMPLICIT BUCKLE`
- `*CONTROL IMPLICIT EIGENVALUE`
- `*CONTROL IMPLICIT GENERAL`
- `*CONTROL IMPLICIT SOLUTION`
- `*CONTROL TERMINATION`

For the non-linear analysis the most important keywords to define the analysis are:

- `*CONTROL IMPLICIT AUTO`
- `*CONTROL IMPLICIT DYNAMICS`
- `*CONTROL IMPLICIT GENERAL`
- `*CONTROL IMPLICIT SOLUTION`

- \*CONTROL TERMINATION
- \*CONTROL TIMESTEP
- \*DATABASE BINARY D3PLOT

The keyword \*CONTROL TIMESTEP also needs a curve defined with use of the keyword \*DEFINE CURVE. This curve acts as the maximum timestep, and is also time-dependent. This definition is important for the quality of the results, and for the computational time needed to compute the non-linear analyses.

For the analyses including imperfections the keyword \*PERTURBATION NODE has been used. This keyword needs an input file with the nodal displacements representing the imperfections. Imperfections were computed in two different ways.

The main method used to apply imperfections was to use displacements from the linear or non-linear analysis in LS-DYNA. The nodal displacements were exported to a text file, and a Python-script was written and used to write a file compatible with the \*PERTURBATION NODE keyword. The Python script can be seen in Appendix B.2.

A computed imperfection consisting of a sinusoidal shape along the cylindrical part of the stretched tank was also applied in some of the analyses. The scripts used to compute this imperfection is in Appendices B.3 and B.4.

LS-PREPOST was used as post-processor. Additionally, results such as nodal displacements and element stresses were exported to files and post-processed using scripts in Python. Several scripts were made written to process the data from LS-PREPOST, in most cases to produce relevant plots. This was in most cases either to see how the displacement and stress distribution developed with increasing load. The scripts to plot the force/displacement-relation and the stress development can be seen in Appendix B.5 and B.6.

Scripts representing procedures defined by DNV GL was written, to identify maximum allowable stresses for spheres and cylinders. These procedures are described in Sections 3.4 and 3.5, and the scripts are in Appendices B.7 and B.8.

## 6 Mesh Convergence Study

In order to obtain reliable results it is important to verify that the mesh is suitable for the analysis. In addition to consulting literature and Class Guidelines to identify a proper mesh, a mesh convergence study has been carried out. Non-linear analysis can be very time consuming, and to limit required computational effort is also a purpose of such a study.

In the Class Guidelines from DNV GL concerning LNG-tankers, some guidelines are given regarding mesh size and element type. The guidelines advise the use of 8-node shell elements with a mesh size of  $r/30$ . The alternative is the use of 4-node quadrilateral elements. If this is the case, DNV GL advises the mesh size to be around  $r/150$ . In the modelling software Patran, it was not possible to use 8-node quadrilateral elements for spherical structures, and as a consequence 4-node quadrilateral elements were chosen. According to DNV GL the mesh size should then be in the order of 0.25 meters. The mesh-convergence study was carried out using a Python-script to automatise the analyses. This script is appended in Appendix B.1.

This study was done to see how the results and the computational time of the analysis depended on the size of the mesh. Additionally, visual inspection of each model has been done to compare the buckling shapes. A rule of thumb when it comes to buckling of shell structures is that each half-wave should contain eight elements for the mesh to be sufficiently fine.

The parameters of the analysis should represent typical thicknesses for the simple model of a non-spherical LNG-tank. Figure 28 shows the non-spherical tank before meshing, and the most important parameters of the model can be seen in Table 3.

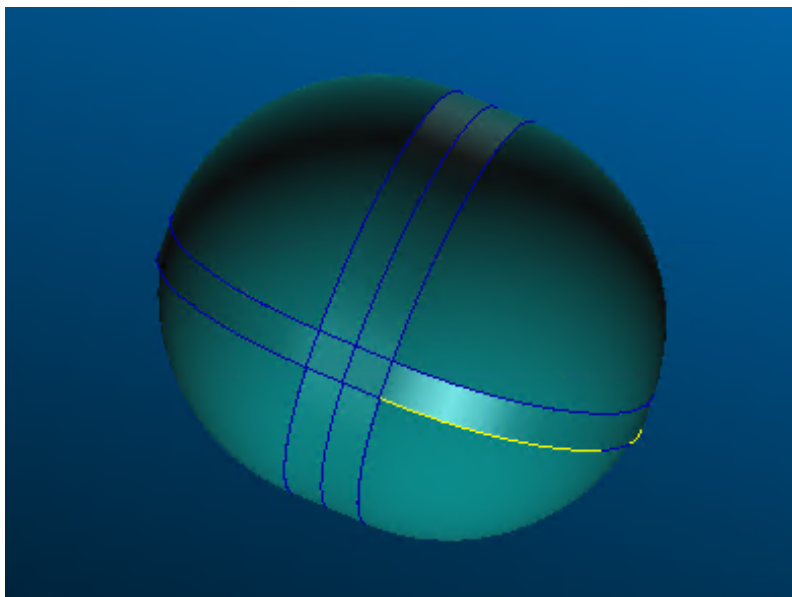


Figure 28: Tank Model Before Meshing in Patran



Table 3: Mesh Convergence Analysis Parameters

Radius of Half-spheres and Cylinder	21.5 m
Length of Cylindrical Section	8 m
Height of Skirt	4 m
Thickness Cylinder	100 mm
Thickness Skirt	70 mm
Thickness Sphere	50 mm
Material	Aluminium
Boundary Conditions	Skirt edge restricted in all 6 DOFS
Load	External Pressure

In this mesh convergence study a total of nine mesh-sizes have been tested. However, the process was not streamlined, as some of the mesh sizes chosen at first was not a good fit for the geometry of the tank. For some mesh-sizes Patran was unable to connect the spherical and the cylindrical sections. However, additional attempts with small changes to the mesh sizes lead to nine models with mesh sizes ranging from 0.25 to 2.0 meters. Some of the mesh sizes are shown in the figures below:

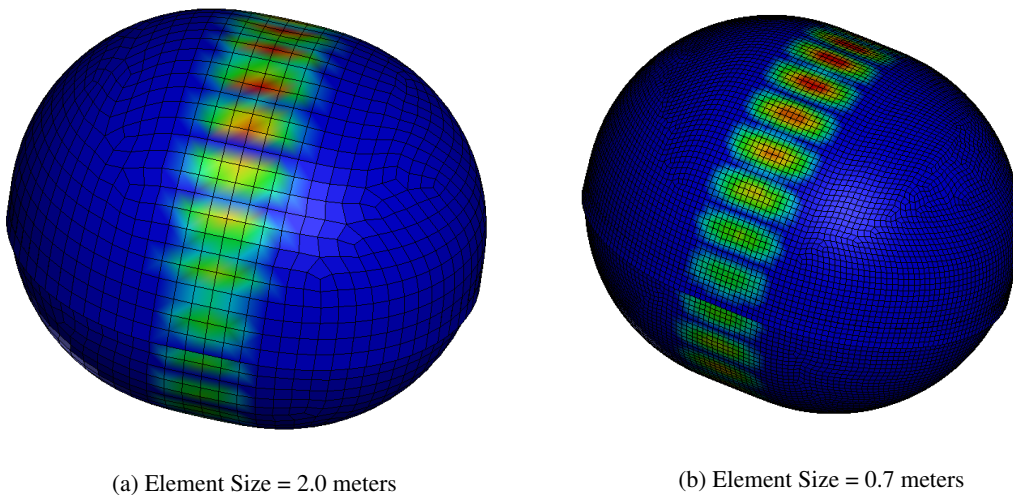


Figure 29: Mesh Convergence Study, 1. Eigenmodes with Different Mesh Sizes

Figure 29a shows a very coarse mesh of 2.0 meters. Even though the buckling shape looks similar to the more refined mesh models, it can be seen that the mesh is very coarse. In this case we can see that one half-wave contains only three elements, which is not sufficient. Additionally, the plot in Figure 31 shows that the accuracy of the buckling load is low. However, the interesting and positive results from the analyses with such a coarse mesh, is that the buckling shape of the cylindrical part is not very dependant on the mesh size. This is also confirmed by comparison of the remaining buckling modes.

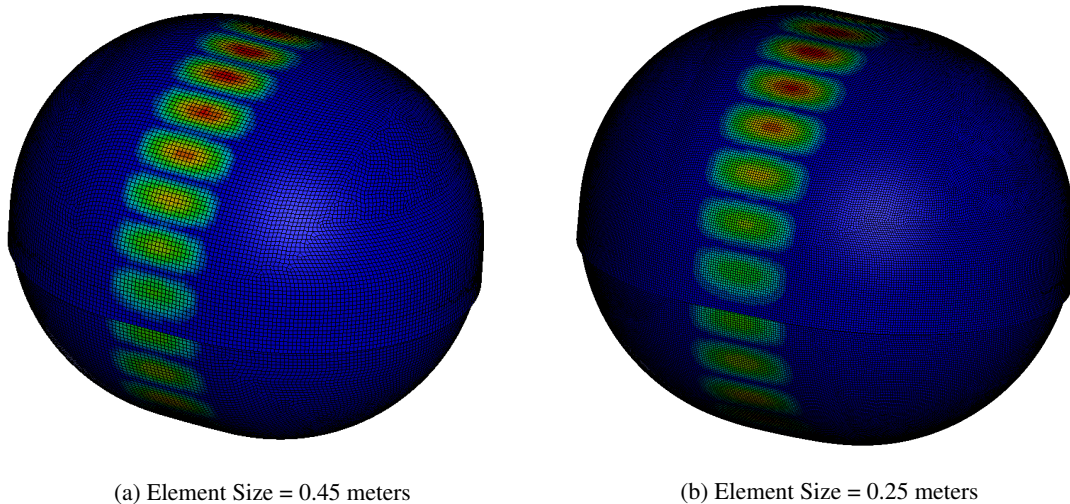


Figure 30: Mesh Convergence Study, 1. Eigenmodes with Different Mesh Sizes (2)

Figure 31 shows that the linear buckling pressure converges asymptotically towards a limit. It is as expected that the smaller the mesh, the lower the buckling pressure. This can be explained by at each node connecting two elements, the curvature of the spherical or cylindrical section will lead to an angle between two neighbouring elements. This angle induces bending moments on each element, increasing with the angle, which again increases for coarse meshes. These bending moments will have major significance for such a thin-walled structure with very limited resistance to bending. Hence, the way the critical buckling pressure converges is as expected.

As mentioned, DNV GL recommended a mesh size of approximately 0.25 meter for a spherical structure with the same radius as the half-spheres in this stretched tank. Based on Figure 31 one can see that the buckling pressure converges, and would probably continue to decrease for even smaller mesh sizes. However, the difference between the analyses with a 0.25 meter mesh and the 0.45 meter mesh is small. Figure 32 shows that the computational time becomes very large for the finest model. The main part of this project is to run several parametric studies to see how the strength of the stretched tank is affected by changing different parameters, i.e. thickness relationships between sections. The analyses will also be non-linear which is more time-consuming. Therefore, for the purpose of this work, a mesh size of 0.45 meter is chosen as a suitable value, where a balance between accuracy and computational effort is found.

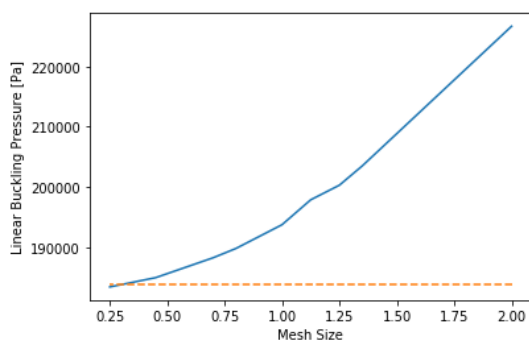


Figure 31: Mesh Convergence: Critical Load

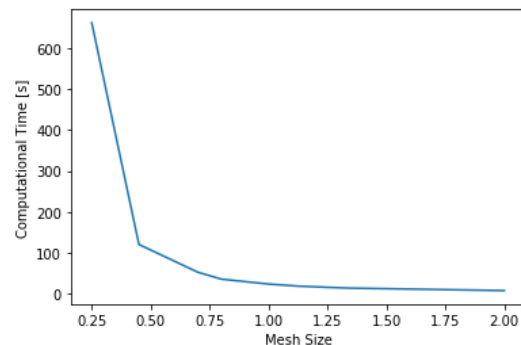


Figure 32: Mesh Convergence: Computational Time

## 7 Buckling Analyses of Stretched Tank Exposed to External Pressure

In the Class Guidelines by DNV GL it is assumed that one can see the cylindrical part by itself and the spherical part by itself. On page 68 in DNVGL-CG-0134, DNV GL writes "Common for tank systems deviating from the ideal spherical shape is that the tank shell needs to be thicker to compensate for the extra membrane and bending stresses in the tank shell. Cylindrical shells will in general need to be twice as thick as spherical shells." [7] To investigate the validity of this assumption is a key aspect of this project, comparing FEM-results with current Class regulations. Both linear eigenvalue analyses and non-linear analysis without imperfections are carried out. The most important parameters of the analyses can be seen in Table 4.

Table 4: Parameters for Thickness Relationship Study

Radius of Half-spheres and Cylinder	21.5 m
Length of Cylindrical Section	8 m
Height of Skirt	4 m
Thickness Cylinder	100 mm
Thickness Skirt	70 mm
Thickness Sphere	30-70 mm
Mesh Size	0.45
Material	Al 5083-0
Boundary Conditions	Skirt edge restricted in all 6 DOFS
Load	External Pressure

### 7.1 Calculating Elastic Buckling Pressure according to DNV GL

DNVGL-RP-C202 concerns the buckling of shells [6]. The critical stress is calculated as shown below by the use of certain factors from tables in the DNV GL document. The elastic buckling strength of unstiffened cylinders is the same as mentioned in Section 2.1, where  $\psi$  represents a plate buckling coefficient,  $\xi$  represents a curvature parameter, and  $\rho$  is a knock-down factor. These equations are also used in the procedure to calculate limits of design stresses, but in this part, only the elastic buckling stress and corresponding pressure are of importance.

$$\sigma_E = C \frac{\pi^2 E}{12(1-\nu^2)} \left(\frac{t}{l}\right)^2 \quad (36)$$

$$C = \psi \sqrt{1 + \left(\frac{\rho \xi}{\psi}\right)^2} \quad (37)$$

Table 5: Buckling Coefficients for Hydrostatic Pressure - DNV GL

$\psi$	2
$\xi$	$1.04 \sqrt{Z}$
$\rho$	0.6

where:

$$Z_l = \frac{l^2}{rt} \sqrt{1-\nu^2} \quad (38)$$

The buckling pressure is then found directly from the critical stress by the known equation:

$$P_{cr} = \sigma_E \frac{t}{R} \quad (39)$$

The value of 2 for  $\psi$  takes into account the axial stresses due to end caps on such a cylinder. The axial stresses in a submerged cylinder will be half the circumferential stress. For a cylinder with only lateral load, there will be no axial stress induced from the end caps. In that case,  $\psi$  should be 4. In the table below some critical buckling pressures for different combinations of the coefficients are listed, to be used for comparison with the results from the FEA.

Table 6: Critical Buckling Pressures for Important Combinations of Coefficients

$\psi$	$\xi$	$\rho$	$P_{cr}$
2	$1.04 \sqrt{Z}$	0.6	0.181
2	$1.04 \sqrt{Z}$	1.0	0.275
4	$1.04 \sqrt{Z}$	0.6	0.243
4	$1.04 \sqrt{Z}$	1.0	0.319

## 7.2 Linear Analyses

Firstly, linear analyses were carried out for the stretched tank. The thickness of the cylinder was set to 100 mm, and the thickness of the sphere was in the range of 30-70 mm, and analyses were done for every 5 mm interval. The most interesting observation was the thickness ratio which was the limit concerning which part of the structure buckles at the lowest external pressure.

Figure 33a and 33b show two out of the ten buckling modes produced with a 50 mm spherical section. All ten buckling modes look very similar, and no buckling on the spherical parts can be observed for any mode. This was also the case for all thicknesses between 50 and 70 mm, as expected.

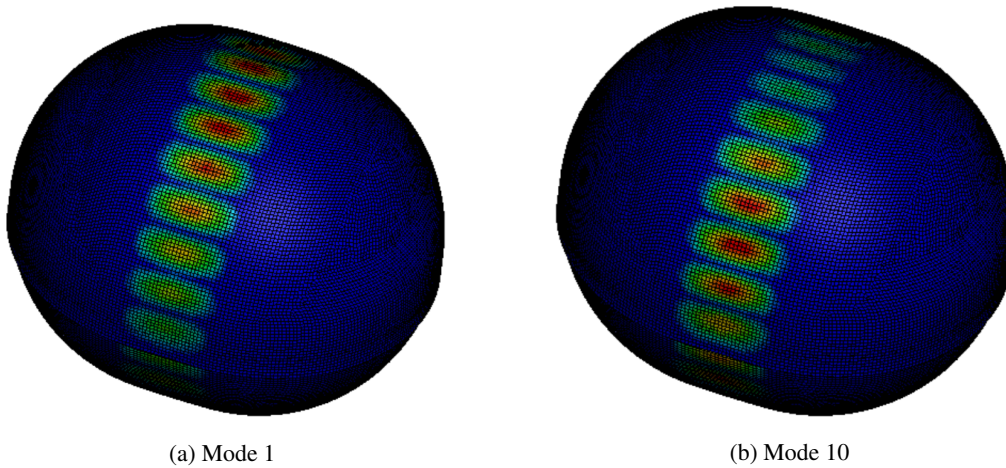


Figure 33: Linear Analysis: Sphere: 50 mm, Cylinder: 100 mm

Table 7: Buckling Pressure for 50 mm Sphere, Linear Analysis

Linear Buckling Pressure	0.185 MPa
--------------------------	-----------

Approximately the same buckling modes can be seen when the sphere thickness is reduced to 35 mm, and

in the range between 35 and 55 mm. All modes show buckling only on the cylindrical part. However, the critical buckling pressure is reduced, which indicates an effect on the cylinder buckling strength from changing the sphere thickness.

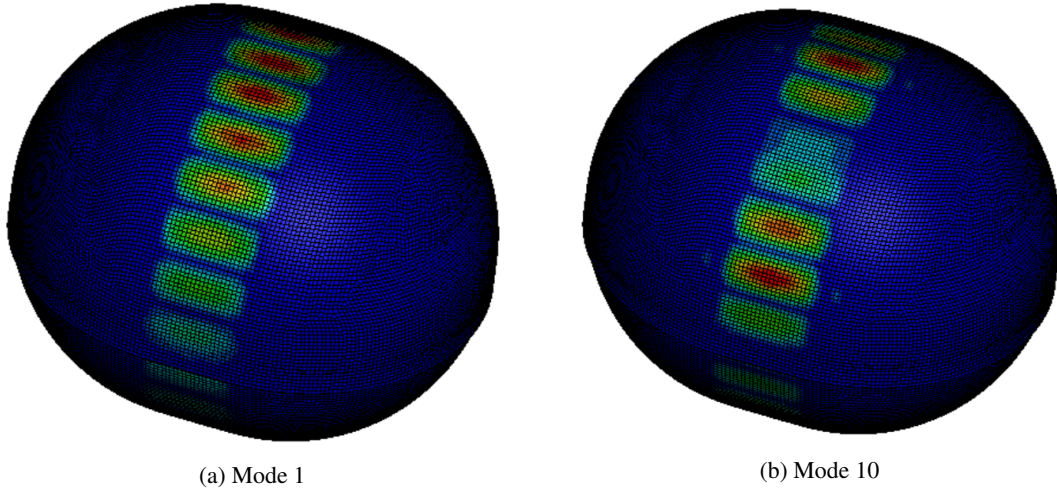


Figure 34: Linear Analysis: Sphere: 35 mm, Cylinder: 100 mm

Table 8: Buckling Pressure for 35 mm Sphere, Linear Analysis

Linear Buckling Pressure	0.169 MPa
--------------------------	-----------

For a sphere thickness of 30 mm the buckling modes changed. For the first eight modes the buckling mode is largest on the cylinder, but closer investigation shows that the buckling mode is a combination of buckling on the cylinder and on the spherical sections. For modes 9 and 10, only spherical buckling occurs, which indicates that a sphere thickness of 30 % of the cylinder thickness is the limit between cylindrical and spherical buckling. It would be interesting to decrease the thickness of the spherical section further. However, such attempts have been made but the linear solver has problems with finding eigenvalues on the structures, and produces no results. This might be due to significant discontinuities between the spherical and the cylindrical part. The issue concerning large discontinuities for such tanks is addressed in Section 2.3.

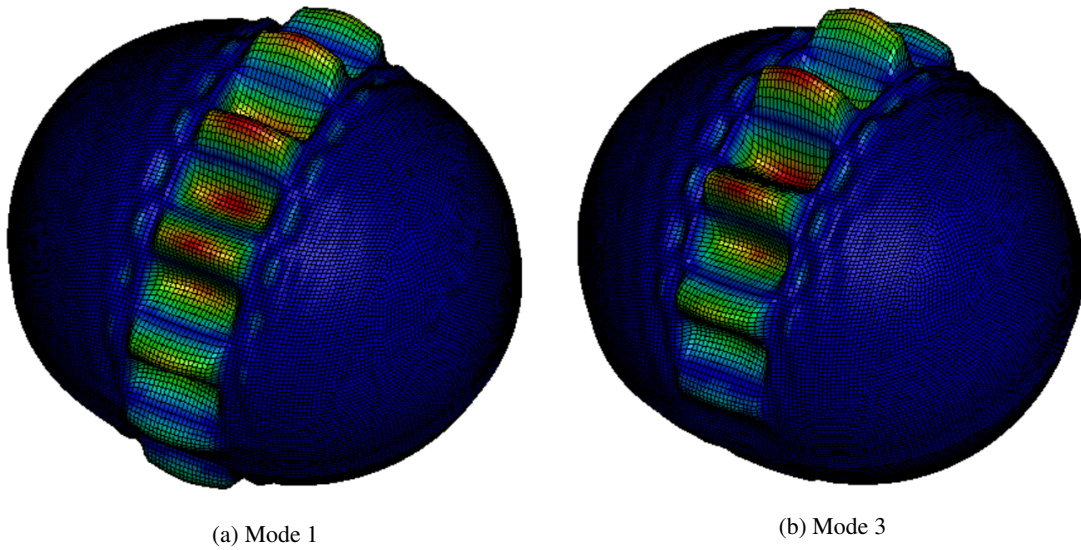


Figure 35: Linear Analysis: Sphere: 30 mm, Cylinder: 100 mm

Table 9: Buckling Pressure for 30 mm Sphere, Linear Analysis

Linear Buckling Pressure	0.158 MPa
--------------------------	-----------

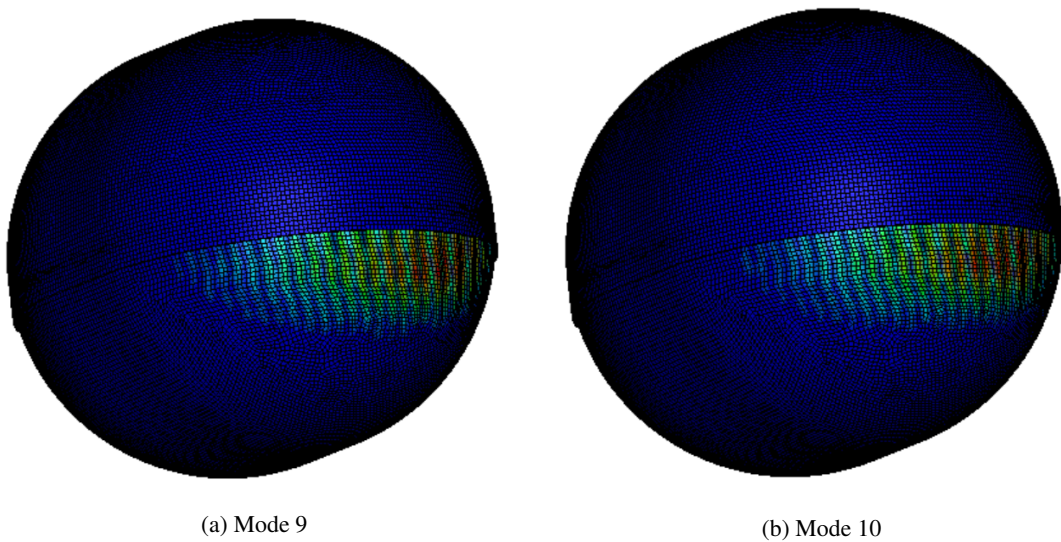


Figure 36: Linear Analysis: Sphere: 30 mm, Cylinder: 100 mm

However, the results show that a thickness relationship between sphere and cylinder of 30 % seems to be the limit between buckling on the cylindrical or the spherical part, exposed to external pressure. The results will be discussed further and compared with the results from the non-linear analysis and DNV GL regulations in Section 7.4.

### 7.3 Non-Linear Analyses

The non-linear analyses are almost identical to the linear analyses. However, the material is modelled differently. As explained in Section 4.3.1 the elasto-plastic aluminium is modelled to follow a Ramberg-Osgood

curve.

Additionally, the solution procedure is changed. The difference between linear and non-linear analysis is explained in Chapter 4. These non-linear analysis has been carried out without imperfections, which means that there is no geometrical difference between the linear and the non-linear model.

As expected, the tanks with a spherical section of 50 and 35 mm, show a similar buckling mode as seen in the linear analysis. The critical pressures for different spherical thicknesses can be seen in Table 10 and the buckling shapes can be seen in Figures 37 and 38.

Table 10: Linear Elastic Buckling Pressures for Stretched Tank

Sphere Thickness	Linear Buckling Pressure
50 mm	0.185 MPa
35 mm	0.169 MPa
30 mm	0.158 MPa

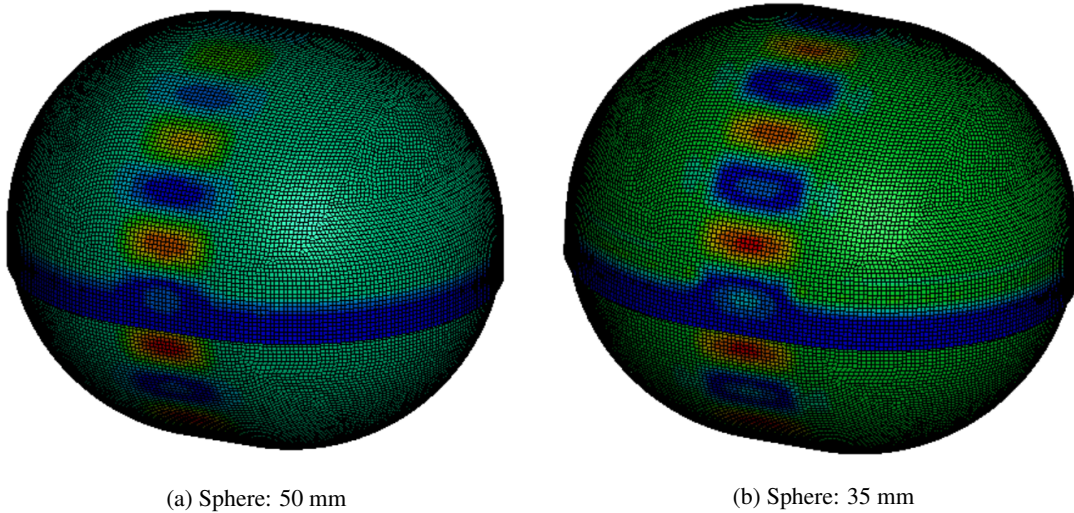


Figure 37: Non-Linear Analysis: Cylinder: 100 mm

When the thickness of the spherical sections reaches 30 mm or less, the deformation of the structure changes drastically. The result is a local buckling mode following the connection between the cylindrical and the spherical part. The deformation is largest in the corners, closest to the skirt. As expected, the thin sphere will be more deformed than the cylinder. This leads to significant curvature in the connections. These curvatures induce bending moments which are crucial to thin-walled shell structures.

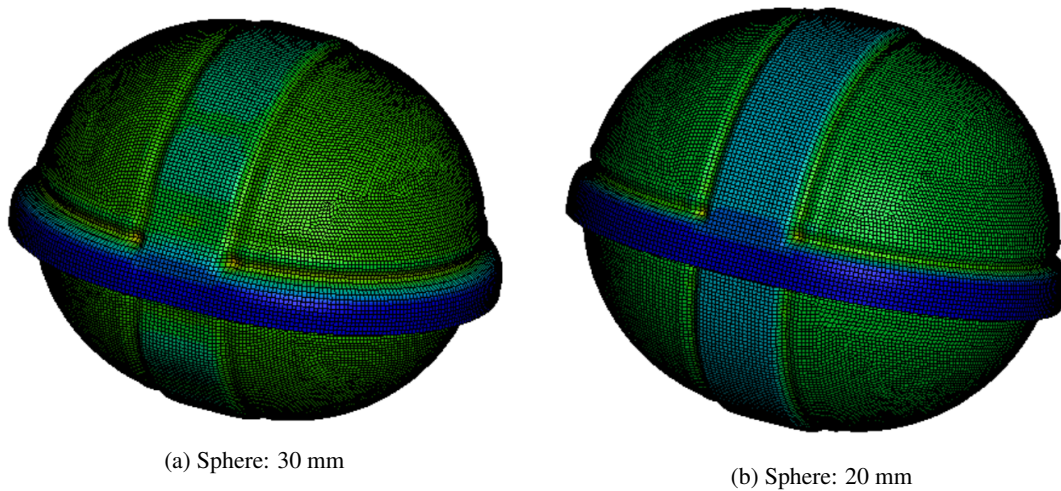


Figure 38: Non-Linear Analysis: Cylinder: 100 mm (2)

#### 7.4 Comparison of Results

The plot in Figure 39 shows the results from the linear and non-linear analyses. The linear buckling pressure is slightly higher than the non-linear pressure. This is believed to be due to the effect of non-linear material behavior introduced in the model. Additionally, one can see that the correlation between the linear and the non-linear buckling pressure is similar for the whole range of sphere thicknesses. However, the most interesting point of the plot is the change between 35 and 30 mm, where the buckling shape is expected to change from only buckling of the cylindrical part, to buckling of the spherical part, or a combined buckling shape. The drop in buckling pressure is higher for the non-linear analysis, which might imply that the non-linear material model leads to a more elasto-plastic buckling. This can be explained by the significant curvature in the connection area.

Section 7.1 explains DNV GLs procedure of calculating the buckling pressure for cylinders. The knock-down factor  $\rho$  should be set to 0.6. From Figure 39 one can see that 0.6, and a cylinder thickness of 100 mm yields a very good correlation with the FEA-results. However, in order to compare the classical elastic buckling strength of the sphere and the cylinder,  $\rho$  has to be 1, as there is no knock-down factor in the Zoelly buckling pressure equation.

Both a  $\rho$  of 0.6 and 1.0 was used, and the comparison can be seen in Figure 39. Even though the classical linear elastic buckling pressure without any imperfections is supposed to be calculated without any knock-down factor, a knock-down factor of 0.6 seems to fit very well with the results from the analyses. This can be seen as the crossing between the Zoelly buckling pressure and the analytic result with  $\rho=0.6$  occurring at approximately 31 mm sphere thickness.



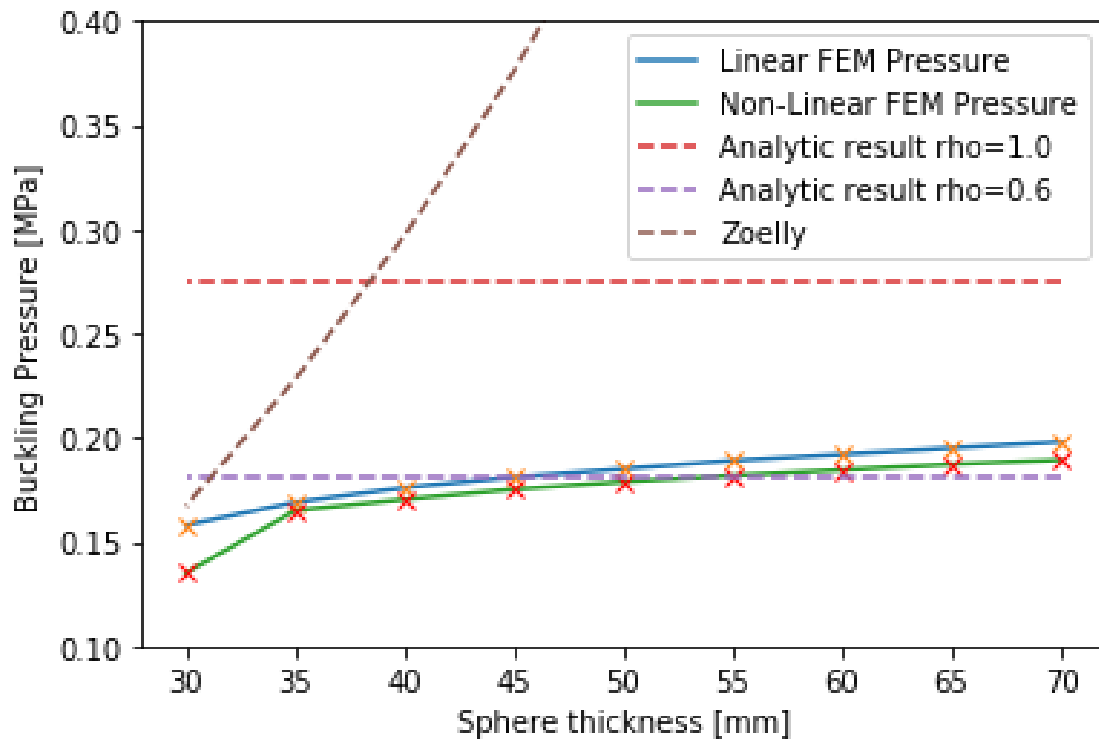


Figure 39: Comparison of Results from FEA and Relevant Formulas

## 7.5 Comparison of Simple Cylinder and Half-sphere

Due to uncertainty concerning the knock-down factor of 0.6 in the DNV GL Recommended Practice, some additional investigation of the buckling strength of cylinders and spheres, and the effect of combining them was carried out. For the cylinder, a knock-down factor of 0.6 was recommended, and from the analyses up to this point, it seems like a good fit. For the sphere, the Zoelly equation without a knock-down factor was used and also seemed to be a good fit. However, the application of a knock-down factor for the cylinder, but not for the half-spheres did not seem logical, which lead to further studies.

### 7.5.1 Only Cylinder

A comparison of the buckling load of a stand-alone cylinder, compared to one with two spherical end caps was done. The cylinder has a thickness of 100 mm, and is retained in all translations, but not rotations in both ends of the cylinder. The difference between this cylinder is not only the new boundary conditions at the ends instead of the sphere caps, but that the bearing from the skirt is removed.

Note that  $\psi$  is changed from four, to two, as the cylinder is only exposed to lateral pressure, and not axial pressure induced by the end caps. In this case, the strength from the numerical results exceeded the result from the equation, and the buckling strength of the same cylinder is increased from 0.185 to 0.351 MPa, which is an increase of 90 %, by replacing the sphere with boundary conditions. That the numerical results are higher than the results from the DNV GL recommendation, is unexpected, but it seems that the new boundary conditions strengthen the cylinder considerably.

The buckling modes of the cylinder can be seen in Figure 40a and 40b, and look similar to the ones obtained in the previous analyses.

Table 11: Result from Cylinder Analysis

Analysis	Theoretical Buck. Load $\rho = 1.0$ [MPa]	Num. Buck. Load [MPa]
Linear Analysis	0.275	0.351
Non-Linear Analysis	0.275	0.373

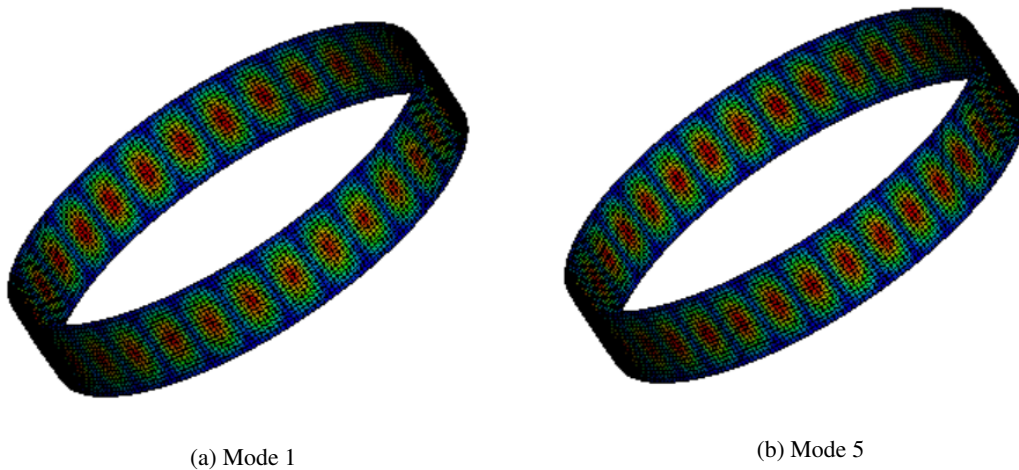


Figure 40: Linear Analysis of Cylinder with Thickness 100 mm

### 7.5.2 Only Hemisphere

The half-sphere did not seem to have the same reduction in strength due to combining the two shapes. The half-sphere analysed here has a thickness of 50 mm, and has the same boundary conditions as the stand-alone cylinder, which means that all end nodes are retained in all three translations.

Table 12 shows that the linear analysis of the half-sphere corresponds well with the linear elastic buckling pressure from the Zoelly equation. The buckling strength drops when the analysis is non-linear, which is the opposite of the non-linear analysis of the stand-alone cylinder where the buckling strength was increased for the non-linear analysis.

Table 12: Result from Half Sphere Analysis

Analysis	Zoelly [MPa]	Numerical Result [MPa]
Half Sphere (50 mm) Linear Analysis	0.465	0.471
Half Sphere (50 mm) Non- Linear Analysis	0.465	0.33

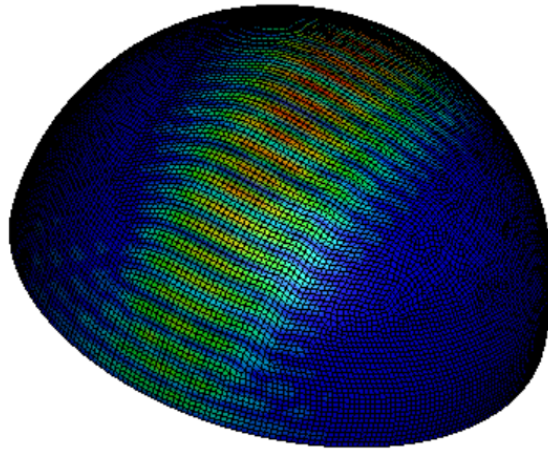


Figure 41: Linear Analysis of Half Sphere with Thickness 50 mm

## 7.6 Results of Comparison

The results of these two comparisons give reason to believe that the cylinder is more vulnerable, when it comes to combining the two shapes, and therefore changing the boundary conditions. For the cylinder this is probably a combination of the effect from the sphere, and the effect from the skirt. This might be the reason for applying the knock-down factor of 0.6, but as emphasized, this is not clear in DNVGL-RP-C202 [6]. This issue is studied further in Chapter 8.

## 8 Study of the Impact of Cylinder Length in Stretched Tank

A parametric study of the effect of the length of the cylindrical part has been carried out. In addition to study how the strength of the tank is affected by the length of the cylindrical part, the aim is to compare the results with the Class Guidelines from DNV GL, similar to the work done in Chapter 7. Section 7.1 describes the procedure for calculating elastic buckling pressure. In this study the only load to the structure is external pressure. It is important to emphasize that this study is limited to linear elastic buckling strength related to external pressure and that the strength against other types of loads, i.e. sloshing can be different. The main parameters of the study can be seen in Table 13, and the results from the linear buckling analyses can be seen in Table 14.

Table 13: Parameters for Study Effect of Cylinder Length

Radius of Half-spheres and Cylinder	21.5 m
Height of Skirt	4 m
Thickness Cylinder	100 mm
Thickness Skirt	70 mm
Thickness Sphere	50 mm
Mesh Size	0.45
Material	Al 5083-0
Boundary Conditions	Skirt edge restricted in all 6 DOFS
Loads	External Pressure

Table 14: Results of Cylinder Length Parameter Test

Cyl. Length [m]	Pc FEA [MPa]	Pc DNV GL [MPa]	% Offset	Buck. Stress FEA [MPa]
4	0.291	0.637	118.9	62.6
8	0.185	0.275	48.6	39.8
12	0.135	0.177	31.1	29.0
16	0.107	0.131	22.4	23.0
20	0.089	0.104	17.1	19.2
32	0.060	0.064	8.35	12.9
48	0.043	0.043	0.396	9.2
64	0.034	0.032	-4.32	7.3

In Chapter 7 the reliability of the equations of linear elastic buckling pressure in DNVGL-CG-0314 was discussed and questioned. In those analyses, the cylindrical part was eight meters, and the comparison of results from the FEA and Class Guidelines did not yield satisfactory results, especially due to uncertainties concerning the knock-down factor  $\rho$ . For this comparison of FEA-results and elastic buckling pressure based on Section 7.1,  $\rho$  is set to 1. That value should correspond to the classical linear elastic buckling pressure, without any imperfections. A comparison between the buckling pressure obtained in the analyses and by the equation in DNV GL can be seen in Figure 42, which is based on Table 14. The comparison shows that the results of the equations and the FEA are very different for short cylinders, and that the difference in percentage decreases as the cylinder length increases. For the 48 meters cylinder, they are practically the same, and for the 62 meter cylinder the FEA yields higher buckling strength than the equations for the first time.

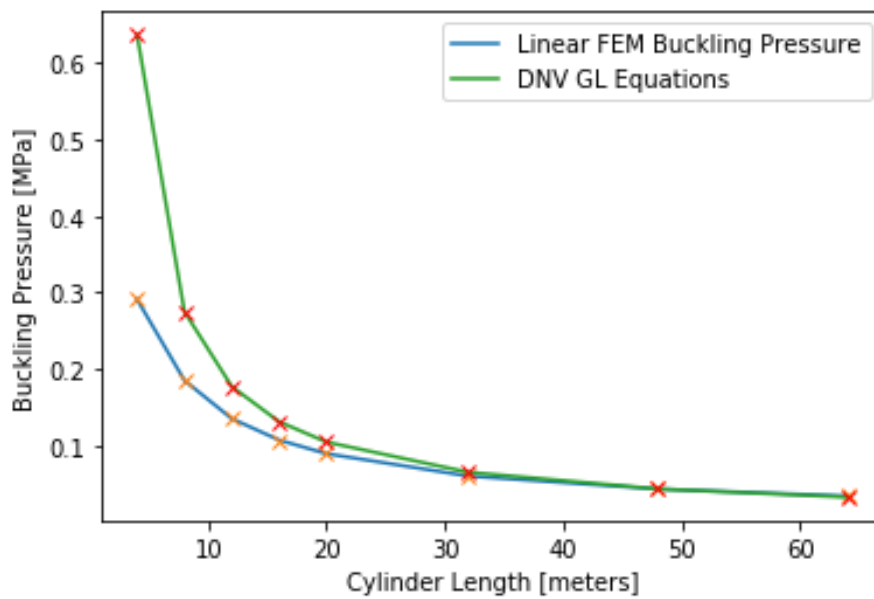


Figure 42: Comparison of FEA-results and DNV GL Equations

Figure 43 shows the percentage difference between the FEA-results and the Class Guidelines. The plot clearly shows that for cylinders of less than 30 meters there are major deviations between the FEA-results and Class Guidelines. Based on the results obtained, it seems like the procedure recommended by DNV GL to find elastic buckling pressure of unstiffened circular cylinders is unsuitable for cylinders where the length of the cylinder is less than the diameter. As a consequence, the equations seem unsuitable to calculate buckling pressures for the cylindrical parts of LNG-tanks as they have a very small length/diameter-ratio. This is possibly due to the interaction with the boundary conditions, which may affect a short cylinder more.

The circumferential stresses in the cylinder corresponding to the critical pressures for the different lengths are not close to the yield stress. This implies that the buckling is very elastic, which again implies that the correspondence between FEA and DNV GL equations should comply. If the stresses were closer to the yield stress, the effect of plasticity would have been taken into account, and the buckling strength could have been reduced drastically.

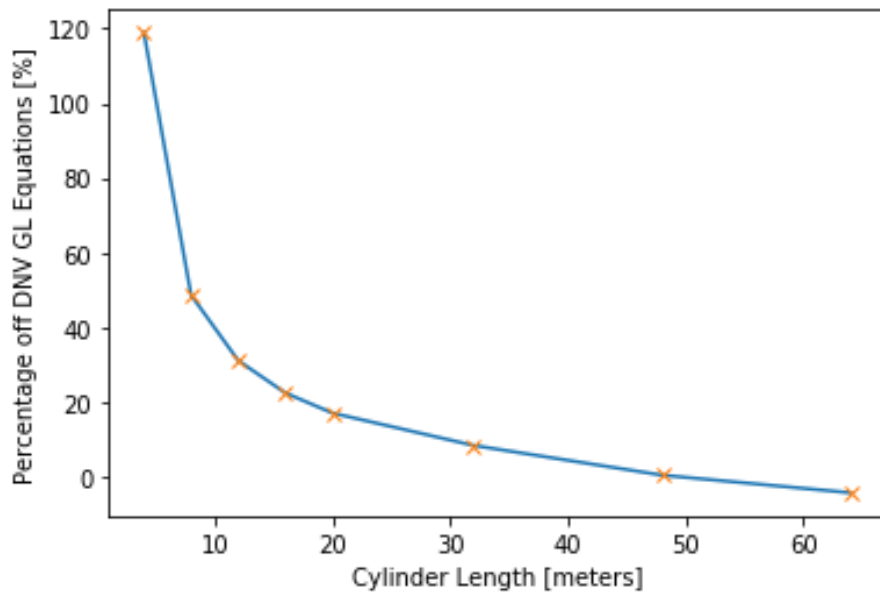


Figure 43: % Offset of FEA-Results from DNV GL equations

Contour plots of the first buckling mode of all tanks of different lengths can be seen in Appendix A.

### 8.1 Comparison with Vertically Stretched Tank

Based on the results showing unsatisfactory compliance between the equations from DNV GL and FEA results, possible sources of error were considered. In this project, stretching the tanks longitudinally is studied. However, the most common way to stretch the tanks is vertically. In this case the magnitude of elongation is very limited due to the increase of the center of gravity leading to stability issues. The stretched tanks in DNVGL-CG-0134 seem to be vertically stretched, and these differ from the longitudinally stretched tank in terms of boundary conditions.

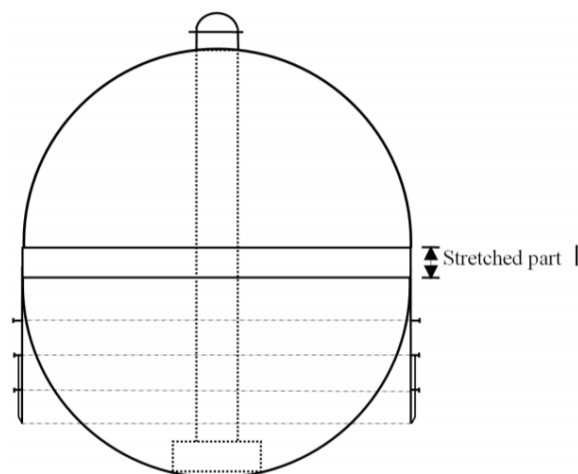


Figure 44: Illustration of Stretched Tank from Class Guidelines [7]

For the vertically stretched tank the connection between the skirt and the tank is at the weld between the lower half-sphere and the cylinder. Hence, the skirt is circular and very similar to the skirt for a fully spherical tank. For the longitudinally stretched tank the skirt is changed, which affects both the skirt and the tank. For the longitudinal tanks, the skirt goes along with the cylinder, as seen in Figure 45. To verify

the results comparing the FEA-results and the DNV GL regulations, a comparison between the horizontally and vertically stretched tank was done. The only comparison was the eight meter cylindrical part, which is a realistic cylinder length. Table 15 shows that there is a significant difference in strength, and that the buckling strength is reduced by the skirt along with the horizontal cylinder. However, the results of the vertically stretched tank does not comply with the buckling pressure from the DNV GL regulations, and does not change the significance of the results. The model of the vertically stretched tank with boundary conditions and the first buckling mode can be seen in Figure 46 and 47.

Table 15: Comparison of Strength of Horizontal and Vertical Tank

Horizontal Tank	0.1850 MPa
Vertical Tank	0.1997 MPa
DNV GL Equations	0.275 MPa



Figure 45: Boundary Conditions for Horizontal Tank

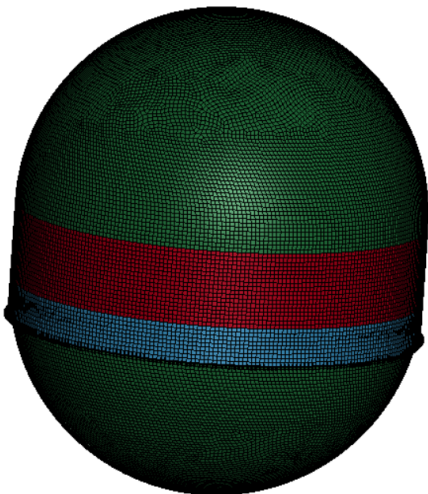


Figure 46: Vertical Tank Model

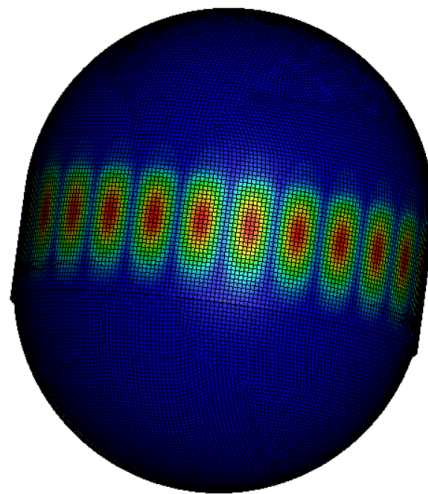


Figure 47: Vertical Tank, Mode 1

## 9 Imperfection Sensitivity Study

This chapter describes the tanks sensitivity to imperfections, compared with the expected sensitivity. Two different imperfections have been applied; one based on the first eigenmode from the linear analysis, and one computed imperfection modelled as a sinusoidal imperfection shape on the cylindrical part.

### 9.1 DNV GL Class Guidelines

DNV GLs recommended way to model the imperfections of spherical LNG tanks is by modelling the spherical shell as a shape close to spherical, with the same nominal radius as the sphere. The imperfection amplitude is defined as  $\delta_i$  and is the amplitude of the light opening between the spherical shell and the imperfect and almost spherical shell structure.  $\delta_1$  is defined as:

$$\delta_1 = \frac{0.01g}{1 + g/R} \quad (40)$$

where:

$$g = 4\sqrt{Rt} \quad \text{if} \quad \frac{\sigma_{20}}{\sigma_{10}} > 0 \text{ (comp. - comp. )} \quad (41)$$

or

$$g = \left(4 + 2\frac{\sigma_{20}}{\sigma_{10}}\right)\sqrt{Rt} \quad \text{if} \quad -1 < \frac{\sigma_{20}}{\sigma_{10}} < 0 \text{ (comp. - tens. )} \quad (42)$$

$\delta_1$  is compared with the length of each segment, preferably a half-wave differing from the spherical shape. This length is defined as:

$$\ell_1 = 2\sqrt{Rt_{\max}} \quad (43)$$

DNV GL has also defined  $\ell_2$  and  $\delta_2$ :

$$\delta_2 = \frac{r}{750} \quad (44)$$

$$\ell_2 = 4\sqrt{Rt_{\max}} \quad (45)$$

Both  $\delta$ -values should be appropriate imperfection amplitudes for the given imperfection length  $\ell_2$ , although DNV GL also writes: "The value of  $\delta_1$  to be used in the calculations will be decided by the Society taking into consideration the manufacturers experience from previous production, shell thickness, and type of material." [7] However, the obtained values of  $\delta$  are seen appropriate as a basis for the analyses carried out in this project.

Often, the imperfections are eigenmodes, as these are supposed to be the shape that reduces the strength the most. They can also be chosen deviations to the shape based on experience, experiments etc. However, this will be easier in situations where the buckling shapes are more obvious, i.e. in a stiffened plate panel.

### 9.2 Eigenmodes as Imperfections

A common way to apply imperfections to shell structures is in the form of eigenmodes. The main reason for this is that the eigenmodes correspond to the weakest shape of the structure towards the load in question. Hence, using eigenmodes will in most cases lead to the largest knock-down factor, for a given imperfection amplitude. This is also described more thoroughly in Section 2.4.1.

In this section, the impact of the imperfection amplitude is studied. Initially, a linear eigenvalue analysis was done for a stretched tank with an eight meter long cylindrical part, using a linear material model. The main parameters of the tank can be seen in Table 16.



Table 16: Parameters for Study Effect of Cylinder Length

Radius of Half-spheres and Cylinder	21.5 m
length of Cylinder	8 m
Height of Skirt	4 m
Thickness Cylinder	100 mm
Thickness Skirt	70 mm
Thickness Sphere	50 mm
Mesh Size	0.45
Material	Al 5083-0
Boundary Conditions	Skirt edge restricted in all 6 DOFS
Loads	External Pressure

The linear buckling analysis yielded a buckling pressure of 0.185 MPa which is quite much lower than the expected buckling pressure for an unstiffened cylinder from DNV GL which is 0.275 MPa. This factor is probably due to the effects of the boundary condition, which is more important for short cylinders. This issue is addressed in Chapter 8. The buckling mode seen in Figure 48 was extracted, and used as imperfection for the non-linear analysis, with increasing amplitudes.

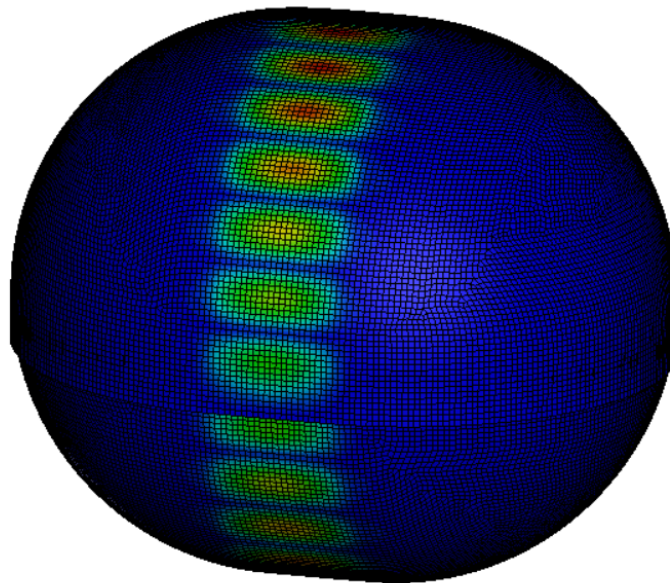


Figure 48: Linear Buckling Analysis, 1. Mode, Buckling Pressure = 0.185 MPa

Initially, a non-linear analysis was done without any geometrical imperfections. However, the material model was changed to an elasto-plastic material model. This is described in Section 4.3. The analysis yielded a buckling pressure of 0.179, and the buckling shape in Figure 49 is seen to be similar to the buckling modes from the linear analysis. The small reduction of buckling strength is believed to be a result of the material model introducing plasticity. However, the stress corresponding to a critical pressure of 0.185 MPa is 39.8 MPa, which is about 25 % of the yield stress. Hence, the buckling is quite elastic, leading to a limited reduction of buckling stress due to non-linear material behavior.

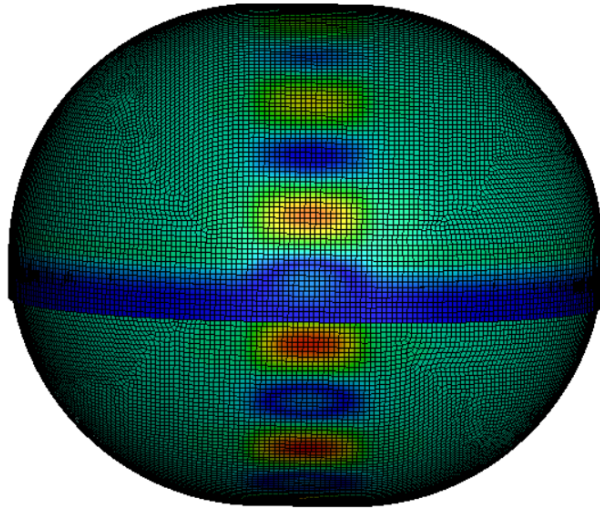


Figure 49: Non-Linear Buckling Analysis, No Imperfection, Buckling Pressure = 0.179 MPa

The imperfection amplitudes range from 5 mm to the cylinder thickness of 100 mm as a maximum. The results from the analyses, and the corresponding knock-down factors can be seen in Table 17.

Table 17: Results of Imperfection Test using 1 Eigenmode as Imperfection

Imperfection Amplitude [mm]	Buckling Pressure from FEA [MPa]	Knock-Down Factor [-]
0	0.179	1.000
5	0.164	0.919
10	0.153	0.854
20	0.134	0.750
30	0.120	0.671
40	0.108	0.606
50	0.099	0.554
60	0.094	0.525
70	0.090	0.502
80	0.086	0.482
90	0.083	0.465
100	0.080	0.450

As described in Section 9.1, DNV GL has two ways to define suitable imperfection amplitudes. It should be emphasised that these are only very simple suggestions, which probably yield suitable estimates. Shell thickness and even the experience of the manufacturers are factors DNV GL considers when deciding a suitable amplitude. The two resulting  $\delta$ -values can be seen below.

$$\delta_1 = 46mm \quad (46)$$

$$\delta_2 = 29mm \quad (47)$$

These delta values correspond to  $\ell_1$  and  $\ell_2$ , with values:

$$\ell_1 = 2933mm \quad (48)$$

$$\ell_2 = 5865mm \quad (49)$$

A study of the applied imperfection yields an estimate for the light opening of mode 1 from the linear analysis. This was simply done by counting the number of half-waves, and calculating the circumference of the cylinder. This resulted in a light opening estimate of:

$$\ell = 4,8m \quad (50)$$

which is between the two suggested light openings by DNV GL. It is observed from the DNV GL equations that a short light opening implies a higher imperfection amplitude. Based on the results, an imperfection amplitude of 40 mm seems like a reasonable value.

It can be seen from Table 17 that an imperfection amplitude of 40 mm yields a knock-down factor of 0.6. The results from Table 17 are plotted in Figure 50. The results show a reasonable imperfection sensitivity, along with the expectations. The development of the buckling strength can be compared with the experimental results of a similar cylinder in Figure 51. Based on the scatter diagram from the experiments, the plot suggests an upper and a lower limit to the imperfection sensitivity. The plot from the FEA-results seems to be approximately in the middle of the upper and lower limit, and based on that, the imperfection sensitivity seems to be reasonable.

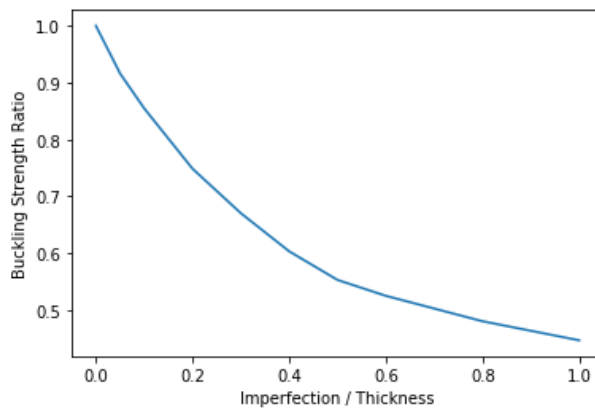


Figure 50: Knock-Down factor With Increasing Imperfection Amplitude

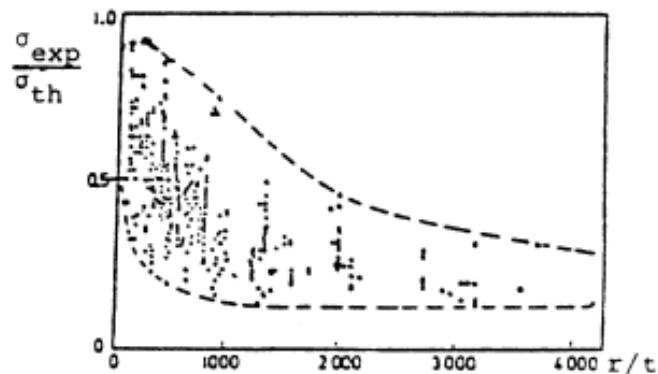


Figure 51: Experimental Test of Imperfections on Buckling of Cylinder [1]

### 9.3 Chosen Imperfection Shapes

Instead of using eigenmodes, one can based on educated guessing and experience, use self-made imperfection shapes. These will in many cases be quite similar to the eigenmodes, as they should lead to large knock-down factors. However, they can also reflect usual imperfections that may occur from manufacturing of the structure. For shell structures, any weld can be seen as an imperfection, and weaken the structure. For some scenarios it will be easier to compute imperfection-shapes than others. A stiffened plate panel is a good example, as it is easy to predict the possible buckling shapes, and these shapes will again be easily computed by use of trigonometric functions. For a larger, irregular structure, it might be hard to predict the buckling shape, and a linear analysis will probably be useful to produce mode shapes. All though, also in these cases it might be useful to model some imperfections representing imperfections from manufacturing, or likely ruptures due to impact with other structures.

Two Python-scripts were developed where a trigonometric imperfection was introduced on the cylindrical part. The scripts can be seen in Appendices B.3 and B.4. In order to make imperfections similar to the eigenmodes, a number of 14 sinusoidal waves was chosen. This is the same number as the first linear eigenmode, which leads to a light opening of approximately 4.8 meters. The same study was done by increasing the imperfection amplitude and plotting the effect.

It can be seen in Figure 52 that the results of the two types of eigenmodes are very similar for the smaller imperfection amplitudes. For the eigenmodes as imperfections, the buckling strength decreases continuously. However, the steepness of the plot decreases as the imperfection amplitude increases. The buckling pressures with computed imperfections are almost identical to the buckling pressures with eigenmodes, up to an imperfection amplitude of 30 mm, which is 30 % of the shell thickness. Somewhere between 30 and 40 mm, the buckling pressure flattens, and is practically constant to the largest imperfection amplitude of 100 mm. It is hard to identify the reason for this, but based on the results, the use of eigenmodes from linear analysis might be a more suitable solution.

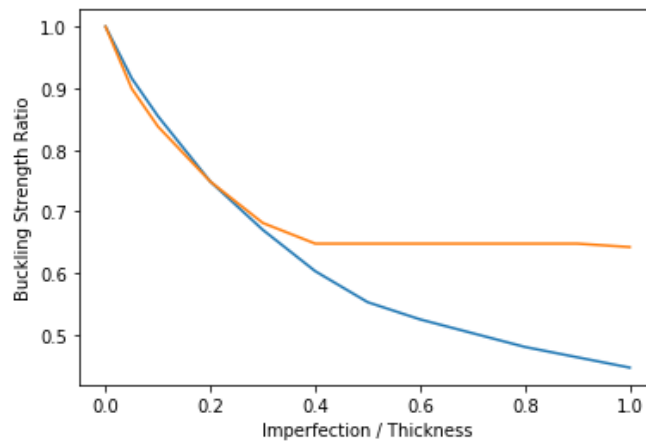


Figure 52: Imperfection Sensitivity Study with Computed Imperfections

## 10 Non-Spherical LNG-tank With Different Thicknesses

As described in the Chapter 1, the Moss LNG-tanks are divided into sections with varying thicknesses. As the highest impacts on the tank are near the bottom, because this is where the hydrostatic pressure is highest, it would be a waste of weight and material to have the same thickness on the whole tank. A non-spherical tank was modelled, based on Figure 6, in Section 1.3. The thicknesses for the spherical part was decided based on scantlings provided by Moss Maritime, and the thicknesses for the cylindrical parts were set to double the corresponding spherical sections.

Table 18 contains the thicknesses of the sectioned model, and the meshed model can be seen in Figure 53.

Table 18: Thicknesses for Sectioned Non-Spherical Tank

Zone	Zone Height	Thickness Spherical Part	Thickness Cylindrical Part
Zone 7	2000	40	80
Zone 6	6500	32	64
Zone 5	10000	51	102
Zone 4 U	2400	57	114
Equator	1200	195	390
Zone 4 L	2400	71	142
Zone 3	10000	66	132
Zone 2	6500	53	106
Zone 1	2000	53	106
Skirt	4000	70	70



Figure 53: Meshed Model With Different Thicknesses

### 10.1 Comparison of Linear Analysis with External Pressure

The main target of this study was to identify the differences in terms of strength for the model divided into sections and the models analysed up to this part, with one thickness for the cylinder and one for the

spherical parts. For the sectioned model, the thicknesses listed in Table 18 were used. The thickness of the cylindrical and spherical parts of the homogeneous model was set to be equal to the lowest thickness from the sectioned tank, which is 64 and 32 mm, respectively. This is a reduction compared to the studies done up to this point, where 100 and 50 mm have been used. For the linear analyses, a linear elastic material model for aluminium was used, and the only load was external pressure. The parameters in common for both tanks are listed in Table 19. The thicknesses for the homogeneous model are listed in Table 20.

Table 19: General Parameters for Homogeneous and Sectioned Model

Radius of Half-spheres and Cylinder	21.5 m
Length of Cylindrical Section	8 m
Height of Skirt	4 m
Mesh Size	0.45
Material	Al 5083-0
Boundary Conditions	Skirt edge restricted in all 6 DOFS
Loads	External Pressure

Table 20: Thicknesses for Homogeneous Model

Thickness Cylinder	64 mm
Thickness Skirt	70 mm
Thickness Sphere	32 mm

Figures 54a and 54b show the buckling patterns for the respective models. One can see a more local buckling for the sectioned model, where the deflection is largest in the section with the smallest thickness. The bottom of the sectioned model has significantly higher thickness. Hence, only the upper part of the cylinder buckles.

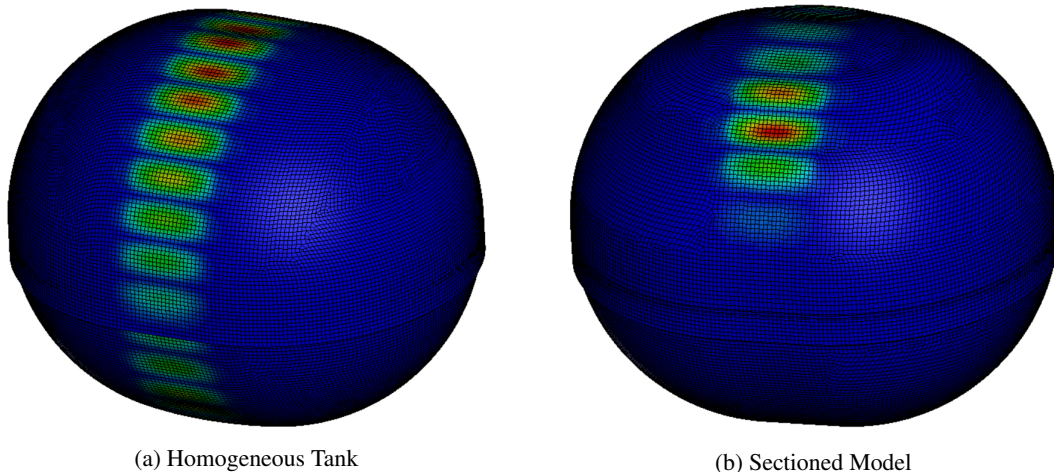


Figure 54: Linear Analysis

Table 21 shows that the strength is higher for the sectioned model. Most of the cylinder, which is the critical part of the structure, is thicker than the homogeneous model. It is seen as likely that the thicker sections, especially the sections neighboring Zone 6, stiffen the weaker sections, leading to higher strength.

Table 21: Linear Buckling Pressures

Buckling Pressure Homogeneous Model	0.0643 MPa
Buckling Pressure Sectioned Model	0.0805 MPa

## 10.2 Comparison of Non-Linear Analysis with External Pressure, Without Imperfections

By introducing a non-linear material model, a non-linear analysis was done, without the use of imperfections. As this problem is quite elastic, changing from an elastic to an elasto-plastic material model does not yield any significant difference when it comes to the buckling pressure. The deformation can be seen in Figure 55a and 55b, and the buckling pressures can be seen in Table 22.

Table 22: Non-Linear Buckling Pressures Without Imperfections

Buckling Pressure Homogeneous Model	0.0642 MPa
Buckling Pressure Sectioned Model	0.0765 MPa

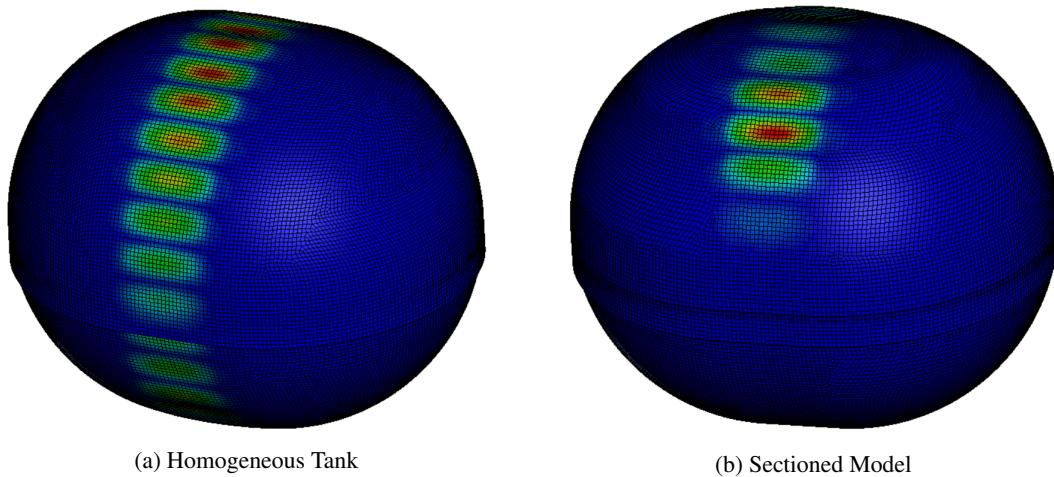


Figure 55: Non-Linear Analysis Without Imperfection

## 10.3 Comparison of Non-Linear Analysis with External Pressure, With 1. Mode as Imperfection

In addition to studying the difference between a sectioned model and the model with homogeneous thickness on the spherical and cylindrical part, imperfections were introduced to both models to study if the effect of imperfections was different for the two models. The amplitude of the imperfection is set to 40 mm for both cases, and is introduced as the first mode from the respective linear analysis, but scaled to an amplitude of 40 mm. The deformation of the tanks can be seen in Figures 56a and 56b, and the buckling pressures and knock-down factors can be seen in Table 23. The knock-down factor is seen to be slightly smaller for the sectioned model, which might indicate that the sectioned model is slightly more sensitive to imperfections than the homogeneous model.

However, the difference is not especially high, and based on all of the comparisons, a simpler model, with the same thickness as the lowest thickness on the actual tank, can be used for structural analyses with external pressure as load. These simpler analyses will probably give conservative values concerning buckling

strength. This might not be the case for more advanced loading conditions, and is limited to external pressure only.

Table 23: Non Linear Buckling Pressures With 1. Mode as Imperfection

Model	Imperfection Amplitude	Buckling Pressure	Knock-Down Factor
Homogeneous Model	40 mm	0.0351 MPa	0.55
Sectioned Model	40 mm	0.0375 MPa	0.49

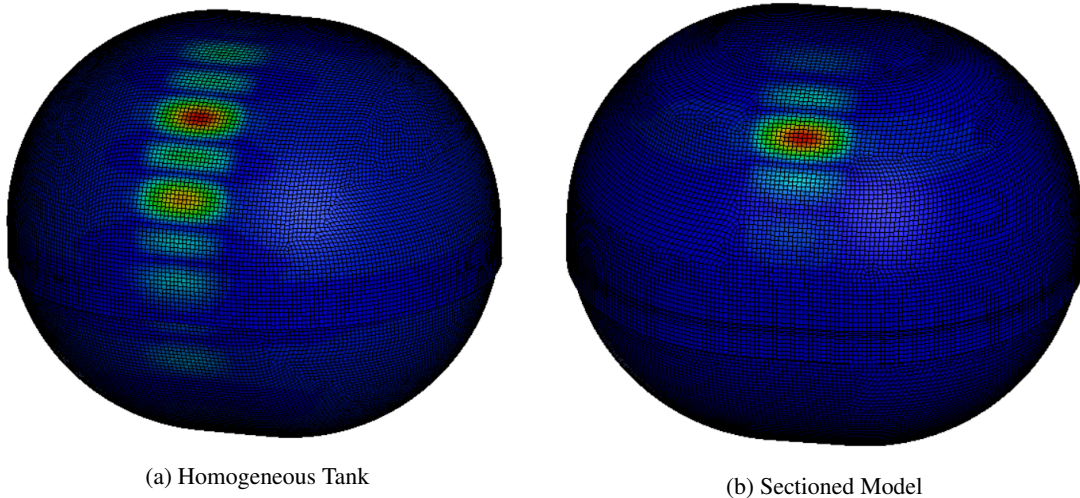


Figure 56: Non-Linear Analysis With 1. Eigenmode as Imperfection

#### 10.4 Comparison of Non-Linear Analysis with External Pressure, Computed Imperfection

A chosen imperfection shape represented by a sinusoidal imperfection was also applied to the cylindrical part, and the effect was investigated. The amplitude and length of the imperfection matched the length and amplitude of the first mode, identified by the linear analysis. The reduction of the buckling strength due to the computed imperfections can be seen as slightly smaller than for the imperfection based on the first mode from the linear analysis. The results can be compared by using Tables 23 and 24. The difference may be explained by the fact that the buckling shape from the linear analysis should be the deformation shape in which the tank is weakest. Even though the computed imperfection is very similar, the tank will probably be slightly stronger with the computed imperfection, than for the tank with an imperfection based on the linear analysis. However, the difference in buckling strength is not deterrent, and the computed imperfection seems like a proper way of introducing imperfections. However, one might need a slightly more conservative imperfection amplitude, and know with certainty that the computed imperfection is close to the shape that will give the largest strength reduction.

Table 24: Non-Linear Buckling Pressures With Computed Imperfections

Model	Imperfection Amplitude	Buckling Pressure	Knock-Down Factor
Homogeneous Model	40 mm	0.0381 MPa	0.59
Sectioned Model	40 mm	0.0432 MPa	0.54



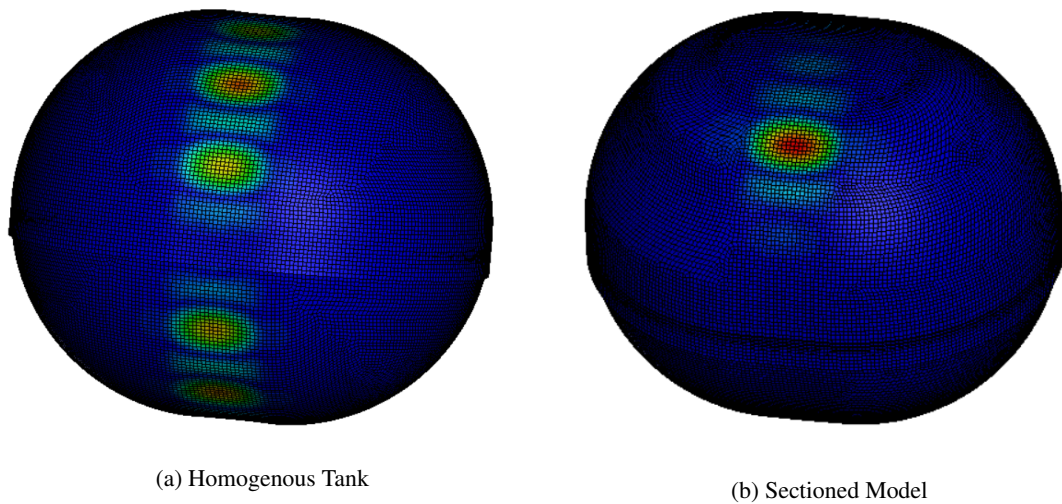


Figure 57: Non-Linear Analysis With Computed Imperfection

The comparisons of the behaviour of the homogeneous tank analysed up to this Chapter, and a more realistic tank may be seen as a verification of the results up to this point. It seems like the homogeneous tank is similar to the sectioned tank in behaviour against external pressure. This increases the reliability of the analyses done up to this point, described in Chapters 7, 8 and 9.

## 11 Sloshing Analyses with Conservative Thicknesses

Up to this point, only external pressure has been applied to the structure. At this point, more loads will be applied and studied, according to Class Guidelines. The loads that will be applied are:

- External Pressure
- Gravity Load, including insulation
- Acceleration on material due to ship motion
- Sloshing Load

The gravity loads include the added weight due to the insulation of the tank. The weight of the insulation is set to be  $15 \text{ kg/m}^2$ . The gravity and the acceleration of material are combined. As they are not assumed to be a dimensioning load, the load combining gravity and acceleration to the material is the first load to be applied. Following the gravity load, the external pressure will be applied similarly to what has been done up to this point.

As described in Chapter 3, interaction forces between the tank and the hull should be included in these analyses. However, this leads to the need of a FEM-analysis of a cargo hold model to obtain these interaction forces. This has not been included in these analyses, which is a simplification of the analyses, as all necessary loads are not included.

### 11.1 Acceleration on Material

The acceleration on the tanks should be found by direct hydrodynamic analyses for the vessel in question, unless data is available from similar ships [7]. In this case, the additional acceleration components  $a_z$  and  $a_y$  are  $0.45 \text{ g}$  and  $0.5 \text{ g}$ , respectively. In the vertical direction, the acceleration due to gravity of  $1 \text{ g}$  is added. This yields an acceleration resultant of  $15.05 \text{ m/s}^2$ , vertically.

### 11.2 Sloshing Load

A more critical load to the LNG-tanks is the sloshing load from the LNG. Although the sloshing load is dynamic, it is modelled as a static load, more specifically as hydrostatic pressure in accordance with Class [7]. The LNG is assumed to have a density of  $500 \text{ kg/m}^3$ . As mentioned, the sloshing force is modelled as hydrostatic pressure, with an increased acceleration than only acceleration of gravity, to account for fluid momentum. This acceleration is defined as  $a_R$ . Figure 58 illustrates the simplification of the sloshing force.

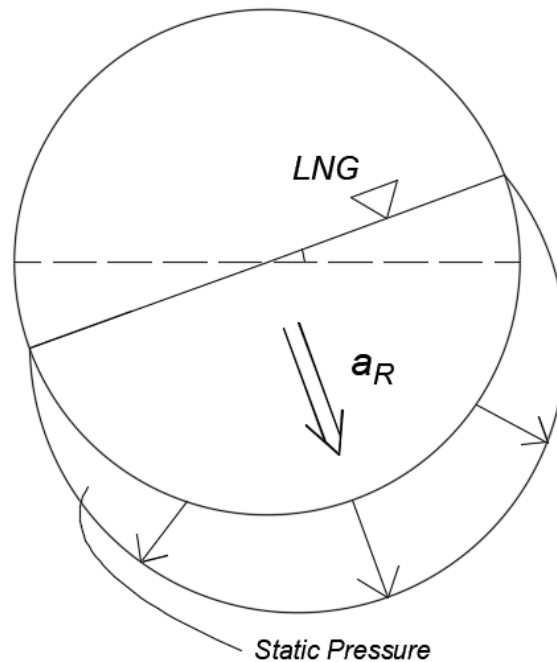


Figure 58: Illustration of Sloshing Load as Hydrostatic Pressure

In terms of buckling strength, the most critical state will be when the lower level of the LNG is below the equator. The weight of the cargo will induce meridional tensile stresses in the tank. Through contraction, these tensile stresses will yield compressive stresses in the circumferential direction. It is emphasized that fillings of more than 50 %, with a skew angle, can be below the equator. Such a load condition will lead to higher stresses due to the increased weight of the cargo, and will in most cases be critical in terms of buckling strength.

### 11.2.1 Difference Between Spherical and Non-Spherical Tank

DNV GL describes the difference in calculating the sloshing load for a spherical and a stretched tank in DNVGL-CG-0134 [7]. For a limited extension of the stretched part the sloshing will be similar compared to the spherical tank. It may be suitable to use a tank diameter equal to the tank length for calculating the sloshing force. This is interpreted as important for sloshing longitudinally. For transverse sloshing, the same radius as for the sphere is used, and the same load will be applied to both tanks. For longitudinal sloshing it would be more appropriate to use a radius for calculation of the sloshing load equal to half the tank length. Even though the load will increase for such a configuration, the effect on the tank will probably be more similar to a sphere, than for transverse sloshing.

### 11.2.2 Application of Loads

This section describes how the loads are applied for both linear and non-linear analyses. One important factor is that the sloshing load is assumed to be the critical load, and this is important for the order of load application, in the non-linear analyses. Figure 59 illustrates how the loads are applied. For the non-linear analysis, the initial time is set to zero. As the analysis goes on, the time increases with appropriate step-sizes. Between  $t=0$  and  $t=1$ , the acceleration of the material is applied. This acceleration includes both gravity and acceleration due to ship motion. During the next time interval, of equal length, the external pressure is applied, increasing with time. At  $t=2$ , the external pressure has reached its maximum and the sloshing load is applied. As this is seen as the critical load, this will increase until failure.

The procedure is different for the linear analysis. The linear analysis only happens at one specific time, this is specified to be at  $t=3$ , to include all loads in the analyses. This time is illustrated in Figure 59, by a red dotted line. The linear analysis will then find an eigenvalue, which will be a scale factor to be multiplied with the value of all three loads at  $t=3$ . The combination of those loads will then be the critical load for linear buckling. However, one analysis does not give a clear picture of what loads are more critical than the other. Therefore, it is suitable to investigate this by trying different combinations of load amplitudes, and comparing the results. To exemplify, if the maximum value for acceleration on the material is multiplied by a factor of ten, but the eigenvalue remains the same, the acceleration on the material is likely of minor significance for the strength of the structure.

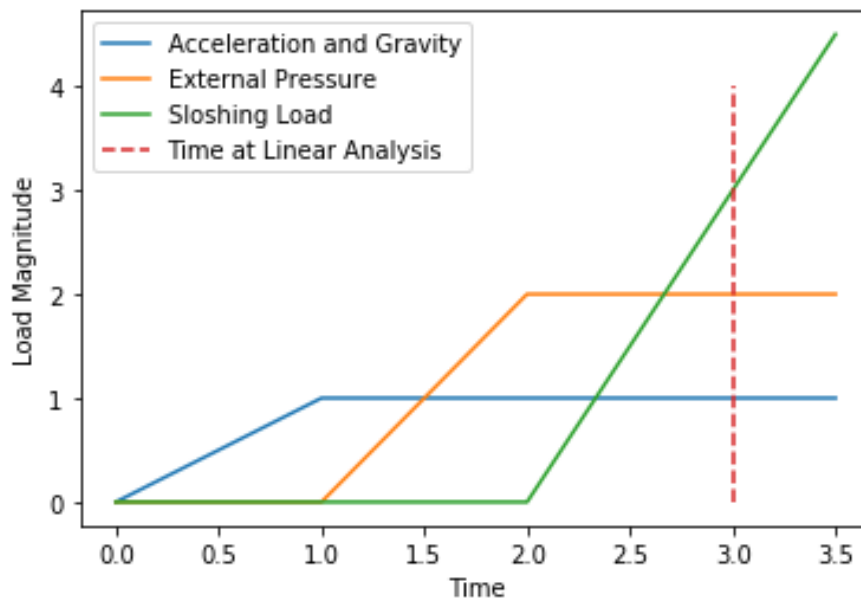


Figure 59: Plot Illustrating the Application of Loads

Linear eigenvalue analysis was attempted in order to produce suitable imperfections for the non-linear analyses. However, the linear analyses proved more difficult than anticipated, when including the sloshing load. As mentioned, the sloshing load is modelled as hydrostatic pressure, leading to tensile stresses. These tensile stresses lead to compressive stresses of approximately the same magnitude in parts of the tank above the surface of the liquid. The linear eigenvalue analysis in LS-DYNA only produces negative eigenvalues for the sloshing load. The physical interpretation is that the hydrostatic pressure is negative, leading to high compressive stresses where the absolute value of the hydrostatic pressure is largest. It seems reasonable that a negative sloshing load will be more crucial in terms of buckling. However, the nature of the loading is unphysical, and leads to a deformed shape that is different than the buckling deformation that occurs when the pressure is positive. Consequently, the linear analysis was shelved, and a non-linear analysis was used to produce suitable imperfections.

Due to the problems concerning the linear analysis, the imperfections for the further analyses have been produced by non-linear analysis. For each loading situation, a non-linear analysis has been carried out without any imperfection. The buckling deformation from these analyses was extracted, scaled, and applied to the model, and a new analysis with imperfection was done.

In the following analyses, a filling level of 29 % was planned, as that is one of the three important filling levels to analyse according to DNV GL. The additional filling levels are 50 and 65 %, measured in volume.

However, due to a mistake the filling level was 23 % for the following analyses of spherical, and stretched tank exposed to both transverse and longitudinal sloshing. The thicknesses used for these analyses, was based on scantlings provided by Moss Maritime. At a later point it was discovered that the original scantlings were very conservative. However, these analyses are important to verify the application of the loads, and these initial analyses are the basis for the further analyses.

### 11.3 Spherical Tank, 23 % Filling, 20°

The expectation of these analyses is that the sloshing load will be the most critical, and that the external pressure and the acceleration to the material will be of minor significance. To study this hypothesis, several analyses were run for the spherical tank, with different external pressures. As mentioned, the water level was wrongly set to 23 %. An illustration of the level of the LNG in the tank can be seen in Figure 60.

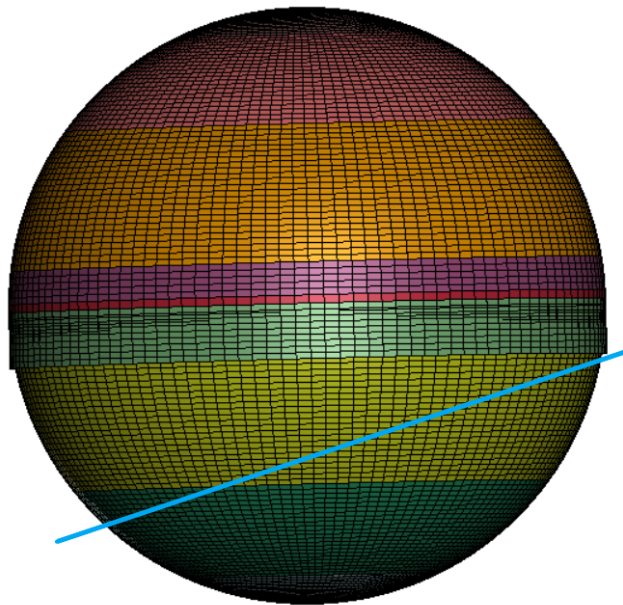


Figure 60: Sloshing Load on Spherical Tank with 23 % Filling, and 20° angle

Initially, analyses were run with four different external pressures to study the sensitivity towards the external pressure, compared to the sloshing load. Table 25 shows the critical accelerations for the analyses with different values for the external pressures. For the analyses in Table 25, imperfections were applied.

The results in Table 25 indicate that the sloshing load is the dominating load. It is unexpected that an external pressure of 0.005 and 0.02 MPa yield approximately the same strength, and that 0.01 and 0.05 MPa does the same. As increasing the external pressure will lead to higher compressive stresses, it is assumed that an increase in external pressure will lower the critical acceleration. A possible explanation to the inconsistency of the results is that the buckling shape might change slightly due to changes in the external pressure. Such a change in buckling shape might lead to an increase in critical acceleration due to an increase of the external pressure. However, the analysis with the lowest external pressure of 0.005 MPa is continued with, and as a consequence, the external pressure is set to 0.005 MPa for the analyses of the stretched tank.

Table 25: Sloshing Analysis on Sphere with Different External Pressures and Imperfections

External Pressure	Imp. Amplitude	Critical Acc. [ $m/s^2$ ]
0.005 MPa	40 mm	110
0.01 MPa	40 mm	104.1
0.02 MPa	40 mm	109.5
0.05 MPa	40 mm	105

### 11.3.1 External Pressure of 0.005 MPa

The upscaled buckling deformation can be seen in Figure 61. The deformation is according to the expectations. Figure 63 and 64 shows the meridional and the circumferential stress in the critical area. As expected, the sloshing load leads to tensile stresses in the part of the sphere just above the lower edge of the fluid surface. This is illustrated well in Figure 61. The part of the tank that buckles is "hanging" from equator, and the high tensile stresses in the meridional direction induce compressive stresses of equal magnitude in the circumferential direction. The stresses are seen to be very high when the tank buckles, and can be seen in Figures 63 and 64. Figure 65 shows very high von Mises stress in the part that buckles. This indicates a very elasto-plastic buckling. This is also confirmed by Figure 66 which is the force/displacement relation for the analyses, with and without imperfections. The impact of the imperfection is not as high as expected, but the small strength reduction due to the imperfection as well as the high stresses seen in Figure 63 to 65 indicate large effects of plasticity.

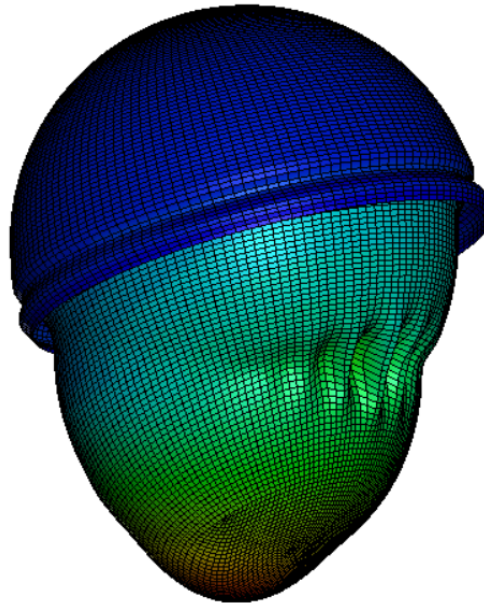


Figure 61: Displacement Scaled With a Factor of 100

LS-DYNA keyword deck by LS-PrePost  
 Time = 2.7655  
 Contours of Resultant Displacement  
 min=0, at node# 35100  
 max=0.114725, at node# 42963

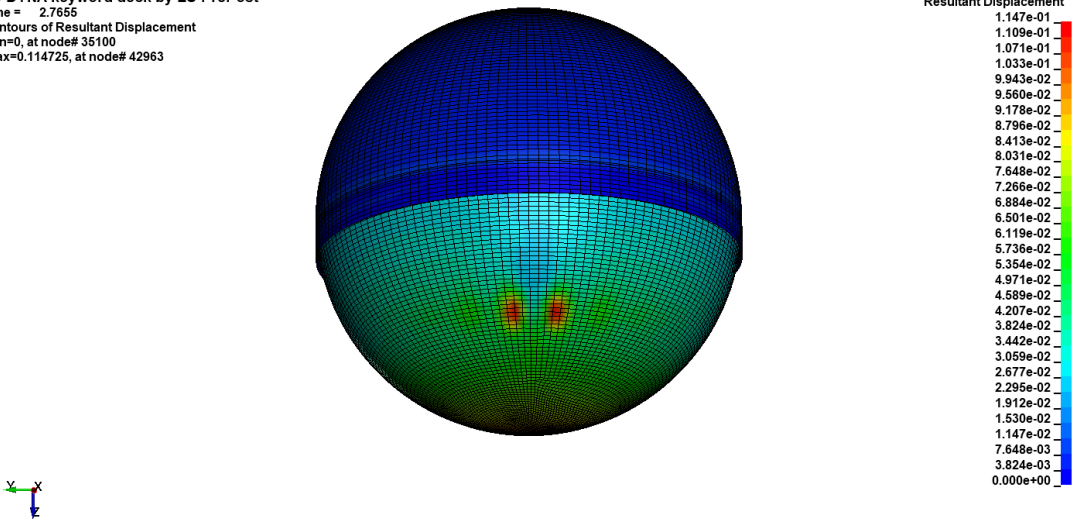


Figure 62: Sphere: 20 deg pitch, 23 % Filling; Buckling Deformation

LS-DYNA keyword deck by LS-PrePost  
 Time = 2.8004  
 Contours of Z-stress  
 max IP. value  
 min=-6.58053e+07, at elem# 9520  
 max=7.30666e+07, at elem# 16062

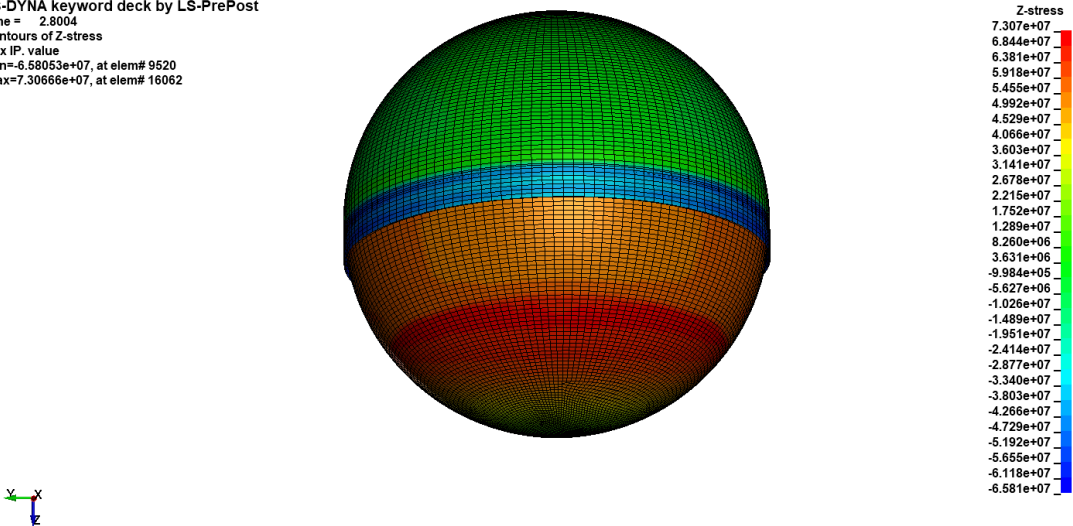


Figure 63: Sphere: 20 deg pitch, 23 % Filling; Meridional Stress

LS-DYNA keyword deck by LS-PrePost  
 Time = 2.8004  
 Contours of Y-stress  
 max IP. value  
 min=-7.70546e+07, at elem# 14863  
 max=1.49049e+08, at elem# 16595

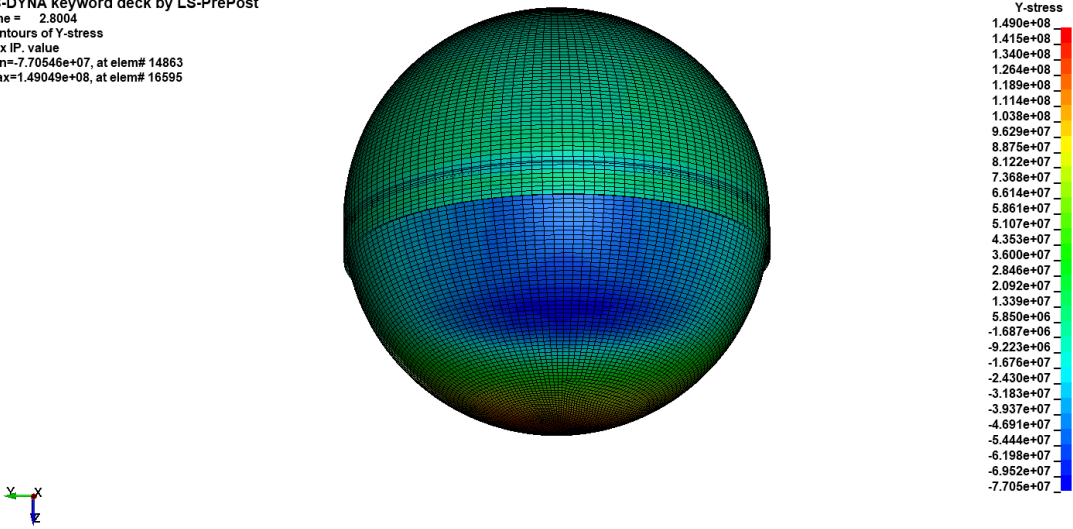


Figure 64: Sphere: 20 deg pitch, 23 % Filling; Circumferential Stress

LS-DYNA keyword deck by LS-PrePost  
 Time = 2.8051  
 Contours of Effective Stress (v-m)  
 max IP. value  
 min=913493, at elem# 8208  
 max=1.48193e+08, at elem# 16595

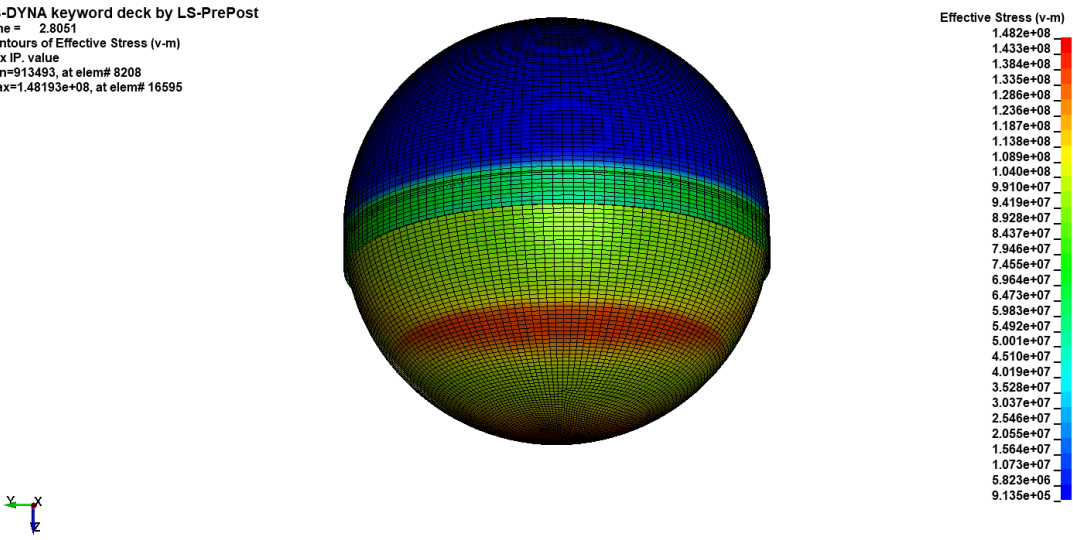


Figure 65: Sphere: 20 deg pitch, 23 % Filling; von Mises Stress

The force/displacement relation for the analysis is shown in Figure 66. It is seen that the imperfection leads to a reduction of critical acceleration from approximately 90 to 75  $m/s^2$ . This also indicates a high degree of plasticity in the failure.



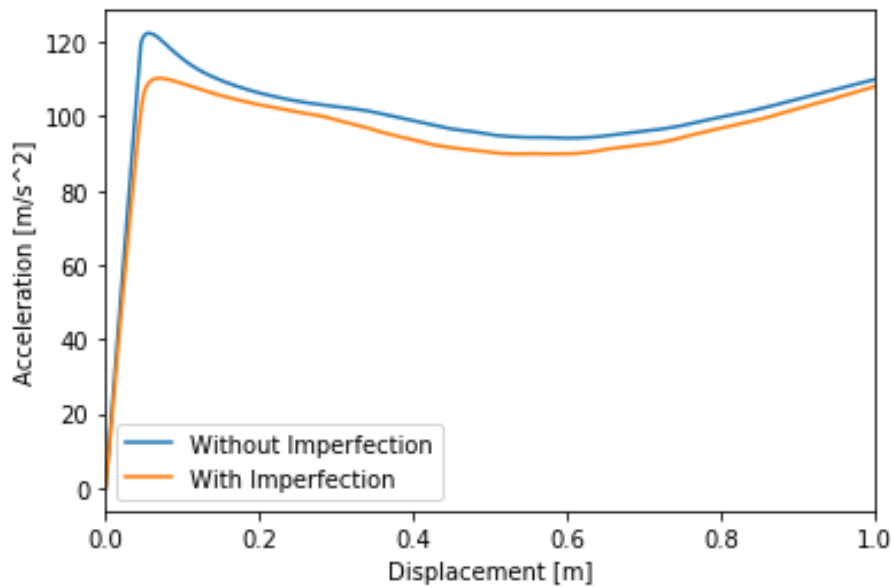


Figure 66: Force/Displacement Relation Sphere (23 % Filling)

#### 11.4 Stretched Tank, Longitudinal Sloshing, 23 % Filling, 20°

The same load conditions were applied to the tank with an angle of 20°, rotated around the beam axis. That includes the external pressure of 0.005 MPa. The angle of 20° might seem as an unrealistic pitch value. However, the physical interpretation of the angle is not that it is a pitch angle. In the longitudinally stretched tank, the fluid will be able to accelerate, and hit the tank walls with a certain momentum. This momentum is not necessarily aligned with the direction of gravity. As Class does not specify otherwise, an angle of 20° is used also for the longitudinal sloshing.

The tank, with an illustration of the fluid level when rotating the tank 20° is shown in Figure 67. The thicknesses of the different sections can be seen in Table 26. A minor modification was done to the thicknesses compared to the thicknesses used in Chapter 10. It was noted that doubling the thickness from the spherical part of the equator led to an unrealistic thickness of 290 mm for the equator on the cylindrical part. This was reduced to 260 mm. The equator does not seem as a critical part. Hence, the thickness reduction is expected to be of minor importance.

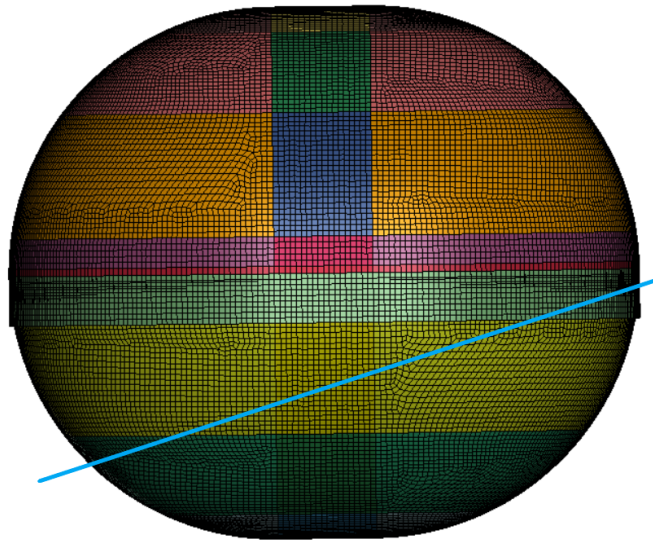


Figure 67: Longitudinal Sloshing Load on Stretched Tank with 23 % Filling, and 20° angle

Table 26: Thicknesses for Sectioned Non-Spherical Tank

Zone	Zone Height	Thickness Spherical Part	Thickness Cylindrical Part
Zone 7	2000	40	80
Zone 6	6500	32	64
Zone 5	10000	51	102
Zone 4 U	2400	57	114
Equator	1200	195	260
Zone 4 L	2400	71	142
Zone 3	10000	66	132
Zone 2	6500	53	106
Zone 1	2000	53	106
Skirt	4000	70	70

Figure 68 shows the buckling deformation of the tank exposed to longitudinal sloshing. The buckling seems to occur just above the liquid surface, in the upper connection between the spherical and the cylindrical part. The deformation is in accordance with the expectations.

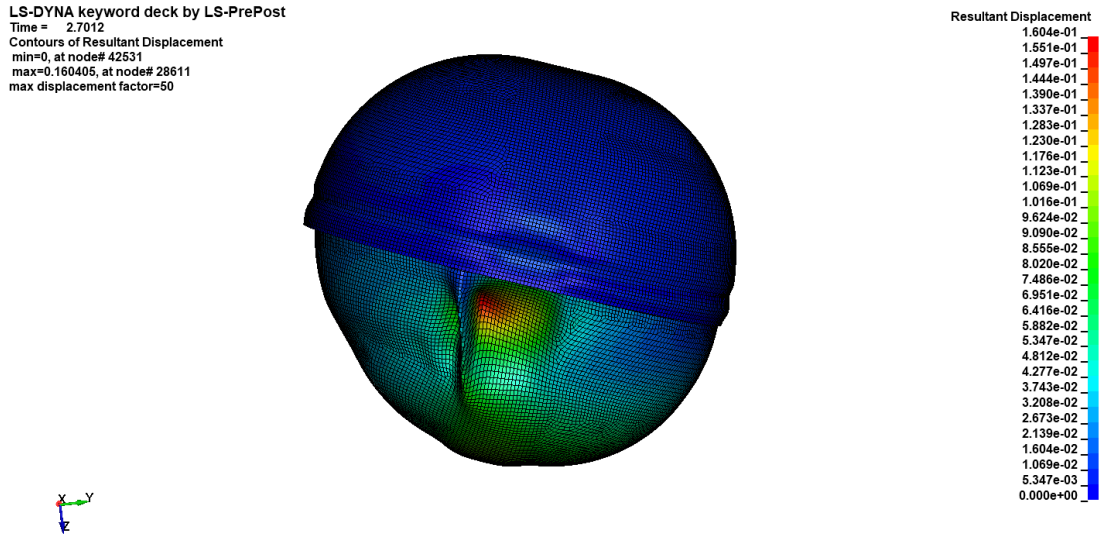


Figure 68: Longitudinal Sloshing, 20 deg pitch, 23 % Filling: Scaled Displacement of Tank (Factor=50)

Figure 69 and 70 shows the vertical and longitudinal membrane stresses before failure. Similarly to the sphere, large compressive stresses occur in the longitudinal direction, induced by the high tensile stresses in the vertical direction. As for the sphere, the magnitudes of the stress component are very high when buckling occurs. A stress situation with high tensile and compressive stress in each direction leads to high values of von Mises stress. The von Mises stress can be seen in Figure 71, and reaches magnitudes of more than 154 MPa. This is significantly larger than the yield stress and indicates a high degree of plasticity. However, the Ramberg-Osgood model used in this analysis yields a maximum strength of more than 300 MPa, although this is at very high strain values. The force-displacement relation for both the analysis with and without imperfection can be seen in Figure 72.

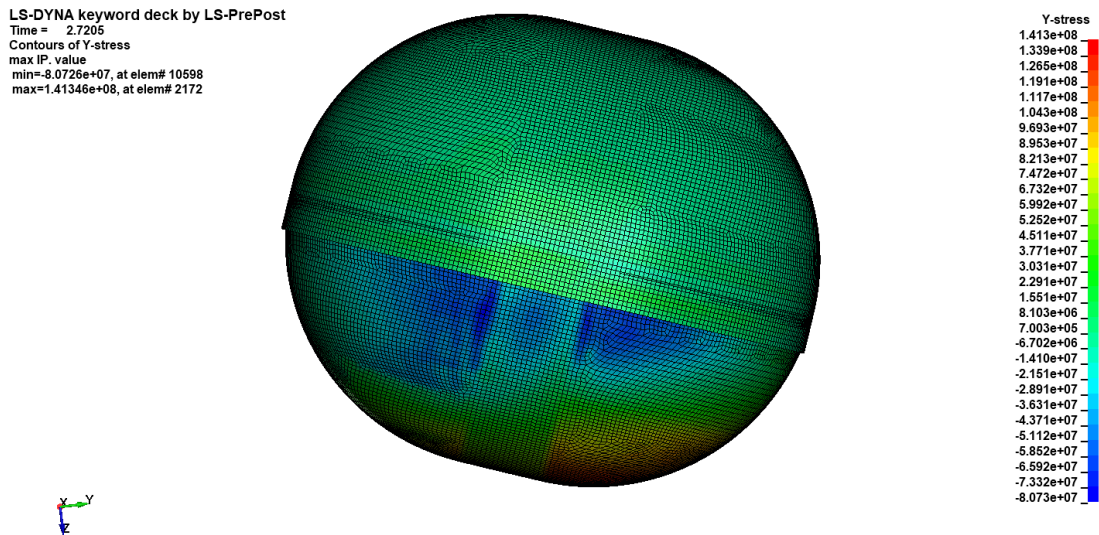


Figure 69: Longitudinal Sloshing, 20 deg pitch, 23 % Filling: Longitudinal Stress

LS-DYNA keyword deck by LS-PrePost  
 Time = 2.7205  
 Contours of Z-stress  
 max IP. value  
 min=-6.81951e+07, at elem# 18166  
 max=9.75945e+07, at elem# 9883

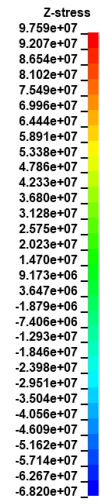
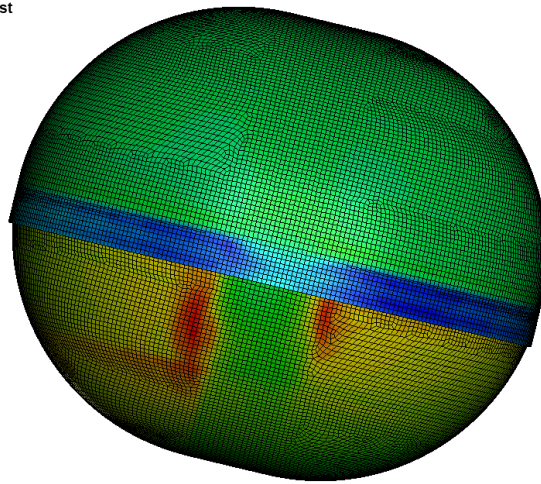


Figure 70: Longitudinal Sloshing, 20 deg pitch, 23 % Filling: Vertical Stress

LS-DYNA keyword deck by LS-PrePost  
 Time = 2.7205  
 Contours of Effective Stress (v-m)  
 max IP. value  
 min=564684, at elem# 34620  
 max=1.54337e+08, at elem# 6360

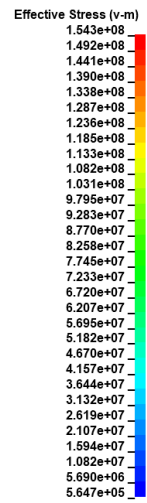
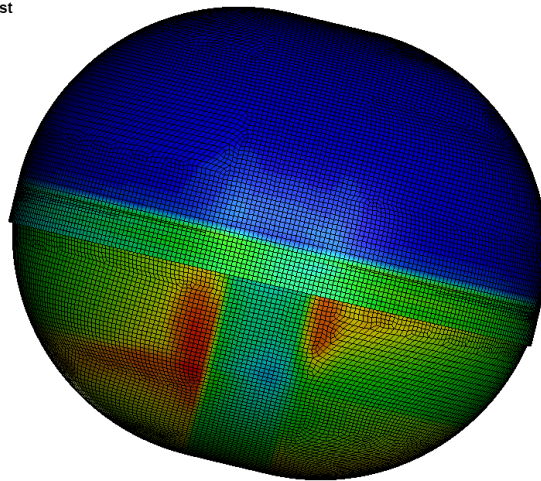


Figure 71: Longitudinal Sloshing, 20 deg pitch, 23 % Filling: Von Mises Stress

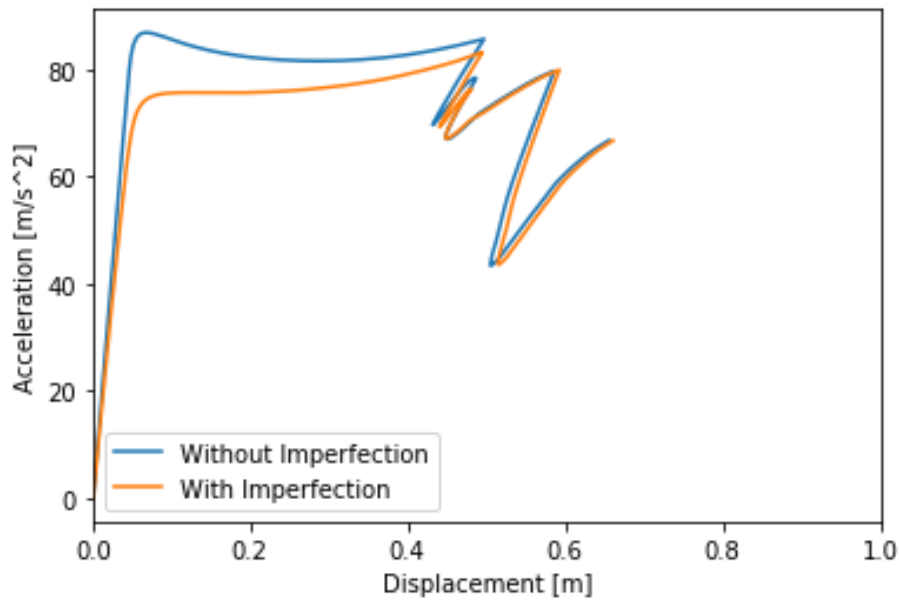


Figure 72: Force/Displacement Relation, Longitudinal Sloshing (23 % Filling)

### 11.5 Stretched Tank, Transverse Sloshing, 23 % Filling, 20°

For the transverse sloshing, the stretched tank is given a heel angle of 20°. The tank including fluid level, seen from the aft or the bow is illustrated in Figure 60 in Section 11.3. Except the orientation of the tank, the tank exposed to transverse sloshing is identical to the tank exposed to longitudinal sloshing. The thicknesses of the tank sections can be seen in Table 26.

The deformation of the tank is in order with the expectations. The buckling occurs in the part of the tank just above the fluid level. Figure 74 shows that considerable compressive stresses are induced in the part of the tank, "hanging" from the equator. In this part, high tensile stresses in the vertical direction can be seen in Figure 75. Prior to buckling the tensile stresses seem to concentrate to the two connections between the cylinder and the spherical parts. This leads to very large von Mises stress in the same parts. The von Mises stress can be seen in Figure 76. Also in this case, the von Mises stress is larger than the yield stress before buckling, which indicates a large degree of plasticity. The buckling shape seems to be a combined shape, in the connection between the cylinder and the spherical parts. This might be due to discontinuities in the connection, leading to considerable local curvature and bending stresses. This aspect was explained in Section 2.3.

LS-DYNA keyword deck by LS-PrePost  
 Time = 2.5383  
 Contours of Resultant Displacement  
 min=0, at node# 42531  
 max=0.212246, at node# 27405  
 max displacement factor=20

Resultant Displacement

2.122e-01
2.052e-01
1.981e-01
1.910e-01
1.839e-01
1.769e-01
1.698e-01
1.627e-01
1.556e-01
1.486e-01
1.415e-01
1.344e-01
1.273e-01
1.203e-01
1.132e-01
1.061e-01
9.905e-02
9.197e-02
8.490e-02
7.782e-02
7.075e-02
6.367e-02
5.660e-02
4.952e-02
4.245e-02
3.537e-02
2.830e-02
2.122e-02
1.415e-02
7.075e-03
0.000e+00

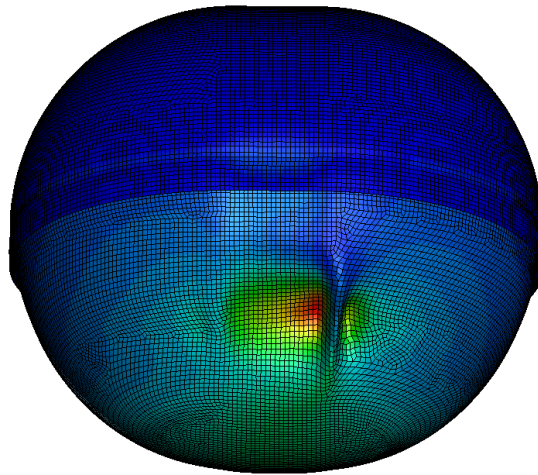


Figure 73: Transverse Sloshing, 20 deg heel, 23 % Filling: Scaled Displacement of Tank (Factor=20)

LS-DYNA keyword deck by LS-PrePost  
 Time = 2.528  
 Contours of Y-stress  
 max IP. value  
 min=-7.41036e+07, at elem# 5531  
 max=1.11101e+08, at elem# 1627

Y-stress

1.111e+08
1.049e+08
9.875e+07
9.258e+07
8.641e+07
8.023e+07
7.406e+07
6.789e+07
6.171e+07
5.554e+07
4.937e+07
4.319e+07
3.702e+07
3.085e+07
2.467e+07
1.850e+07
1.233e+07
6.162e+06
-2.164e+04
-6.195e+06
-1.237e+07
-1.854e+07
-2.472e+07
-3.089e+07
-3.706e+07
-4.324e+07
-4.941e+07
-5.558e+07
-6.176e+07
-6.793e+07
-7.410e+07

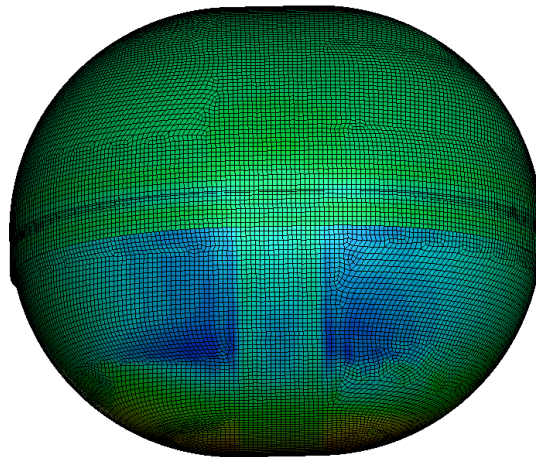


Figure 74: Transverse Sloshing, 20 deg heel, 23 % Filling: Longitudinal Stress

LS-DYNA keyword deck by LS-PrePost  
 Time = 2.528  
 Contours of Z-stress  
 max IP. value  
 min=-4.31132e+07, at elem# 17817  
 max=8.20254e+07, at elem# 5529

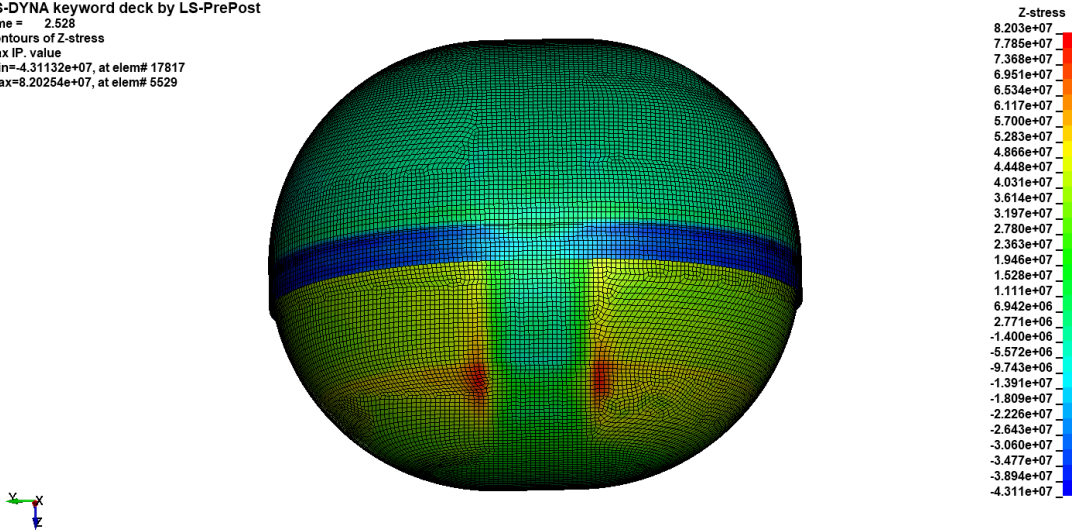


Figure 75: Transverse Sloshing, 20 deg heel, 23 % Filling: Vertical Stress

LS-DYNA keyword deck by LS-PrePost  
 Time = 2.528  
 Contours of Effective Stress (v-m)  
 max IP. value  
 min=808432, at elem# 33810  
 max=1.36998e+08, at elem# 6129

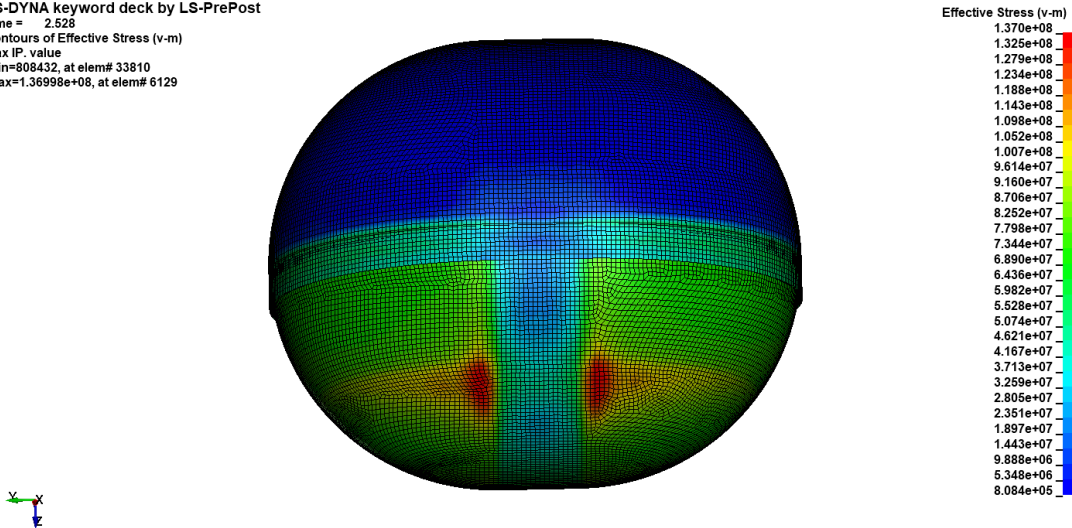


Figure 76: Transverse Sloshing, 20 deg heel, 23 % Filling: Von Mises Stress

Similarly to the spherical tank and the stretched tank exposed to longitudinal sloshing, the effect of imperfections seem to be quite low, even though a strength reduction of approximately 20 % seems to be normal. As for the other load conditions, the quite low imperfection sensitivity indicates a high degree of plasticity.

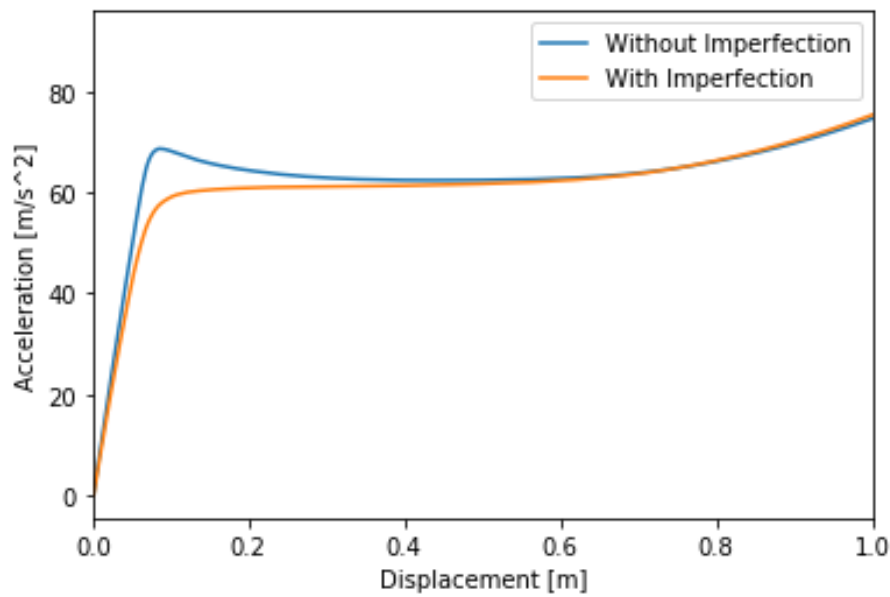


Figure 77: Force/Displacement Relation, Transverse Sloshing (23 % Filling)

## 11.6 Summary of Section 11

This section will briefly evaluate the results obtained in the three analyses in Chapter 11. The spherical tank seems to be significantly stronger than the stretched tank, exposed to the same sloshing load. Transverse sloshing seems to be the more critical sloshing load on the stretched tank. This is also believed to be the more likely load, due to large heel motions of ships compared to pitch.

Table 27: Comparison of Critical Buckling Loads

	Imp. Amplitude	Critical Acc. [ $m/s^2$ ]
Sphere	40 mm	110
Longitudinal Sloshing	40 mm	75
Transverse Sloshing	40 mm	57

As mentioned, the filling ratio was not correct, and was supposed to be 29 % instead of 23 %. Additionally, the thicknesses of both the spherical and the stretched tank were taken as very conservative, and it was discovered that the thicknesses should be reduced significantly to represent a realistic LNG-tank.

The imperfection sensitivity has been addressed and seems to be approximately the same for all three analyses. The failure due to sloshing load, seems to be of a more plastic character than the failure for a tank only exposed to external pressure. This is also based on the stress values being very high, with a von Mises stress higher than the material yield stress.

Transverse sloshing seems to be more critical to the stretched tank than longitudinal sloshing. Hence, only transverse sloshing of the stretched tank will be subject to further analysis. The spherical tank will also be subject to further analysis, for comparison with the stretched tank. Several filling levels will also be analysed in the further sloshing analyses, in order to identify the most critical load condition.



## 12 Analysis of Spherical Tank Exposed to Only Vertical Acceleration

Large critical sloshing accelerations were obtained when analysing the sloshing load, which is believed to be the decisive load. Before continuing the analysis of the sloshing load with updated thicknesses etc. a simple analysis with only vertical accelerations was done, in order to evaluate the impact of the vertical acceleration. The scantlings are the same as used in Chapter 13, but the load is reduced to only vertical acceleration.

Initially, a linear eigenvalue analysis was done. Furthermore, the first mode was used as an imperfection in the following non-linear analysis. The critical accelerations are listed in Table 28, and contour plots for both the linear and the non-linear analysis can be seen in Figures 78 and 79, respectively.

Table 28: Imperfection Effect on Longitudinal Sloshing (20 deg heel and 29 % Filling)

	Imp. Amplitude	Critical Acc. [ $m/s^2$ ]	Knock-Down Factor
Linear Analysis	N.A.	1535 (153 g)	N.A.
Non Linear Analysis	40 mm	581 (58 g)	0.38

The critical accelerations are seen to be very high, and even the non-linear analysis with a knock-down factor of 0.38 yields a critical acceleration corresponding to 58 g. Based on these results, it is deemed unlikely that the acceleration on the material has a major impact on the strength of LNG-tanks. Initially, the purpose of these analyses was also to compare the results with similar results for the stretched tank. However, a combination of very large accelerations, and difficulties with running a successful linear analysis of the stretched tank, lead to the decision of shelving the analysis of the stretched tank, and continue with the sloshing analyses of both a spherical and a non-spherical tank with realistic thicknesses.

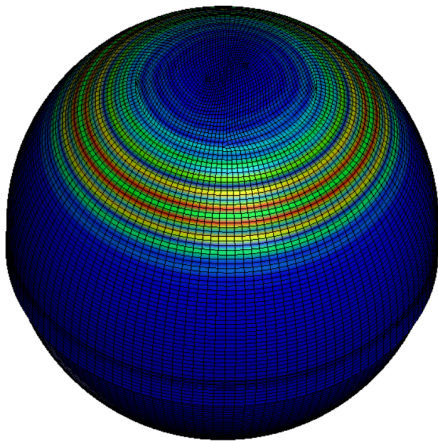


Figure 78: 1. Eigenmode, Linear Analysis

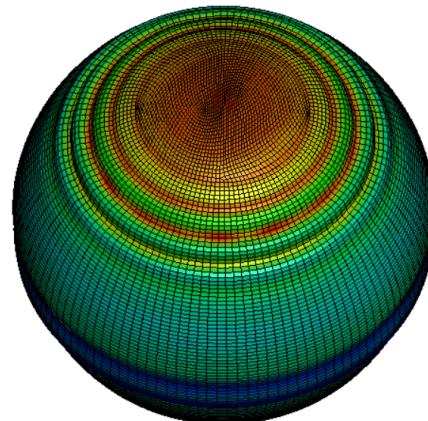


Figure 79: Displacement, Non Linear Analysis

## 13 Sloshing Analyses With Realistic Thicknesses

During the project it was discovered that the scantlings used for the different sections up to this point were very conservative. Consequently, it was decided to reduce the thicknesses, based on new, more realistic scantlings provided by Moss Maritime. In addition to the general reduction in thickness, some additional changes were done between the analyses described in Chapter 11, and the analyses in this chapter.

Additional load factors were applied to both the external pressure, and the acceleration on the material due to gravity and ship motions. This was done in accordance with Class Guidelines [7]. The external pressure was multiplied by a load factor of 1.5, which increased the pressure from 0.005 to 0.0075 MPa. The acceleration on the material was multiplied with a load factor of 1.2, which lead to a design acceleration of the tank of  $18.06 \text{ m/s}^2$  instead of  $15.05 \text{ m/s}^2$ .

Additionally, the filling level was changed. As described in Section 11.6, the level of the LNG was wrong in the last analysis, as the filling level was 23 % instead of 29 %. This was corrected, and analyses with a filling level of 29 % were carried out. In addition, analyses with a filling level of both 50 and 65 % were done according to the Class Guidelines [7]. The presented results are the results from the analysis with a filling level of 50 %, as this proved to be the most severe filling level. The heel angle for the analyses remains unchanged and is set to  $20^\circ$ . An illustration of the fluid level for the sloshing level can be seen in Figure 80.

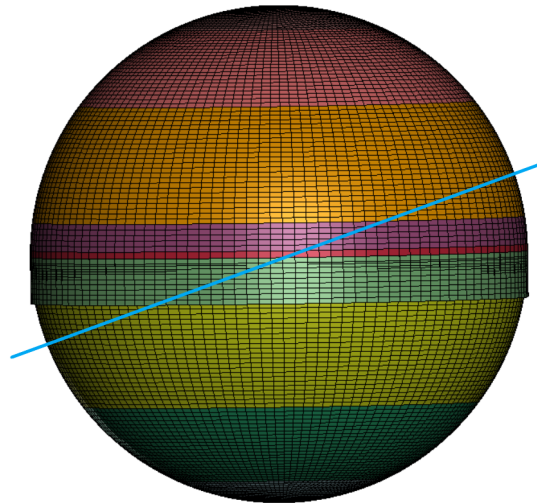


Figure 80: Illustration of Sloshing Load with 50 % Filling, and  $20^\circ$  angle

For the two following tanks, both spherical and stretched, the contour plots showing the different stress components are taken from the analysis without any imperfection. The reason for this is to be able to extract stress values that increases linearly with acceleration, to compare with DNV GL Class Guidelines. For the analyses with imperfection, the stress development is expected to be more irregular, than for the analyses without imperfection.

### 13.1 Spherical Tank, $20^\circ$ Heel and 50 % Filling

Initially, the spherical tank with realistic scantlings was analysed. The scantlings of the tank are presented in Table 29, and the load parameters are presented in Table 30. The loads are applied in the same way as illustrated in Figure 59.

Table 29: Realistic Thicknesses For Spherical Tank

Zone	Zone Height [mm]	Thickness [mm]
Zone 7	2000	30
Zone 6	6500	29
Zone 5	10000	40
Zone 4 U	2400	47
Equator	1200	169
Zone 4 L	2400	57
Zone 3	10000	48
Zone 2	6500	39
Zone 1	2000	41
Skirt	4000	70

Table 30: Load Table for Analysis of Tanks with Realistic Thicknesses

External Pressure	0.0075 MPa
Acceleration on Material	18.06 $m/s^2$
Sloshing Acc.	Increasing until failure

Figure 81 shows the force-displacement relation for the spherical tank. The imperfection of 40 mm leads to a reduction of the critical acceleration of approximately 20 %. The curve implies a noteworthy post-buckling capacity. However, the displacements become significantly larger than what can be tolerated.

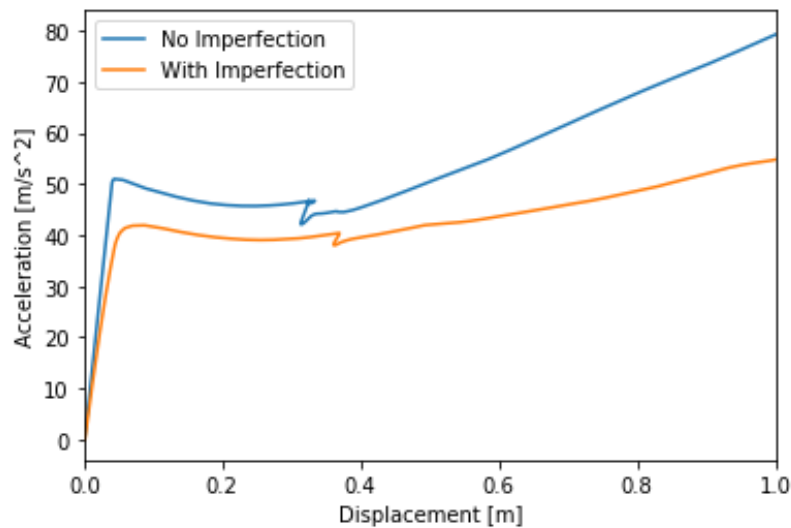


Figure 81: Spherical Tank with Realistic Scantlings: Displacement/Force Relation

Table 31: Imperfection Effect on Spherical Tank (20 deg heel and 50 % Filling)

	Imp. Amplitude	Critical Acc. [ $m/s^2$ ]	Strength Reduction Factor
No Imperfection	N.A.	52	N.A.
With Imperfection	40 mm	42	0.81

Figure 82 shows the buckling shape of the spherical tank. The deformation is in line with the expectations. The compressive stresses in Figure 83 are large between the equator and the surface of the LNG when the tank is rotated 20°. The meridional stresses act as tensile stresses of approximately the same magnitude as the compressive stresses. Even higher meridional stresses occur close to the bottom of the tank, where the pressure is highest. Figure 85 shows that the von Mises stress is very high in the part of the tank that buckles. This indicates that the collapse is of elasto-plastic nature.

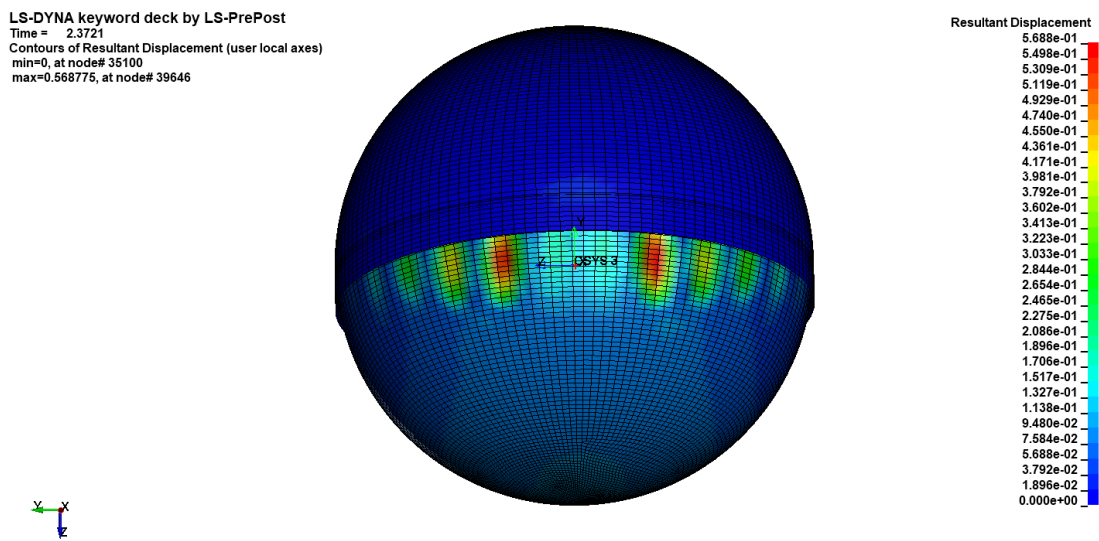


Figure 82: Sphere with Realistic Scantlings: Buckling Deformation

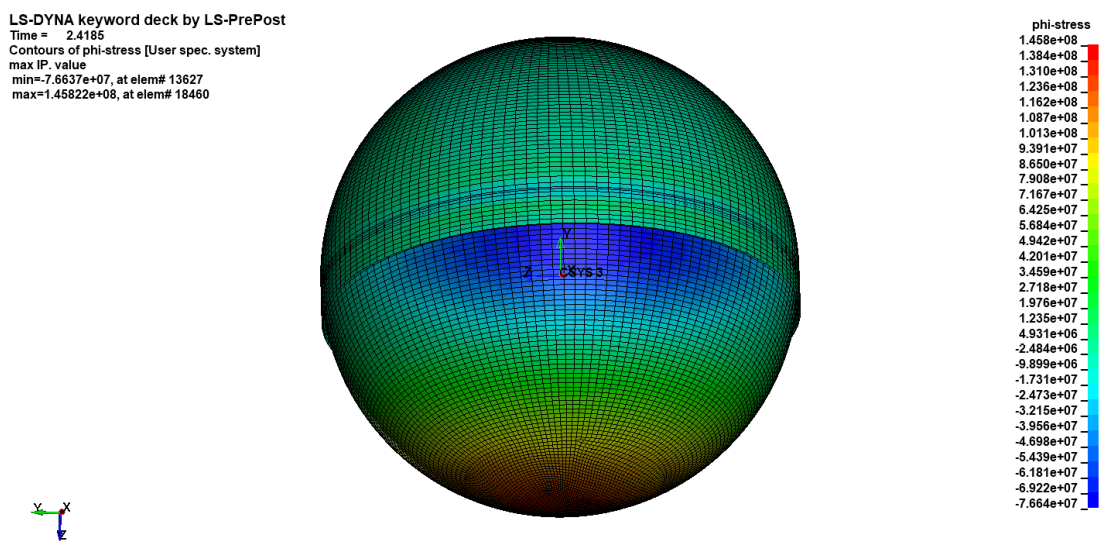


Figure 83: Sphere with Realistic Scantlings: Circumferential Stress

LS-DYNA keyword deck by LS-PrePost  
 Time = 2.4185  
 Contours of theta-stress [User spec. system]  
 max IP. value  
 min=-5.35686e+07, at elem# 9806  
 max=1.43619e+08, at elem# 15141

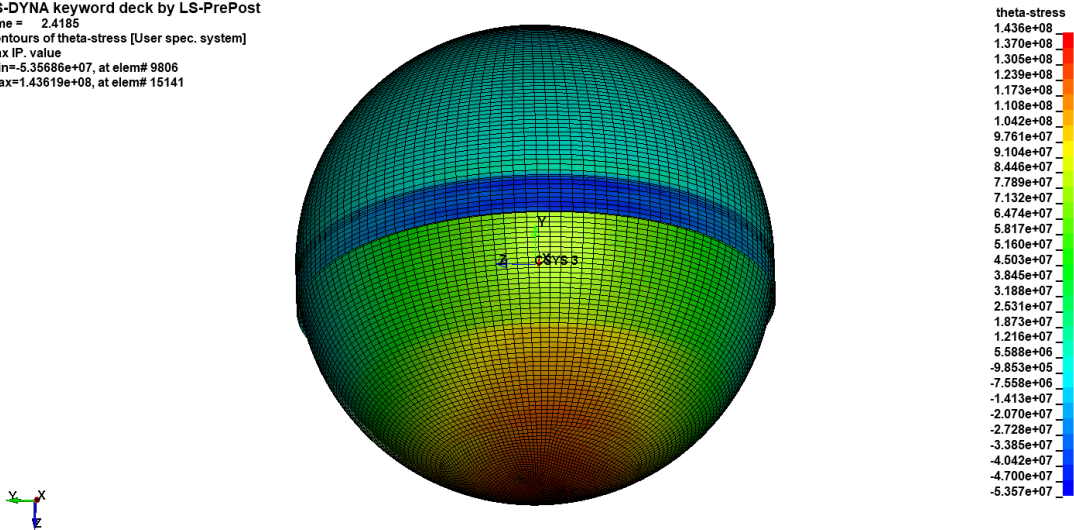


Figure 84: Sphere with Realistic Scantlings: Meridional Stress

LS-DYNA keyword deck by LS-PrePost  
 Time = 2.4185  
 Contours of Effective Stress (v-m)  
 max IP. value  
 min=592814, at elem# 7889  
 max=1.43622e+08, at elem# 13774

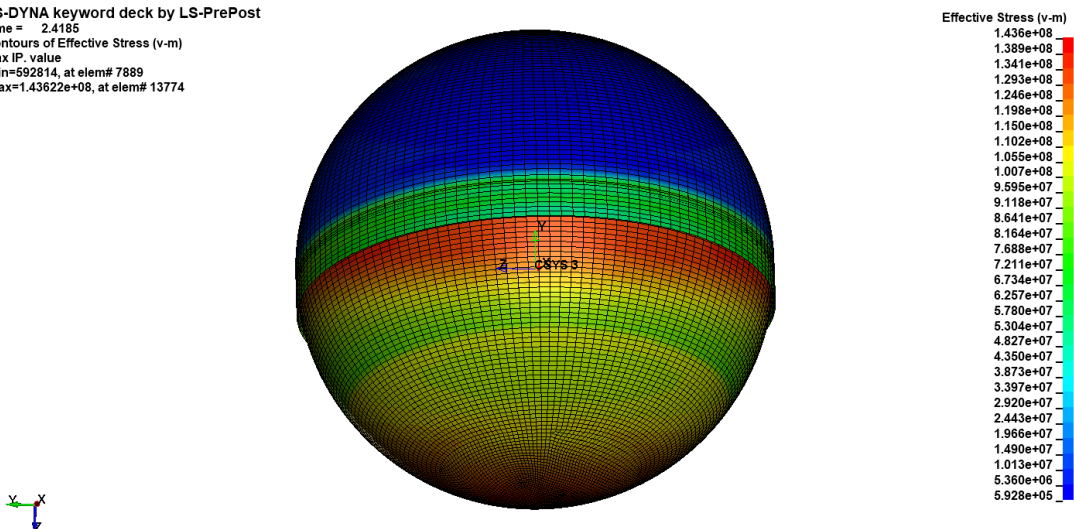


Figure 85: Sphere with Realistic Scantlings: Von Mises Stress

### 13.2 DNV GL Buckling Check of Spherical Tank

Section 3.4 describes a procedure defined by Class where the input is design stresses in the tank, either found by simplified calculations or by FEM-analysis. In this case the stresses induced by the sloshing load at different accelerations are used in the buckling check. The script used to perform the buckling check can be seen in Appendix B.7. The buckling check is performed with the extracted stresses at the green dots in Figure 86. The criteria to be fulfilled in the buckling check is:

$$g > 0 \text{ and } h > 1.0 \tag{51}$$

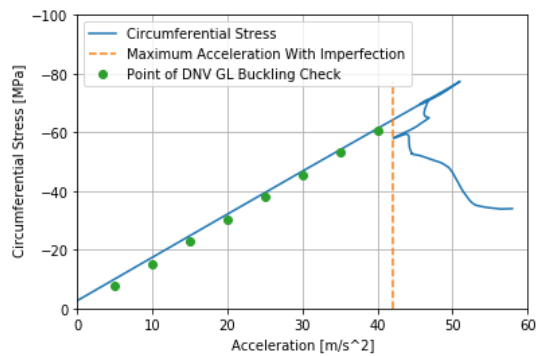
The results of the buckling check can be seen in Table 32. The stresses induced by an acceleration of  $20 \text{ m/s}^2$  passes the test narrowly. The calculation of a design sloshing load, based on Class Guidelines yields a design acceleration of  $13.7 \text{ m/s}^2$ . Multiplying this with a load factor of 1.2, yields a maximum of  $16.4 \text{ m/s}^2$ . Thus, the critical acceleration of  $20 \text{ m/s}^2$  is well above the design acceleration.

This may indicate a safety factor of 1.22. However, how to interpret the safety factor is more complicated than in most cases. One part of the acceleration is simply due to gravity, inducing an acceleration of  $9.81 \text{ m/s}^2$ . Hence, one could argue that only  $6.6 \text{ m/s}^2$  is due to sloshing of the fluid for the design acceleration, and  $10.2 \text{ m/s}^2$  for the maximum acceleration passing the buckling check. Such an interpretation yields a safety factor of 1.55.

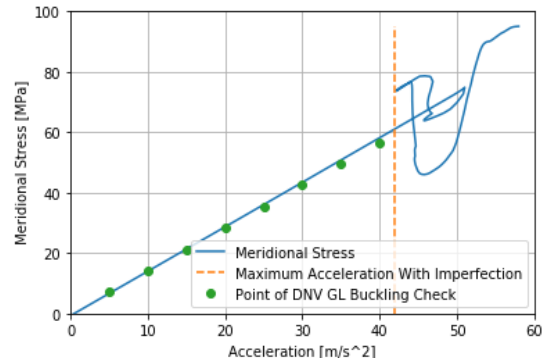
Additionally, the FEA performed in LS-DYNA indicates a capacity of  $40 \text{ m/s}^2$ , which is twice the limit of the DNV GL buckling check. As the stresses increase approximately linearly with increasing acceleration, the maximum compressive and tensile stresses induced by the acceleration are also approximately twice the maximum allowed stresses by Class.

Table 32: Buckling Check (DNV GL) with Extracted Stresses

Accelerations	Circumferential Stress[MPa]	Meridional Stress [MPa]	$g$	$h$	Test
5	-7.6	7.08	4.40	4.0	Passed
10	-15.2	14.16	1.47	2.0	Passed
15	-22.8	21.24	0.49	1.34	Passed
20	-30.4	28.32	0.008	1.005	Passed
25	-38	35.4	-0.29	0.80	Failed
30	-45.6	42.48	-0.48	0.67	Failed
35	-53.2	49.56	-0.62	0.57	Failed
40	-60.8	56.64	-0.72	0.50	Failed



(a) Circumferential Stress



(b) Meridional Stress

Figure 86: Spherical Tank: Principal Stress Components

### 13.3 Transverse Sloshing in Stretched Tank, 20° heel and 50 % Filling

A similar analysis as the sloshing analysis for the spherical tank was done for a stretched tank. The sloshing load is applied as transverse sloshing with a heel angle of 20°. The scantlings for the tank are presented in Table 33, and the loads are the same as for the spherical tank, see Table 30.

Table 33: Realistic Thicknesses for Sectioned Non-Spherical Tank

Zone	Zone Height [mm]	Thickness Spherical Part [mm]	Thickness Cylindrical Part [mm]
Zone 7	2000	30	60
Zone 6	6500	29	58
Zone 5	10000	40	80
Zone 4 U	2400	47	94
Equator	1200	169	216
Zone 4 L	2400	57	114
Zone 3	10000	48	96
Zone 2	6500	39	78
Zone 1	2000	41	82
Skirt	4000	70	70

Figure 87 shows the force-displacement relation of the stretched tank exposed to transverse sloshing. The nature of the collapse is different to that of the spherical tank. For the analysis with no imperfection, the relationship is linear up to an acceleration of approx.  $29 \text{ m/s}^2$ . At that point, a plateau relationship occurs, where the acceleration is constant in the vicinity of  $29 \text{ m/s}^2$ , while the displacement increases drastically. The plot for the analysis with imperfection shows that the relationship becomes non-linear earlier. It is more complicated to extract a critical value based on this plot, but  $23 \text{ m/s}^2$  is deemed suitable. As the acceleration increases, the analysis with imperfection seems to reach the same plateau as the one without imperfection. This indicates a strength reduction of approximately 20 % also for the stretched tank.

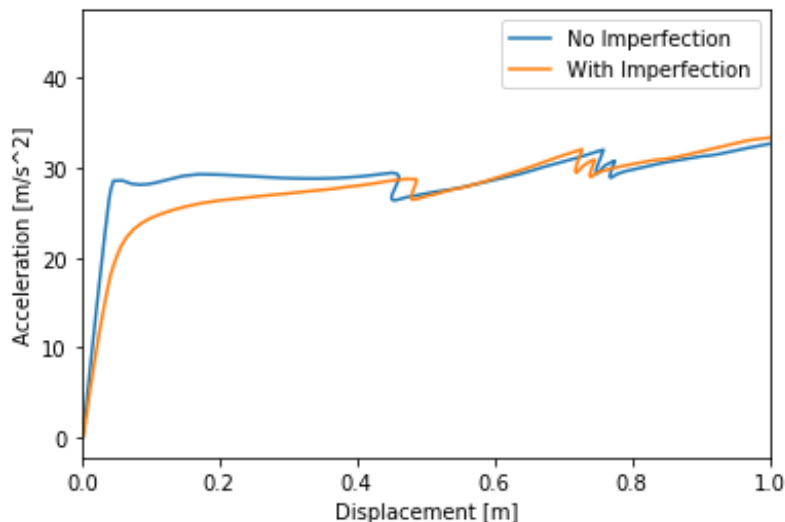


Figure 87: Stretched Tank with Realistic Scantlings: Displacement/Force Relation

Table 34: Imperfection Effect on Transverse Sloshing (20 deg heel and 50 % Filling)

	Imp. Amplitude	Critical Acc. [ $m/s^2$ ]	Strength Reduction Factor
No Imperfection	N.A.	29	N.A.
With Imperfection	40 mm	23	0.79

Figure 88 shows the buckling deformation of the tank. The tank seems to buckle in the spherical part, close to the cylinder. This is confirmed by the large von Mises stresses in this regions prior to the buckling, seen in Figure 89. Figure 90 shows that the compressive stresses are larger in the spherical parts. The relationship between compressive stress in the spherical parts and cylinder seem to be related to the thickness of the cylinder being twice to that of the sphere. Figure 91 shows that the vertical tensile stress seems to concentrate in the corner of spherical parts, the cylinder, and the skirt, leading to the high von Mises stress in this area.

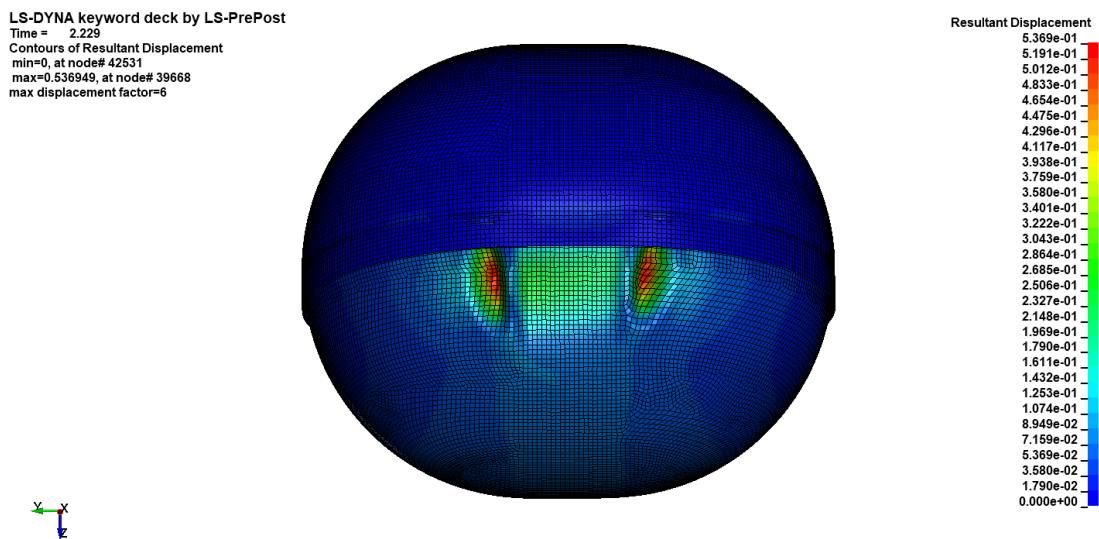


Figure 88: Stretched Tank with Realistic Scantlings: Buckling Deformation

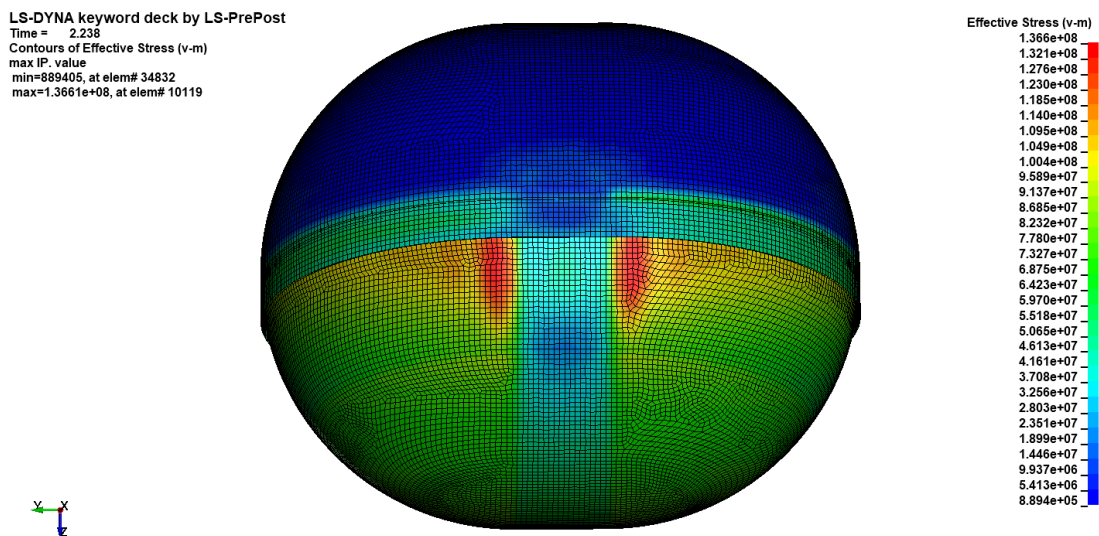


Figure 89: Stretched Tank with Realistic Scantlings: von Mises Stress



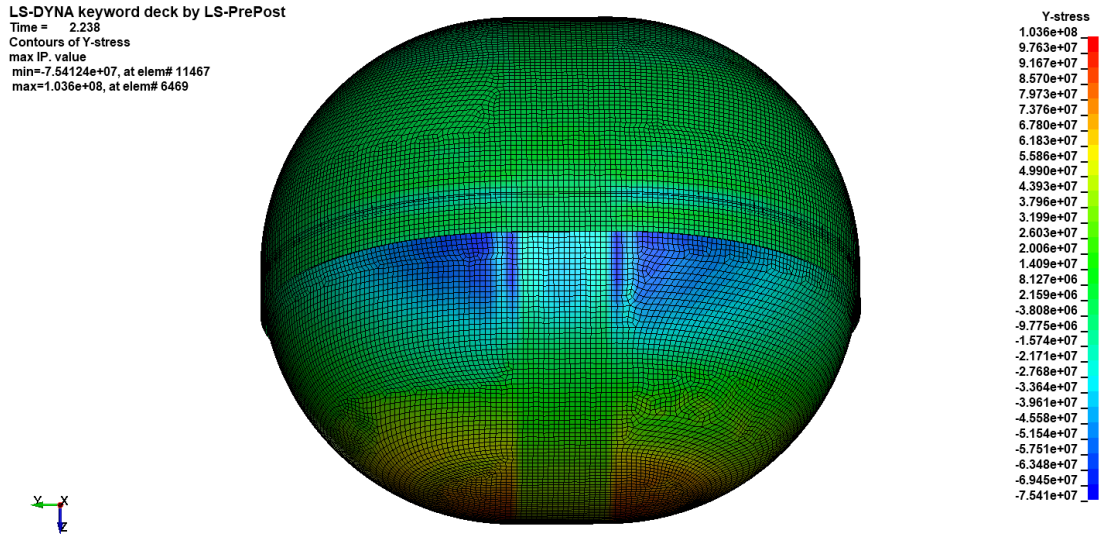


Figure 90: Stretched Tank with Realistic Scantlings: Longitudinal Stress

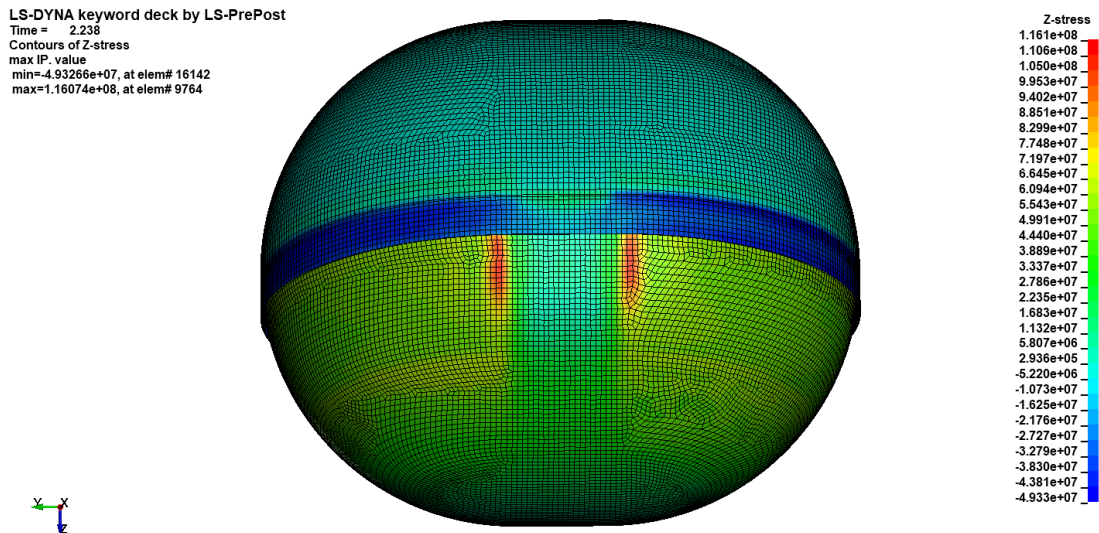


Figure 91: Stretched Tank with Realistic Scantlings: Vertical Stress

### 13.4 DNV GL Buckling Check of Stretched Tank

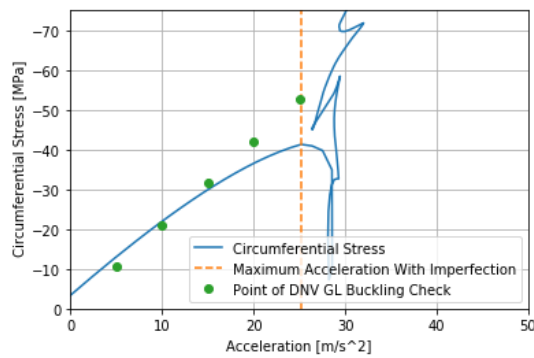
The buckling check procedure using extracted stresses by DNV GL was also done for the stretched tank. DNV GL has one buckling check procedure for the spherical tank, and one for the cylindrical part. The procedure for the highest compressive stresses in the sphere is the same as the one used in Section 13.2. The buckling check for the cylindrical part has also been written as a script, see Appendix B.8.

#### 13.4.1 Spherical Caps

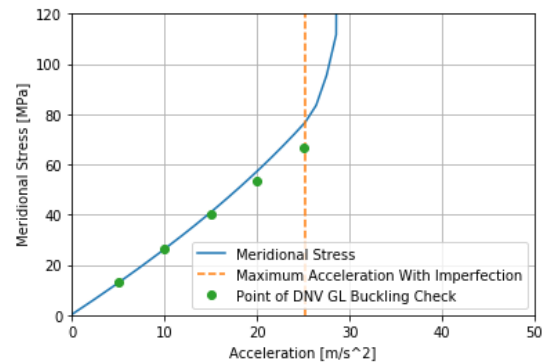
The results of the buckling check of the spherical part are presented in Table 35. An acceleration of  $15 \text{ m/s}^2$  barely passes the test, and interpolation indicates that the maximum acceleration is  $15.6 \text{ m/s}^2$ . This is below the design acceleration of  $16.4 \text{ m/s}^2$ . This indicates that this tank would not pass the sloshing test, and the tank would require strengthening.

Table 35: Buckling Check (DNV GL) For Spherical Caps

Accelerations	Circumferential Stress [MPa]	Meridional Stress [MPa]	$g$	$h$	Test
5	-10.515	13.31	3	3.1	Passed
10	-21.03	26.62	0.789	1.55	Passed
15	-31.545	39.93	0.05	1.03	Passed
20	-42.06	53.24	-0.32	0.78	Failed
25	-52.575	66.55	-0.54	0.62	Failed



(a) Longitudinal Stress



(b) Meridional Stress

Figure 92: Stretched Tank: Principal Stress Components in Spherical Part

### 13.4.2 Cylindrical Part

The buckling check for the cylinder does not use the same parameters  $g$  and  $h$  as the buckling check for the sphere. The output of the procedure is a usage factor, and a maximum allowable usage factor. If the usage factor is smaller than the maximum allowed value, the test is passed. This procedure also includes shear stress. For this analysis the shear stress is set to 1 MPa for all accelerations, which is an upper limit, as the shear stresses are of negligible size.

Table 36 shows the results from the buckling check at the same accelerations as for the spherical parts. The green dots in Figure 93 represents the stresses used in the buckling check.

The buckling check is passed by a serious margin. This confirms that the spherical part is the most critical in this load condition. In this analysis, the circumferential direction is defined as stresses in planes parallel to the equator. Meridians correspond to the longitudinals drawn from the two poles, or in this case, the top and the bottom of the tank. Hence, the meridional stresses will in this case correspond to what is usually referred to as circumferential stresses in cylinders, being stresses in the ring-direction. Furthermore, the stresses described as circumferential will correspond to what is usually referred to as axial stresses in a cylinder. A cylinder with a small length/radius relation, such as this one, will be more vulnerable to compressive stresses in the ring-direction. Table 36 shows that the meridional stresses are tensile, and will not be critical to buckling. The compressive stresses will act as axial stresses on the cylinder, in which the cylinder is strong. This might to some extent explain that the spherical parts will be the weaker part of a longitudinally stretched tank exposed to sloshing.

Table 36: Buckling Check (DNV GL) for Cylindrical Part

Acc. [ $m/s^2$ ]	Circ. Str[MPa]	Mer. Str [MPa]	Sh Str. [MPa]	Usage Fac.	Max. UF	Test
5	-7.265	1.64	1	0.075	0.84	Passed
10	-14.53	3.28	1	0.141	0.84	Passed
15	-21.795	4.92	1	0.206	0.84	Passed
20	-29.06	6.56	1	0.272	0.84	Passed
25	-36.325	8.2	1	0.34	0.84	Passed

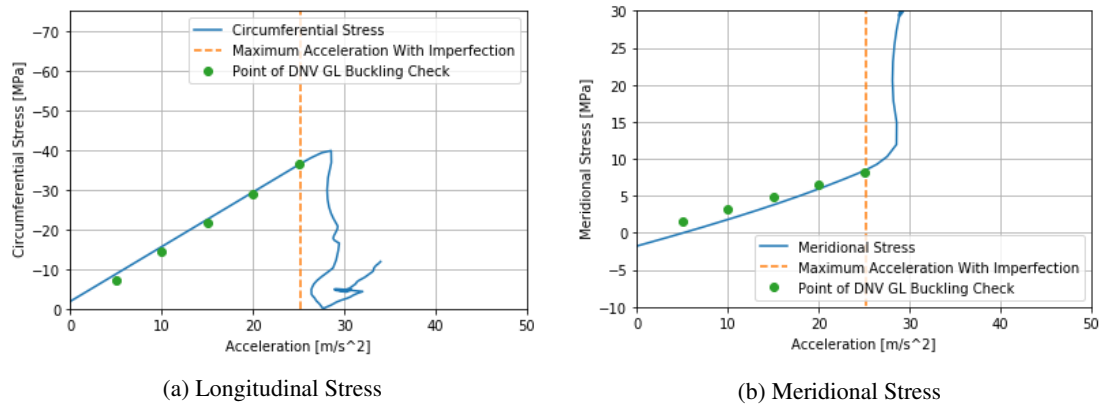


Figure 93: Stretched Tank: Principal Stress Components in Cylindrical Part

### 13.5 Comparison of Spherical and Stretched Tank

Table 37 compares the most important results from the sloshing analysis of both spherical and non-spherical tank with 20° heel, and 50 % filling. It is clear that the addition of a cylindrical part in the original spherical tank significantly weakens the structure exposed to sloshing.

Table 37: Comparison of Spherical and Stretched Tank

	Critical Acc. Buckling Check [ $m/s^2$ ]	Critical Acc. FEA [ $m/s^2$ ]
Spherical Tank	20	42
Stretched Tank	15.6	23

Figure 94 shows the development of the largest compressive stress in the two different tanks based on linear extrapolation. The use of linear extrapolation is based on the grounds that at the lower acceleration, the relationship between the largest compressive stresses and the acceleration is approximately linear. When the acceleration and stress increases, this relationship becomes more non-linear, as the tanks deform. For the buckling checks in DNV GL a linear relationship between the largest compressive stress and load is assumed. Linear extrapolation was used to find a suitable slope.

It can be seen that the slope between the largest compressive stress and acceleration is higher for the stretched tank than for the spherical tank. This is probably a significant part of the reason that the stretched tank is more vulnerable to the sloshing load applied in these analyses. An additional reason for the critical accelerations from the FEA to be smaller for the stretched tank is interaction between the cylinder and the spherical parts. Discontinuities in the connection between the two parts may lead to high local stresses, including bending stresses induced by curvature in the shell structure. Such curvature may have a major

impact on the strength of thin-walled shell structures such as the LNG-tanks.

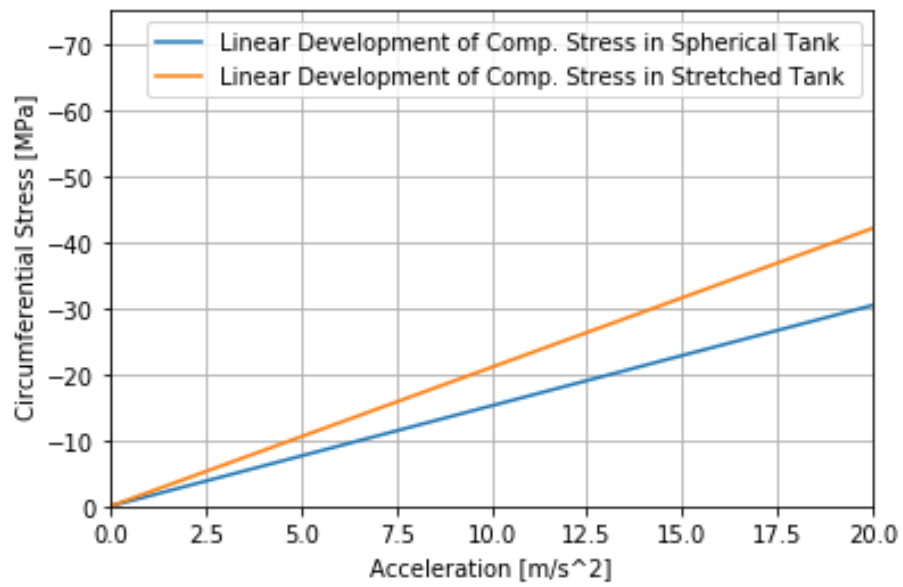


Figure 94: Development of Compressive Stresses in Spherical and Stretched Tank Based on Extrapolation

### 13.6 Attempt with Linear Elastic Material Model

In order to study the degree of plasticity in the buckling, similar analyses were done with a linear elastic material model. The analyses were carried out to observe the relationship between the critical accelerations with the two different material models. The same imperfections as obtained in Section 13.3 were applied. It can be seen from Figure 95 that the buckling strength increases significantly for the linear elastic material model. This observation confirms that the buckling failures of the tanks exposed to sloshing loads in Sections 11 and 13 are of a very plastic nature.

Table 38: Comparison of Spherical and Stretched Tank (Linear Elastic Material Model)

	Elasto-Plastic Mat. Mod. [ $m/s^2$ ]	Linear Elastic Mat. Mod. [ $m/s^2$ ]
Spherical Tank	42	56
Stretched Tank	23	35

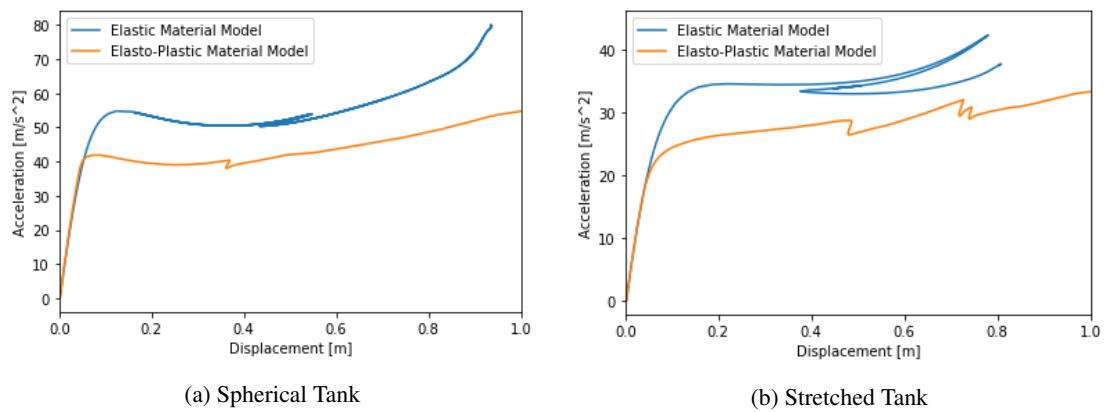


Figure 95: Force/Displacement Relation with Linear Elastic Material

## 14 Discussion

This chapter will discuss the most important limitations in the project and the sources of errors relevant to the analyses. Additionally, the results will be discussed, and based on the results obtained in the FEM-analyses, certain considerations regarding the Class Guidelines from DNV GL will be discussed. Furthermore, a general evaluation of the advantages and disadvantages of non-spherical LNG-tanks is presented.

### 14.1 Limitations of the Project & Sources of Error

In this section, the simplifications of the tank model is addressed. Additionally, the choice of material and the application of imperfections are discussed. Lastly, the determination of buckling load for the sloshing analyses is addressed.

#### 14.1.1 Simplifications of the Tank

Normally, the pump tower should be included in the model for the FEM-analysis of the cargo tanks. This has not been included in this thesis. The tower does not affect the bottom of the tank, but may have significant impact on the top of the tank. However, the two main topics of this thesis are the DNV GL approach to calculate elastic buckling strength of cylinders, and how the strength of the tank against sloshing loads changes for a stretched tank, compared to a spherical tank. For the comparison between the FEM-results and the DNV GL equations concerning buckling strength of cylinders, a simple model has been beneficial. As the tower mainly affects the northern hemisphere, close to the pole, it is reasonable to believe that the tower would have a minor impact on the strength against sloshing loads, as the buckling occurs on the southern hemisphere.

The skirt has been modelled as a 70 mm, unstiffened plate throughout the project. The strength of the skirt has not been of interest and as a consequence, the skirt was designed to be a realistic model of the boundary conditions. This has also been possible as the interaction forces between the tank and the cargo hold have not been included in the analyses. The simplification of the skirt, and neglecting both the static and the dynamic interaction forces are significant simplifications of the analyses.

The effect of thermal loads is also not included in the analyses. The LNG cools the tank, which leads to contraction of the material. This cool-down may lead to significant stresses and deflections. However, thermal loads are not mentioned as a part of the load cases important for the buckling of the LNG-tanks, as they will not affect the buckling strength of the spherical tanks a great deal. However, the thermal loads are believed to have significant impact on the strength of the stretched tank. As the spherical and the cylindrical part will contract differently, significant discontinuities in the connection between the cylinder and the spherical end-caps may occur. This is illustrated by Figure 14 in Section 2.3.

#### 14.1.2 Choice of Material

The choice of material model is described in Section 4.3.1, and was to a great extent based on the experimental data and results from Misovic et al. [23]. However, further studies of the DNV GL regulations indicate that a yield stress of 125 MPa would have been preferred over the chosen value of 134 MPa [12]. Additionally, DNV GL recommends an ultimate tensile strength between 275 and 350 MPa. This is also slightly lower than the value used in the analyses.

However, it is seen as likely that the yield stress of 134 MPa is a suitable value, or even a low value for Al-5083 exposed to low temperatures. Huang et al. did similar experiments, at low temperatures close to  $-163^{\circ}\text{C}$ . The experiments resulted in a minimum value for yield stress of 175 MPa, and an ultimate tensile strength of 420 MPa [14]. This indicates that a yield stress of 134 MPa might have been conservative, and that the Class Guidelines might be too conservative.

### 14.1.3 Application of Imperfections

The application of imperfections is described in Chapter 9. In this thesis, an estimate of a suitable imperfection amplitude has been used, based on simple equations provided by DNV GL. However, these equations are described as an estimate, and according to DNV GL, the imperfection amplitudes will be decided by Class, based on several factors not included in the simple formulas provided by the Class Guidelines. These factors include shell thickness, material, and the manufacturers experience. As the Society will decide the imperfections amplitude, the suitability of the chosen amplitudes is a possible source of error. However, as the estimates provided by DNV GL has been used, the possible error should be of minor importance.

The most common way to introduce imperfections is to do a linear eigenvalue analysis, and make an imperfection based on one or several eigenmodes. This was done for the analyses in the thesis where the load was limited to external pressure. Due to difficulties with the linear analysis with the sloshing loads described in Section 11.2.2, the imperfections were computed based on non-linear analysis. Even though this is not the most common way to introduce imperfections, it is believed to have produced suitable imperfections for these analyses, as the principle of such an imperfection is the same; to apply the most critical imperfection to the structure, with the load in question.

### 14.1.4 Determination of Buckling Load

For the linear analysis, the determination of the buckling load is simple and exact. However, for the non-linear analysis, the buckling load has been decided based on force/displacement-curves such as Figure 96. The force-displacement relation can be quite different for different analyses, and how to extract one specific critical value is subject to interpretation. The blue line in Figure 96 is quite easy to interpret, as the transition from linear to non-linear is abrupt. For the orange line however, the transition between a linear force/displacement relation and a non-linear relation happens more gradually, and the size of the critical load to extract from this curve, depends on the interpretation of the plot. In this project, the critical value has been extracted at the point where the relation becomes significantly non-linear. However, a more consistent method to extract a suitable critical load might have been preferable.

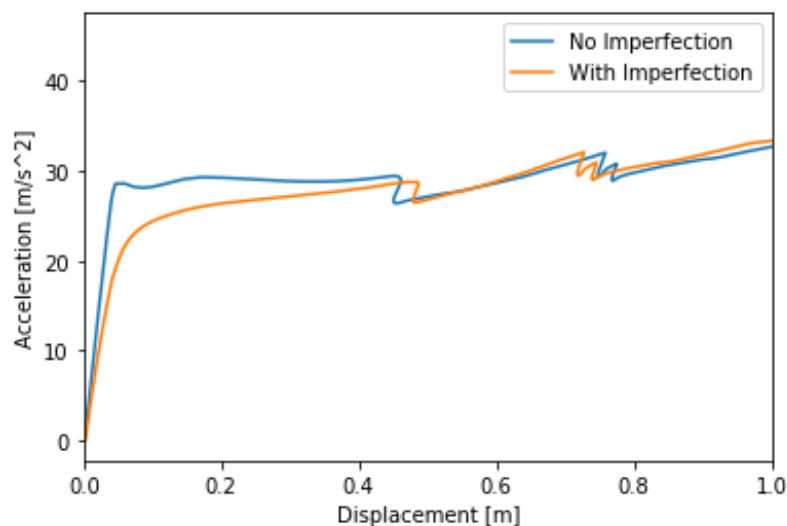


Figure 96: Example of Force/Displacement Relation

## 14.2 Elastic Buckling Stress of Cylinders

The elastic buckling stress of cylinders have been studied in this thesis, and this section will be a discussion of the results obtained on this topic, more specifically Chapters 7 and 8. The findings concerning the equations of the elastic buckling stress of cylinders in Chapter 7, was the basis for the parametric study with increasing cylinder length in Chapter 8. The results from these analyses indicate that the equations provided by DNV GL for the elastic buckling stress of cylinders are unsuitable for cylinders with a very small length/radius-ratio. The results are presented well by Figure 97.

It is clear that the classical elastic buckling stress corresponds well when the length of the cylinder is equal or higher than the cylinder diameter. With a radius of 21.5 meters which is constant in these analyses, and a cylinder length of less than 20, there is a major difference between the FEM-results and the DNV GL equations. This may be because of the high influence from the boundary conditions for very short cylinders, in which the equations does not take into account.

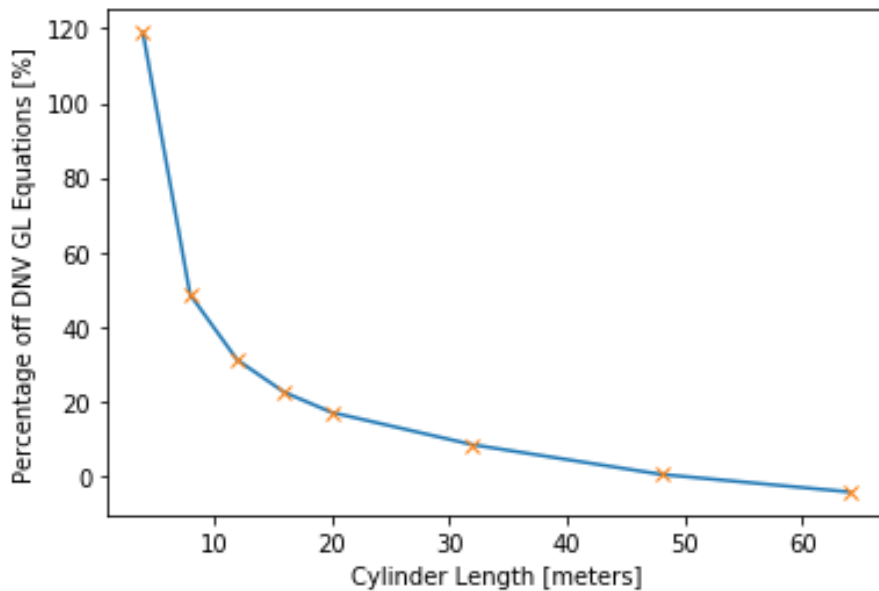


Figure 97: Percentage Offset of FEA-Results from DNV GL equations

As the cylinders of stretched LNG-tanks will have a very low length/radius-ratio, an alteration of the equation for classical elastic buckling stress is suggested, based on the high difference between the FEA-results and the DNV GL equations, seen in Figure 97. The elastic buckling stress for a cylinder is defined as:

$$\sigma_E = C \frac{\pi^2 E}{12(1-\nu^2)} \left(\frac{t}{l}\right)^2 \quad (52)$$

To make the elastic buckling pressure a better fit for cylinders with a length/radius-ratio of less than two, a strength reduction factor is suggested, based on the regression seen in Figure 98. Based on the results obtained in this thesis, a suitable way to calculate the elastic buckling pressure for cylinders is suggested to be:

$$\text{if } L/2R < 1 \quad \sigma_E = \left(0.87 + 0.221 * \log(L/R)\right) C \frac{\pi^2 E}{12(1-\nu^2)} \left(\frac{t}{l}\right)^2 \quad (53)$$



$$\text{if } L/2R \geq 1 \quad \sigma_E = C \frac{\pi^2 E}{12(1-\nu^2)} \left(\frac{t}{l}\right)^2 \quad (54)$$

The reduction factor for short cylinders is the function of the regression-line in Figure 98. It is important to emphasise that the suggestion to make this change in the DNV GL Class Guidelines needs verification. Only eight different cylinder lengths have been analysed, which is a limited amount of data. Hence, to verify this hypothesis, a larger amount of cylinder lengths need to be analysed, preferably in several different software, to confirm the hypothesis.

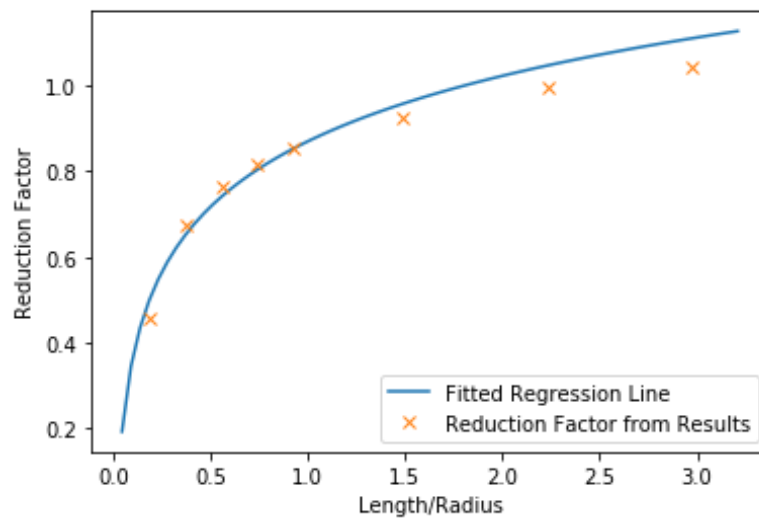


Figure 98: Experimental Results and Fitted Regression Line

### 14.3 Advantages and Disadvantages of Stretched LNG-tanks

The main advantage of stretching the LNG-tanks is to increase the capacity and the utilization of the ship volume. However, if the difficulties of such a configuration are too many and significant, a longitudinally stretched LNG-tank would be unfeasible.

It is hard to evaluate the suitability of longitudinally stretched tanks based on the very narrow scope of this thesis. As the scope of this thesis is limited to buckling of the tank, there are several aspects of a stretched tank that may be more critical to the suitability of such tanks. As explained in Section 14.1.1, the thermal loads are expected to be more critical to the stretched tank, than to the spherical tank. Additionally, significant changes will have to be done to the skirt, and the interaction between the cargo hold and the tank may be different.

From the FEA-results presented in Chapter 13, it is clear that the compressive stresses are higher for the stretched tank exposed to transverse sloshing, leading to a reduced critical load. A possible explanation is that such a stretched tank will room more LNG. This leads to a higher total load on the structure. This might lead to higher stresses, especially as the stresses in the spherical parts are higher for the stretched tank, than for the spherical tank. However, the most exposed part of the stretched tank could be strengthened to enhance the structural capacity. How much additional thickness needed to increase the strength of the stretched tank sufficiently, could be determined by further analyses. There are no indications that an increase in thicknesses in critical areas will fail to improve the tank strength sufficiently. This assumption is based

on the large difference in strength observed in Chapters 11 and 13. The conservative thicknesses applied to both tanks in Chapter 11 yielded satisfactory results in the DNV GL buckling check, and a tank with thicknesses somewhere between the conservative thicknesses used in Chapter 11 and the more optimised tanks in Chapter 13, may prove to be a more optimal longitudinally stretched tank, with an eight-meter cylindrical part. Thus, there is no indication that the buckling of the stretched LNG-tank should make a longitudinally stretched configuration unfeasible. It seems likely that other structural aspects of such a configuration will yield more important challenges, in terms of both feasibility and cost.

## 15 Conclusion

Based on the results obtained in the FEA computed in this thesis, the DNV GL use of the equation for elastic buckling stress for the short cylinders in question in this thesis, seems unsuitable. The FEA-results has been the basis for a suggestion of an alteration to the current procedure defined by DNV GL. The suggested procedure to calculate elastic buckling stress for cylinders can be seen below.

$$\text{if } L/2R < 1 \quad \sigma_E = \left(0.87 + 0.221 * \log(L/R)\right) C \frac{\pi^2 E}{12(1 - \nu^2)} \left(\frac{t}{l}\right)^2 \quad (55)$$

$$\text{if } L/2R \geq 1 \quad \sigma_E = C \frac{\pi^2 E}{12(1 - \nu^2)} \left(\frac{t}{l}\right)^2 \quad (56)$$

The buckling strength of a longitudinally stretched tank is significantly lower than the strength of the original spherical tank. However, increased thicknesses in the stretched tank, especially in the spherical part seem to be a satisfactory solution to increase the buckling strength. Based on the results obtained in this thesis there is no indication that the reduction of buckling strength will be a major challenge and it is deemed likely that other aspects of such a configuration, especially related to thermal effects and other structural elements of the vessel will be more critical to the feasibility of longitudinally stretched LNG-tanks.

Based on the comparison of buckling capacity by use of FEM and the procedures to calculate maximum allowable stress provided by DNV GL, a suitable rule of thumb seem to be that the maximum allowable principal stresses by DNV GL are half the stress magnitudes in the structure prior to failure. This observation indicates that the DNV GL Class Guidelines concerning buckling strength of spherical and non-spherical LNG-tanks are quite conservative. Hence, it seems that allowing higher stress values in the tanks may lead to more cost-efficient LNG-carriers without introducing issues concerning safety. However, as the maximum capacity is expected to be very dependent on several aspects of the analyses such as material model and the simplifications, the results obtained in this thesis will need further verification before any changes can be introduced by Class.

### 15.1 Further Works

In order to realise the longitudinal LNG-tanks, numerous FEM-analyses of the vessel will have to be carried out. This is not only limited to the LNG-tanks but includes other parts of the vessel. The suggested further works, limited to the tanks are listed below.

- Further analyses concerning the suitability of the equations concerning elastic buckling pressure provided by Class could be done. This would possibly include a different software, and a larger range of cylinder lengths than the eight different lengths analysed in this thesis.
- Thermal effects on longitudinally stretched LNG-tank, including comparison with the original spherical design is an important topic to evaluate concerning the feasibility of longitudinally stretched tanks.
- Interaction forces between the tank and the cargo hold could be investigated and included in the analysis to make the results more reliable. If the interaction forces were to be included, it is advised that a more detailed skirt model is modelled. The pump tower or realistic interaction forces between the pump tower and the tank can also be modelled to increase the reliability.

---

## Bibliography

- [1] Amdahl J. TMR4205 Buckling and Ultimate Strength of Marine Structures Compendium: Chapter 5: Buckling of Cylindrical Shells. NTNU Dept. Marine Technology; 2011
- [2] Baumgarten L & Kierfeld J. Buckling of thermally fluctuating spherical shells: Parameter renormalization and thermally activated barrier crossing. TU Dortmund University; 2018
- [3] Bell K. Konstruksjonsmekanikk Del 2: Fasthetslære. Fagbokforlaget; 2019
- [4] JASION P & MAGNUCKI K. Elastic buckling of Cassini ovaloidal shells under external pressure – theoretical study. Poznań University of Technology Institute of Applied Mechanics; 2015
- [5] Digital Engineering 24/7 [Internet]. Linear and Nonlinear Buckling in FEA; 2015 [cited 2020 Feb 10] Available from: <https://www.digitalengineering247.com/article/linear-and-nonlinear-buckling-in-fea/>
- [6] DNV GL, DNVGL-RP-C202 Buckling strength of shells, DNV GL, 2017; pp. 17-20
- [7] DNV GL. DNVGL-CG-0134, Liquefied gas carriers with spherical tanks of type B. DNV GL; 2018
- [8] DNV GL. DNVGL-RP-C208 Determination of structural capacity by non-linear finite element analysis methods. DNV GL; 2016
- [9] DNV GL. DNVGL-RU-SHIP Pt.5 Ch.7 Liquefied gas tankers. DNV GL; 2017
- [10] DNV GL. Classification Note 30.1, *BUCKLING STRENGTH ANALYSIS OF BARS AND FRAMES, AND SPHERICAL SHELLS*, DNV GL, 2004
- [11] Classification Note 30.3, *BUCKLING CRITERIA OF LNG SPHERICAL CARGO TANK CONTAINMENT SYSTEMS – SKIRT AND SPHERE*, DNV GL, 1997
- [12] DNV GL. DNVGL-RU-SHIP Pt.2 Ch.2 Metallic materials, DNV GL; 2017; p. 180
- [13] Evkina AY Lykhachova OV. Design buckling pressure for thin spherical shells: Development and validation. Prydniprov'ska State Academy of Civil Engineering and Architecture; 2018
- [14] Huang C et al. Mechanical properties of AA5083 in different tempers at low temperatures. IOP Conf. Ser.: Mater. Sci. Eng; 2017
- [15] Hutchinson JW, Knockdown factors for buckling of cylindrical and spherical shells subject to reduced biaxial membrane stresses, Harvard University; 2010
- [16] Hutchinson JW, Initial Post-Buckling Behavior of Toroidal Shell Segments. Harvard University; 1967
- [17] International Energy Agency [Internet]. Data and Statistics. [cited 2020 Jan 26] Available from: <https://www.iea.org/data-and-statistics/charts>
- [18] von Karman T Tsien HS. The Buckling of Thin Cylindrical Shells under Axial Compression. Journal of the Aeronautical Sciences; 1941
- [19] Lee A. The Geometric Role of Precisely Engineered Imperfections on the Critical Buckling Load of Spherical Elastic Shell. Massachusetts Institute of Technology; 2016
- [20] Leira BJ. Marine Structures, Basic Course Compendium. NTNU Dept. Marine Technology; 2018
- [21] Livermore Software Technology Corporation. LS-DYNA Theory Manual. LSTC; 2015
- [22] Livermore Software Technology Corporation. LS-DYNA Theory Manual. LS-DYNA; 2019
- [23] Misovic M, Tadic N and Lucic D. Deformation characteristics of aluminium alloys. University of Montenegro; 2016

- [24] Moan T. Finite Element Modelling and Analysis of Marine Structures. NTNU Dept. Marine Technology NTNU; 2003
- [25] Odland J. Dimensjonering av skallkonstruksjoner. Institutt for Marine Konstruksjoner, 1991
- [26] Pranesh SB. Non-linear buckling analysis of imperfect thin spherical pressure hull for manned submersible. Department of Ocean Engineering, Indian Institute of Technology Madras; 2017
- [27] Sanne A. Buckling of Non-spherical Moss-LNG tank. Norwegian University of Science and Technology; Faculty of Engineering; Department of Marine Technology.
- [28] Sano, Matsubara, Izumi Fujikobo, Estimation of Elastic Buckling Strength of a Non-Spherical Tank in the Partially Filled Condition. International Conference on Ocean, Offshore and Arctic Engineering; 2017.
- [29] The Motorship [Internet]. Non-Spherical Moss LNG Tank Gets AIP. [cited 2020 Jan 26] Available from: <https://www.motorship.com/news101/lng/non-spherical-moss-lng-tank-gets-aip>
- [30] U.S. Energy Information Administration [Internet]. Natural Gas Explained.; c2019 [cited 2020 Jan 26]. Available from: [www.eia.gov/energyexplained/natural-gas/](http://www.eia.gov/energyexplained/natural-gas/)
- [31] Vesselfinder [Internet]. DNV GL awards Kawasaki Heavy Industries AiP for new non-spherical (MOSS) LNG tank; 2017 [cited 2020 Jan 26]
- [32] Zhang, Wang, Wang Tang. Buckling of egg-shaped shells subjected to external pressure. Jiangsu University of Science and Technology; 2017
- [33] Zoelly R. Ueber ein Knickungsproblem an der Kugelschale. ETH Zürich; 1915

# Appendices

## A Additional Results Section 8

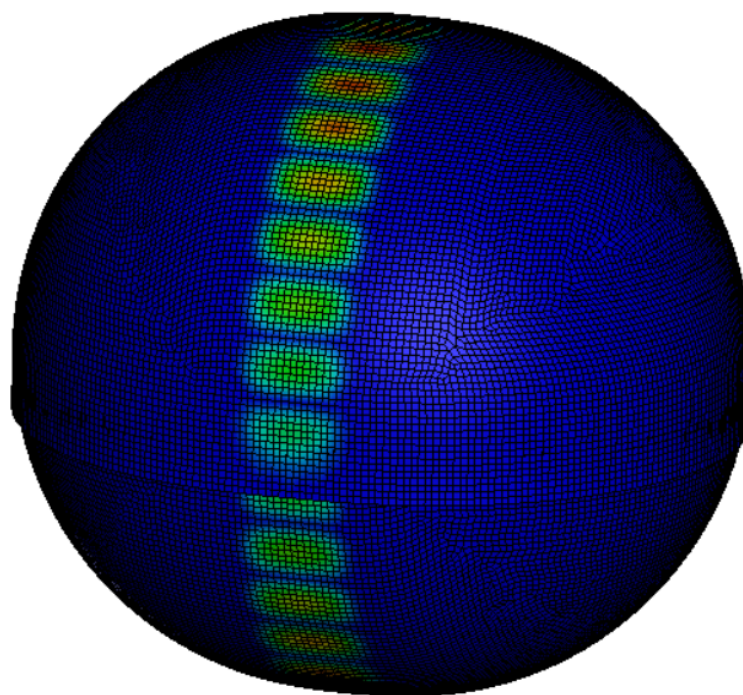


Figure 99: 4 meter Cylindrical Part, Mode 1

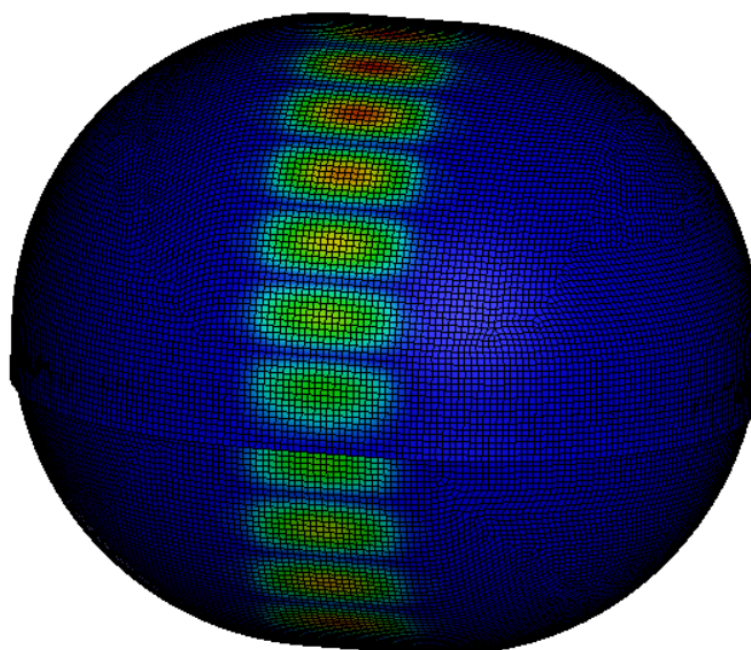


Figure 100: 8 meter Cylindrical Part, Mode 1

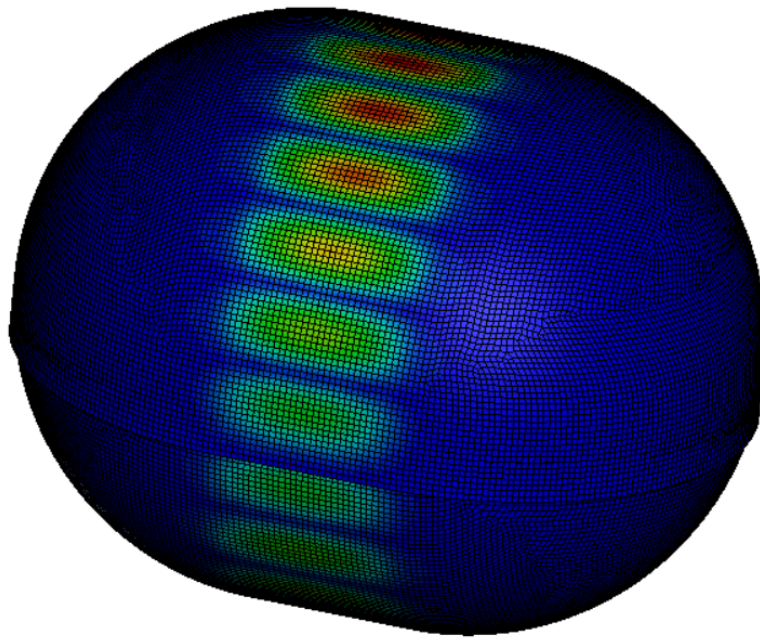


Figure 101: 12 meter Cylindrical Part, Mode 1

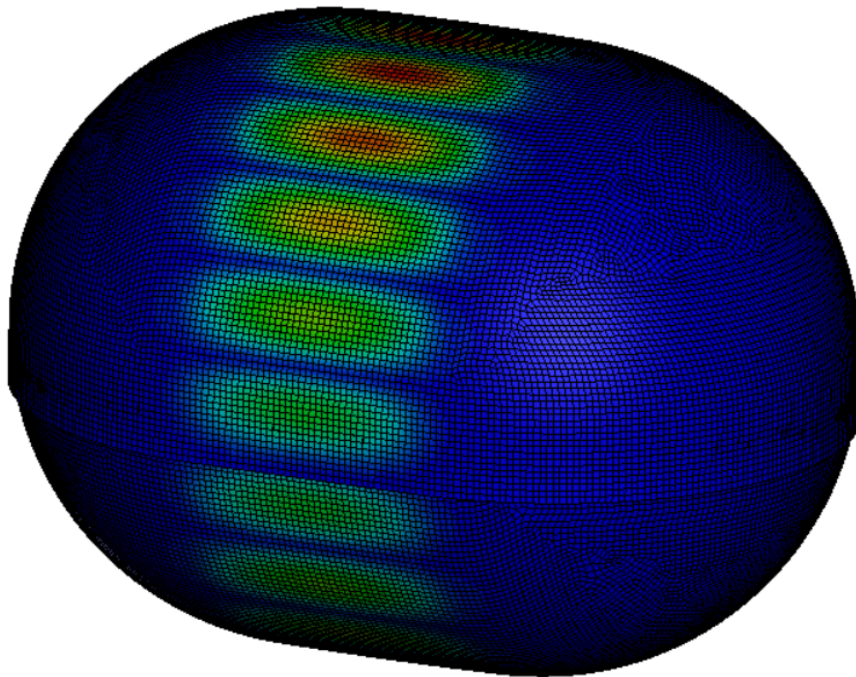


Figure 102: 16 meter Cylindrical Part, Mode 1

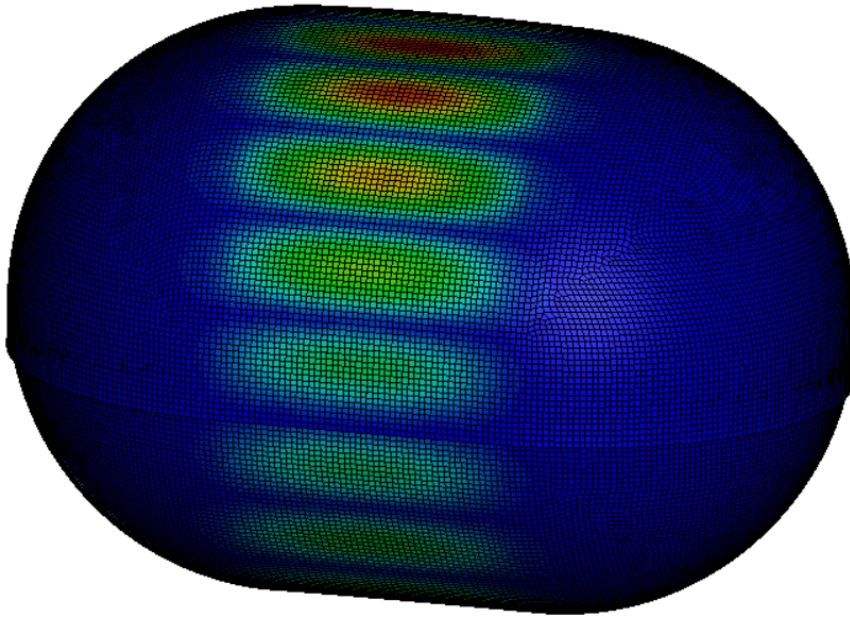


Figure 103: 20 meter Cylindrical Part, Mode 1

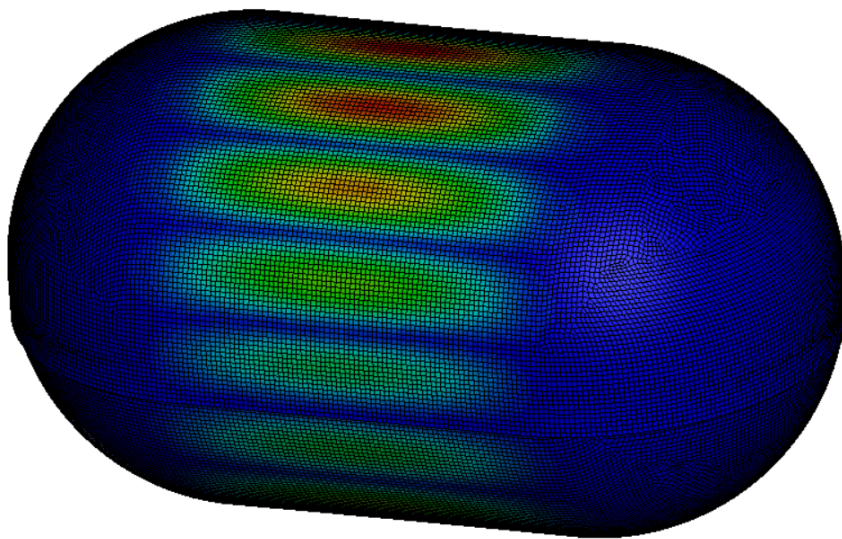


Figure 104: 32 meter Cylindrical Part, Mode 1



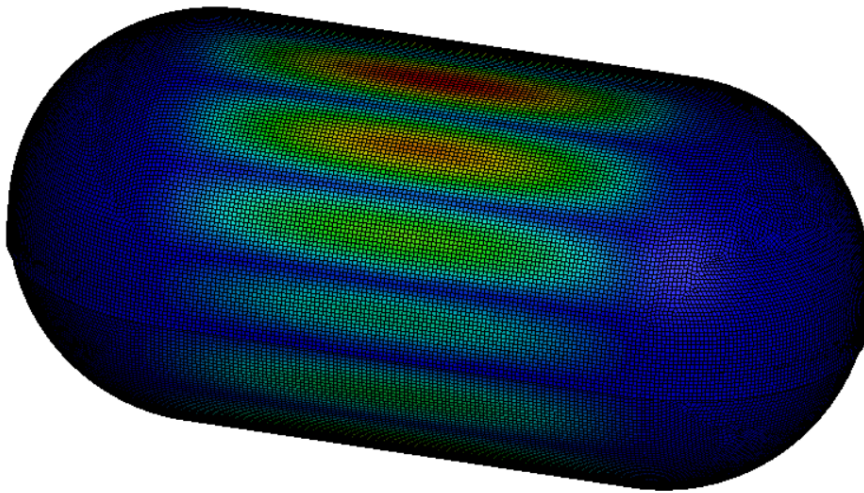


Figure 105: 48 meter Cylindrical Part, Mode 1

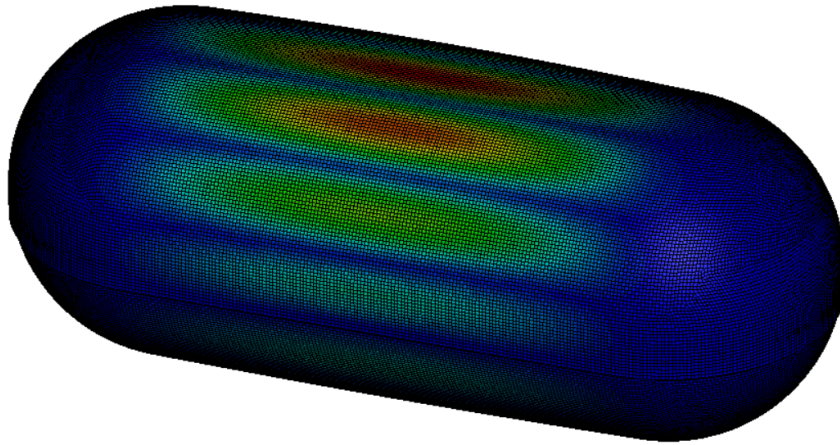


Figure 106: 64 meter Cylindrical Part, Mode 1

## B Python Scripts

### B.1 Mesh Convergence Script

@author: Peder Gjestvang

```
import os
import subprocess
import subfunc
import time
import pandas as pd
import matplotlib.pyplot as plt

os.chdir(r"P:\Master\MeshConvergenceFolder")

mesh_vec=[2.0,1.35,1.25,1.125,1.0,0.8,0.7,0.45,0.25]

P_analytic_vec=[183880,183880,183880,183880,183880,183880,183880,183880,183880]

path=r"P:\Master\MeshConvergenceFolder"
folder=[]

for i in range(len(mesh_vec)):
    mesh=str(mesh_vec[i])
    folder.append(path + "\\\" + mesh)

for i in range(len(mesh_vec)):

    os.chdir(folder[i])
    cwd = os.getcwd()
    print(cwd)

    subprocess.call("batchtest.bat")

    analysis="running"

    while analysis=="running":
        time.sleep(20)
        f_log=open("messag")
        lineList=f_log.readlines()
        f_log.close()

        last_line=lineList[len(lineList)-1]
        print(last_line)
        if last_line.find("N o r m a l"):
            print("Normal Termination")
            analysis="complete"
```

```
        elif last_line.find("E r r o r"):  
            print("Error Termination")  
            analysis="Error"  
  
eigout=[]  
eigenvalues=[]  
  
for i in range(len(mesh_vec)):  
  
    os.chdir(folder[i])  
  
    f=open("eigout","r")  
    eigout.append(f.readlines()[-5])  
    f.close()  
  
    #print(eigout)  
  
    temp_string=eigout[i]  
    eigenvalue_string=temp_string[15:-15]  
    print(eigenvalue_string)  
    eigenvalues.append(float(eigenvalue_string))  
    #  
  
    plt.figure()  
    plt.plot(mesh_vec,eigenvalues)  
    plt.plot(mesh_vec,P_analytic_vec,linestyle='dashed')  
    plt.xlabel("Mesh Size")  
    plt.ylabel("Linear Buckling Pressure [Pa]")  
    plt.show()  
  
    #Plotting the analysis time to compare the mesh sizes  
  
    comp_time_vec=[]  
    messag=[]  
  
    for i in range(len(mesh_vec)):  
  
        os.chdir(folder[i])  
        f=open("messag","r")  
        messag.append(f.readlines()[-12])  
        f.close()  
  
        temp_time_string=messag[i]  
        time_string=temp_time_string[26:-43]  
        print(time_string)  
        comp_time_vec.append(float(time_string))
```

```
plt.figure()
plt.plot(mesh_vec, comp_time_vec)
plt.xlabel("Mesh Size")
plt.ylabel("Computational Time [s]")
plt.show()
```

```
print (messag)
```

## B.2 Script for Making Imperfection Files

@author: Peder Gjestvang

```
import os
import subprocess
import subfunc
import time

os.chdir(r"Write Directory Here")
cwd = os.getcwd()
print (cwd)
f=open("output", "r")
disp=f.readlines()
f.close()

temp_lines=[]
node_numbers=[]
x_disp=[]
y_disp=[]
z_disp=[]

for i in range(len(disp)-8):
    temp_lines.append(disp[i+8])
    temp_string=temp_lines[i]
    node_numbers.append(int(temp_string[1:9]))
    x_disp.append(float(temp_string[10:25]))
    y_disp.append(float(temp_string[26:42]))
    z_disp.append(float(temp_string[43:57]))

f=open("perturb_x", "w")

for i in range(len(node_numbers)):
    temp_string=str(node_numbers[i]) + "\t" + str(x_disp[i]) + "\n"
    f.write(temp_string)
f.close()

f=open("perturb_y", "w")

for i in range(len(node_numbers)):
    temp_string=str(node_numbers[i]) + "\t" + str(y_disp[i]) + "\n"
```

```
f.write(temp_string)
f.close()

f=open("perturb_z","w")

for i in range(len(node_numbers)):
    temp_string=str(node_numbers[i]) + "\t" + str(z_disp[i]) + "\n"
    f.write(temp_string)
f.close()
```

### B.3 Script 1 for Computed Imperfection

@author: Martin Slagstad

```
import os
import numpy as np
import DYNA_pre_updated
set_ID = 3
file_in = r'P: Write Path to input-file here
file_out = r'P: Write Path to output-file here

nodes = DYNA_pre_updated.node_set(file_in,set_ID)

LF =0.04

DYNA_pre_updated.node_imp(file_in,file_out,LF,set_ID)
```

### B.4 Script 2 for Computed Imperfection

@author: Martin Slagstad

```
import numpy as np

def node_set(file_name,set_ID):
    '''
    function finding all nodes in a node set
    input is:
    fille name (including location)
    Set_ID - Set number
    '''
    f = open(file_name,'r')
    nodes = []
    a = 10
    b = 10
    for line in f:
        if '*SET_NODE_LIST_TITLE' in line:
            a = 0
        if a <=3:
            if line.split()[0] == str(set_ID):
                b = 0
        if '*' in line:
            b +=1
```

---

```

    if b == 1:
        node_temp = line.split()
        for i in range(len(node_temp)):
            nodes.append(int(node_temp[i]))
    if '$#' in line:
        b +=1
    a += 1

f.close()
return nodes

def node_imp(file_in, file_out, LF, set_ID):
    '''
    function putting imperfections on nodes in .k file
    Uses the node_set fuction defined in this file
    '''
    R=21.5
    L = 8
    waves=14 #Not halfwaves
    nodes = node_set(file_in, set_ID)
    f_in = open(file_in, 'r')
    f_out =open(file_out, 'w')
    b = 20
    a = 1
    for line in f_in:
        if '*' in line:
            a = 1
        if b == 2:
            a = 0

        if a ==0:
            temp = line.split()
            if int(temp[0]) in nodes:
                x_bar = float(temp[1])
                y_bar = float(temp[2])
                z_bar = float(temp[3])
                #imperfection in y-direction (half wave)
                LF_y = np.cos(np.pi/L*y_bar)
                #imperfection in theta direction
                theta = np.arctan2(z_bar,x_bar)
                LF_R = np.sin(waves*theta)
                #total imperfection
                x = np.abs(np.cos(theta))*LF_y*LF_R*LF*np.sign(x_bar)+x_bar
                z = np.abs(np.sin(theta))*LF_y*LF_R*LF*np.sign(z_bar)+z_bar
                y = y_bar*1

                f_out.write(temp[0]+' %.9f, %.9f, %.9f, 0 ,0 \n' %(x,y,z))

            else:
                f_out.write(line)

```

---

```
    else:
        f_out.write(line)

    if '*NODE' in line:
        b = 0
        b += 1

    f_in.close()
    f_out.close()

    light_opening=2*np.pi*R/(2*waves)
    print("Light Opening")
    print(light_opening)
```

## B.5 Force/Displacement Plot

@author: Peder Gjestvang

```
import os
import subprocess
import time
import matplotlib.pyplot as plt

os.chdir(r"Write Directory of output-file here")
cwd = os.getcwd()
print(cwd)
f=open("disp_time", "r")
file=f.readlines()
f.close()

temp_lines=[]
node_numbers=[]
time=[]
disp=[]
acc=[]

for i in range(len(file)-9):
    temp_lines.append(file[i+8])
    temp_string=temp_lines[i]
    time.append(float(temp_string[4:20]))
    disp.append(float(temp_string[24:40]))

# Plotting parts of the curve

sloshing_time=time[20:]
sloshing_disp=disp[20:]
```

```
for i in range(len(sloshing_time)):
    sloshing_time[i] -= 2
    acc.append(120*sloshing_time[i])

#acc=120*(sloshing_time-2)
no_imp=sloshing_disp
acc_no_imp=acc

os.chdir(r"Write Directory With output-file with Imperfection Here")
cwd = os.getcwd()
print (cwd)
f=open("disp_time","r")
file=f.readlines()
f.close()

temp_lines=[]
node_numbers=[]
time=[]
disp=[]
acc=[]

for i in range(len(file)-9):
    temp_lines.append(file[i+8])
    temp_string=temp_lines[i]
    time.append(float(temp_string[4:20]))
    disp.append(float(temp_string[24:40]))

# Plotting parts of the curve

sloshing_time=time[20:]
sloshing_disp=disp[20:]

for i in range(len(sloshing_time)):
    sloshing_time[i] -= 2
    acc.append(120*sloshing_time[i])

#acc=120*(sloshing_time-2)
with_imp=sloshing_disp
acc_with_imp=acc

plt.figure()
```



```
plt.plot(no_imp, acc_no_imp, label="No Imperfection")
plt.plot(with_imp, acc_with_imp, label="With Imperfection")
plt.xlabel("Displacement [m]")
plt.ylabel("Acceleration [m/s^2]")
plt.xlim(0,1)
plt.legend()
```

## B.6 Script for Stress Development Plots

@author: Peder Gjestvang

```
import os
import subprocess
import time
import matplotlib.pyplot as plt

os.chdir(r"Write Directory of Analysis here")
cwd = os.getcwd()
print(cwd)
f=open("circ_stress", "r")
file=f.readlines()
f.close()

temp_lines=[]
node_numbers=[]
time=[]
circ_stress=[]
acc=[]

for i in range(270):
    temp_lines.append(file[i+8])
    temp_string=temp_lines[i]
    time.append(float(temp_string[4:20]))
    circ_stress.append(float(temp_string[24:40]))

# Plotting parts of the curve

sloshing_time=time[20:]
sloshing_circ_stress=circ_stress[20:]

for i in range(len(sloshing_time)):
    sloshing_time[i] -= 2
    acc.append(120*sloshing_time[i])

for i in range(len(sloshing_circ_stress)):
    sloshing_circ_stress[i]=sloshing_circ_stress[i]*10**(-6)
```

```
#acc=120*(sloshing_time-2)

acc_circ=acc
max_acc_circ=max(acc_circ)

max_acc_with_imperfection=42

max_circ_stress=min(sloshing_circ_stress)

f=open("meri_stress","r")
file=f.readlines()
f.close()

temp_lines=[]
node_numbers=[]
time=[]
meri_stress=[]
acc=[]

for i in range(270):
    temp_lines.append(file[i+8])
    temp_string=temp_lines[i]
    time.append(float(temp_string[4:20]))
    meri_stress.append(float(temp_string[23:40]))

# Plotting parts of the curve

sloshing_time=time[20:]
sloshing_meri_stress=meri_stress[20:]

for i in range(len(sloshing_time)):
    sloshing_time[i] -= 2
    acc.append(120*sloshing_time[i])

for i in range(len(sloshing_meri_stress)):
    sloshing_meri_stress[i]=sloshing_meri_stress[i]*10**(-6)
#acc=120*(sloshing_time-2)

acc_meri=acc
max_acc_meri=max(acc_meri)

# Plotting of the Meridional Stress

max_meri_stress=max(sloshing_meri_stress)
```

---

```

#preallocating for plotting

test_accelerations=[5,10,15,20,25,30,35,40]
test_circ_stress=[]
test_meri_stress=[]

#Finding the slope for the linear stress/force relationship

factor_finding_index=60

lin_fac_circ=sloshing_circ_stress[factor_finding_index]/...
acc_circ[factor_finding_index]
lin_fac_meri=sloshing_meri_stress[factor_finding_index]/...
acc_meri[factor_finding_index]

for i in range(len(test_accelerations)):
    test_circ_stress.append(lin_fac_circ*test_accelerations[i])
    test_meri_stress.append(lin_fac_meri*test_accelerations[i])

plt.figure()
plt.plot(acc_circ,sloshing_circ_stress,label="Circumferential Stress")
plt.plot([max_acc_with_imperfection,max_acc_with_imperfection],...
[0,max_circ_stress],label="Maximum Acceleration With...
Imperfection",linestyle='dashed')
plt.plot(test_accelerations,test_circ_stress,"o"...
,label="Point of DNV GL Buckling Check")

plt.xlim(0,60)
plt.ylim(0,-100)

plt.ylabel("Circumferential Stress [MPa]")
plt.xlabel("Acceleration [m/s^2]")

plt.grid()
plt.legend()

plt.figure()
plt.plot(acc_meri,sloshing_meri_stress,label="Meridional Stress")
plt.plot([max_acc_with_imperfection,max_acc_with_imperfection],...
[0,max_meri_stress],label="Maximum Acceleration With...
Imperfection",linestyle='dashed')
plt.plot(test_accelerations,test_meri_stress,"o"...
,label="Point of DNV GL Buckling Check")

plt.xlim(0,60)
plt.ylim(0,100)

plt.ylabel("Meridional Stress [MPa]")

```

---

```
plt.xlabel("Acceleration [m/s^2]")
```

```
plt.grid()
plt.legend()
```

## B.7 Buckling Check Sphere

@author: Andreas Sanne & Peder Gjestvang

```
import numpy as np
import matplotlib.pyplot as plt
```

```
#Definition of design stresses. Positive in compression, negative in tension
```

```
Sigma10 = 5*10.5*10.0**(6.0)
Sigma20 = -5*13.3*10.0**(6.0)
```

```
# Additional parameters
```

```
E = 7.1*10.0**(10.0)
nu = 0.3
SigmaF = 134.0*10.0**(6.0)
t = 0.048
R = 21.5
```

```
LambdaF = Sigma20/Sigma10
```

```
SigmaCL = ((E)/(np.sqrt(3.0*(1.0-nu**(2.0))))) * (t/R)
```

```
LambdaCL = (SigmaCL)/(Sigma10)
```

```
b = -0.5*np.exp(1)**(1.15*LambdaF)
```

```
if LambdaF<0.0:
    g_tol = (4.0+2.0*LambdaF)*np.sqrt(R*t)
    delta1 = (0.01*g_tol)/(1+(g_tol/R))
```

```
if LambdaF>0.0:
    g_tol = 4.0*np.sqrt(R*t)
    delta1 = (0.01*g_tol)/(1+(g_tol/R))
```

```
delta2 = R/750.0
```

```
delta = delta1+((delta2-delta1)*(np.exp(1)**(2.5*(LambdaF-1.0))))
```

```
my = (delta/t)*np.sqrt(-b)
```

```
Psi = 1.0-(0.375*np.sqrt(my))
```

---

```

GammaP = 1.0/Psi

rhoiterations = np.array([0.5,0.0,0.0,0.0,0.0,0.0,0.0,0.0,0.0,0.0])

#There are two ways to iterate to find rho.
#One will always converge. Choose the one that converges

#if LambdaF<1.0:
for i in range(0,9):
    rhoiterations[i+1] = 1-(((3.0*np.sqrt(3.0))/2.0)*GammaP*np.sqrt(-b)*...
    (delta/t)*rhoiterations[i])** (2.0/3.0)
    rho = rhoiterations[i+1]

#if LambdaF>1.0:
#for i in range(0,9):
# rhoiterations[i+1] = (1.0-rhoiterations[i])** (3.0/2.0)/\
# (((3.0*np.sqrt(3.0))/2.0)*GammaP*np.sqrt(-b)*(delta/t))
# rho = rhoiterations[i+1]

Fe = 1.0/(rho*LambdaCL)

Sigmae0 = np.sqrt(Sigma10**2.0+Sigma20**2.0-Sigma10*Sigma20)

LambdaE = np.sqrt(Fe*(SigmaF/Sigmae0))

LambdaCR = (1.0/(np.sqrt(1.0+LambdaE**4.0)))*(SigmaF/Sigmae0)

LambdaECheck = np.sqrt((SigmaF/Sigmae0)*(Sigma10/SigmaCL))

if LambdaECheck<1.0:
    kappa = 0.925+0.375*LambdaECheck
    GammaSum = kappa*1.15

if LambdaECheck>1.0:
    kappa = 1.3
    GammaSum = kappa*1.15

g=LambdaCR-GammaSum

h=LambdaCR/GammaSum

B.8 Buckling Check Cylinder

@author: Peder Gjestvang

# This code is based on Chapter:
#7.3 Buckling strength analysis for the stretched spherical tank in DNV-CG-0134

```

---

```

import numpy as np

sigma_design_circumferential=6*0.645
sigma_design_axial=6*5.34*10**6
tau_design=1*10**6

L = 8.0
t = 0.096 #cylinder
R = 21.5
nu = 0.3
E = 7.1*10**(10)
ReH=134000000 #Yield Stress

Z = ((L**(2.0))/(R*t))*np.sqrt(1.0-nu**(2.0))

#Defining Table 8 from DNV GL

psi=[1,4,5.34]
zeta=[0.702*Z,1.04*np.sqrt(Z),0.856*Z**(3/4)]
#rho=[0.5*(1+(R/(150*t))**(-0.5)),0.6,0.6]
rho=[1,0.6,0.6]

C_axial=psi[0]*np.sqrt(1+(rho[0]*zeta[0]/psi[0])**2)
C_circumferential=psi[1]*np.sqrt(1+(rho[1]*zeta[1]/psi[1])**2)
C_tors_and_shear=psi[2]*np.sqrt(1+(rho[2]*zeta[2]/psi[2])**2)

if sigma_design_axial < 0.0:
    sigma_design_axial=0.0

if sigma_design_circumferential < 0.0:
    sigma_design_circumferential=0.0

sigma_E_axial=C_axial*(E/(12*(1-nu**2)))*(np.pi*t/L)**2
sigma_E_circum=C_circumferential*(E/(12*(1-nu**2)))*(np.pi*t/L)**2
sigma_E_tors=C_tors_and_shear*(E/(12*(1-nu**2)))*(np.pi*t/L)**2

von_mises=np.sqrt(sigma_design_axial**2+sigma_design_circumferential**...
2-sigma_design_axial*sigma_design_circumferential+3*tau_design**2)

lambda_squared=(ReH/von_mises)*((sigma_design_axial/sigma_E_axial)+...
(sigma_design_circumferential/sigma_E_circum)+(tau_design/sigma_E_tors))

sigma_ecr=ReH/(np.sqrt(1+lambda_squared**2))

```

```
usage_factor=von_mises/sigma_ecr

if np.sqrt(lambda_squared) < 1.0:
    kappa= 0.925+0.375*np.sqrt(lambda_squared)
if np.sqrt(lambda_squared) > 1.0:
    kappa=1.3

maximum_usage_factor=1/(1.15**kappa)

safety_margin=maximum_usage_factor/usage_factor
```

